

NAVAL POSTGRADUATE SCHOOL MONTEREY, CALIFORNIA



19981023 009

THESIS

CAVITATION EFFECTS ON A SHIP-LIKE BOX STRUCTURE SUBJECTED TO AN UNDERWATER EXPLOSION

by

Steven L. Wood

September 1998

Thesis Advisor:

Young S. Shin

Approved for public release; distribution is unlimited

REPORT DOCUMENTATION PAGE			Form Approved OMB No. 0704-0188	
<p>Public reporting burden for this collection of information is estimated to average 1 hour per response, including the time for reviewing instruction, searching existing data sources, gathering and maintaining the data needed, and completing and reviewing the collection of information. Send comments regarding this burden estimate or any other aspect of this collection of information, including suggestions for reducing this burden, to Washington Headquarters Services, Directorate for Information Operations and Reports, 1215 Jefferson Davis Highway, Suite 1204, Arlington, VA 22202-4302, and to the Office of Management and Budget, Paperwork Reduction Project (0704-0188) Washington DC 20503.</p>				
1. AGENCY USE ONLY (Leave blank)		2. REPORT DATE September 1998.		3. REPORT TYPE AND DATES COVERED Master's Thesis
4. TITLE AND SUBTITLE: CAVITATION EFFECTS ON A SHIP-LIKE BOX STRUCTURE SUBJECTED TO AN UNDERWATER EXPLOSION			5. FUNDING NUMBERS	
6. AUTHOR(S) Wood, Steven L.				
7. PERFORMING ORGANIZATION NAME(S) AND ADDRESS(ES) Naval Postgraduate School Monterey CA 93943-5000			8. PERFORMING ORGANIZATION REPORT NUMBER	
9. SPONSORING/MONITORING AGENCY NAME(S) AND ADDRESS(ES)			10. SPONSORING/MONITORING AGENCY REPORT NUMBER	
11. SUPPLEMENTARY NOTES The views expressed here are those of the authors and do not reflect the official policy or position of the Department of Defense or the U.S. Government.				
12a. DISTRIBUTION/AVAILABILITY STATEMENT Approved for public release; distribution is unlimited.			12b. DISTRIBUTION CODE	
13. ABSTRACT (maximum 200 words) Shock trials are required for the lead ship of each new construction shock hardened ship class. Live fire shock trials are both complex and expensive. Finite element modeling and simulation provides a viable, cost effective alternative to live fire shock trials. This thesis investigates the effect of bulk and local cavitation on a three-dimensional ship-like box model. The fluid surrounding the structure is modeled to capture the effect of cavitation. Viable results validate the modeling and simulation method used and provide the basis for further investigation into the use of fluid modeling in underwater explosion simulation.				
14. SUBJECT TERMS Underwater Explosion, Cavitation, Surface Model			15. NUMBER OF PAGES 134	
			16. PRICE CODE	
17. SECURITY CLASSIFICATION OF REPORT Unclassified	18. SECURITY CLASSIFICATION OF THIS PAGE Unclassified	19. SECURITY CLASSIFICATION OF ABSTRACT Unclassified	20. LIMITATION OF ABSTRACT UL	

Approved for public release; distribution is unlimited.

**CAVITATION EFFECTS ON A
SHIP-LIKE BOX STRUCTURE SUBJECTED TO AN
UNDERWATER EXPLOSION**

Steven L. Wood
Lieutenant, United States Navy
B.S., United States Naval Academy, 1992

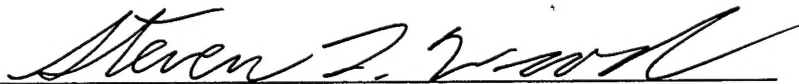
Submitted in partial fulfillment of the
requirements for the degree of

MASTER OF SCIENCE IN MECHANICAL ENGINEERING

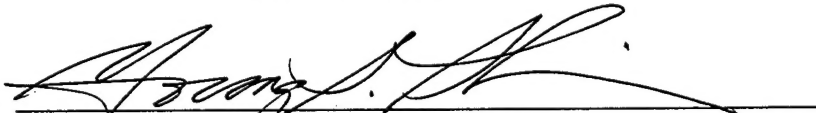
from the


**NAVAL POSTGRADUATE SCHOOL
September 1998**

Author:


Steven L. Wood

Approved by:


Young S. Shin, Thesis Advisor


Terry R. McNeley, Chairman
Department of Mechanical Engineering

ABSTRACT

Shock trials are required for the lead ship of each new construction shock hardened ship class. Live fire shock trials are both complex and expensive. Finite element modeling and simulation provides a viable, cost effective alternative to live fire shock trials. This thesis investigates the effect of bulk and local cavitation on a three-dimensional ship-like box model. The fluid surrounding the structure is modeled to capture the effect of cavitation. Viable results validate the modeling and simulation method used and provide the basis for further investigation into the use of fluid modeling in underwater explosion simulation.

TABLE OF CONTENTS

I.	INTRODUCTION.....	1
	A. BACKGROUND	1
	B. SCOPE OF RESEARCH.....	2
II.	UNDERWATER EXPLOSIONS.....	3
	A. SEQUENCE OF EVENTS.....	3
	B. FLUID-STRUCTURE INTERACTION.....	5
	C. CAVITATION.....	7
	1. Local Cavitation.....	7
	2. Bulk Cavitation.....	9
III.	MODELING AND SIMULATION	15
	A. MODEL CONSTRUCTION AND PRE-PROCESSING.....	16
	1. Three Dimensional Structural Model.....	16
	2. Three-Dimensional Fluid Modeling.....	17
	3. Two-Dimensional Model.....	22
	B. ANALYSIS AND SOLUTION.....	22
	1. Test Description.....	25
	C. POST-PROCESSING	26
IV.	SHOCK SIMULATION RESULTS	29
	A. MODAL ANALYSIS	29
	B. TWO-DIMENSIONAL MODEL	34
	1. Charge Under Keel.....	34
	2. Charge Offset.....	45
	C. THREE-DIMENSIONAL MODEL.....	52
	1. Charge Under Keel.....	52
	2. Offset Charge.....	62
	D. RAYLEIGH DAMPING.....	73
V.	CONCLUSIONS AND RECOMMENDATIONS.....	91
	APPENDIX A. BULK CAVITATION PROGRAM.....	93
	APPENDIX B. HELPFUL FEATURES IN MSC/PATRAN	95

APPENDIX C. FLUID MODELING USING TRUEGRID	101
APPENDIX D. USA/LS-DYNA INPUT DECKS	105
APPENDIX E. USEFUL FEATURES IN LS-TAURUS	113
LIST OF REFERENCES	115
INITIAL DISTRIBUTION LIST	117

LIST OF FIGURES

Figure 1. Shock Wave Profiles From a 300 lb. TNT Charge [Ref. 5]	4
Figure 2. Pressure Wave Profiles [Ref. 7].....	6
Figure 3. Taylor Plate Subjected to a Plane Wave [Ref. 7].....	8
Figure 4. Bulk Cavitation Zone [Ref. 6]	10
Figure 5. Charge Geometry for Bulk Cavitation Equations [Ref. 6]	12
Figure 6. Bulk Cavitation Zones for HBX-1 Charges at the Following Depths: - 50ft, -- 100ft, -. 150ft.....	13
Figure 7. Modeling and Simulation Flow Chart	15
Figure 8. Model Specifications.....	18
Figure 9. Finite Element Mesh	19
Figure 10. Beam Elements	20
Figure 11. Three-Dimensional Fluid Mesh	21
Figure 12. Two-Dimensional Model.....	23
Figure 13. Offset Charge Test Geometry.....	27
Figure 14. Bulk Cavitation Zone for 20 lb. Charge at 15.50-ft	27
Figure 15. Charge Under Keel Test Geometry.....	28
Figure 16. Bulk Cavitation Zone for a 20-lb. Charge at 17.75-ft	28
Figure 17. Two-Dimensional Model Output Nodes	30
Figure 18. Keel Output Nodes (Top View).....	31
Figure 19. Side Output Nodes (Starboard Side)	32
Figure 20. Bulkhead Output Node.....	33
Figure 21. Modes 7 Through 11	35
Figure 22. 2-D Model w/Charge Under Keel (DAA on Wet Surface)	37
Figure 23. 2-D Model w/Charge Under Keel (DAA on Wet Surface)	37
Figure 24. 2-D Model w/Charge Under Keel (DAA on Wet Surface)	37
Figure 25. 2-D Model w/Charge Under Keel (DAA on Wet Surface)	39
Figure 26. 2-D Model w/Charge Under Keel (DAA on Fluid Mesh).....	39
Figure 27. 2-D Model w/Charge Under Keel (DAA on Fluid Mesh).....	39
Figure 28. 2-D Model w/Charge Under Keel Response Comparison (Cavitation Off)....	41

Figure 29. 2-D Model w/Charge Under Keel Response Comparison (Cavitation On)	41
Figure 30. 2-D Model w/Charge Under Keel Fluid Mesh Pressure Profiles.....	42
Figure 31. 2-D Model w/Charge Under Keel Shock Wave Propagation.....	43
Figure 32. 2-D Model w/Charge Under Keel Shock Wave Propagation (Continued)	44
Figure 33. 2-D Model w/Offset Charge (DAA on Wet Surface).....	46
Figure 34. 2-D Model w/Offset Charge (DAA on Wet Surface).....	46
Figure 35. 2-D Model w/Offset Charge Response Comparison (Cavitation Off).....	47
Figure 36. 2-D Model w/Offset Charge Response Comparison (Cavitation Off).....	47
Figure 37. 2-D Model w/Offset Charge Response Comparison (Cavitation On).....	48
Figure 38. 2-D Model w/Offset Charge Response Comparison (Cavitation On).....	48
Figure 39. 2-D Model w/Offset Charge Fluid Mesh Pressure Profiles.....	49
Figure 40. 2-D Model w/Offset Charge Shock Wave Propagation.....	50
Figure 41. 2-D Model w/Offset Charge Shock Wave Propagation (Continued).....	51
Figure 42. 3-D Model w/Charge Under Keel Response Comparison.....	53
Figure 43. 3-D Model w/Charge Under Keel Response Comparison.....	54
Figure 44. 3-D Model w/Charge Under Keel Response Comparison.....	56
Figure 45. 3-D Model w/Charge Under Keel Response Comparison.....	57
Figure 46. 3-D Model w/Charge Under Keel Response Comparison.....	58
Figure 47. 3-D Model w/Charge Under Keel Response Comparison.....	59
Figure 48. 3-D Model w/Charge Under Keel Response Comparison.....	60
Figure 49. 3-D Model w/Charge Under Keel Fluid Mesh Pressure Profiles.....	61
Figure 50. 3-D Model w/Charge Under Keel Shock Wave Propagation.....	63
Figure 51. 3-D Model w/Charge Under Keel Shock Wave Propagation (Continued)	64
Figure 52. 3-D Model w/Offset Charge Response Comparison.....	65
Figure 53. 3-D Model w/Charge Offset Response Comparison.....	66
Figure 54. 3-D Model w/Offset Charge Response Comparison.....	67
Figure 55. 3-D Model w/Offset Charge Response Comparison.....	68
Figure 56. 3-D Model w/Offset Charge Response Comparison.....	69
Figure 57. 3-D Model w/Offset Charge Response Comparison.....	70
Figure 58. 3-D Model w/Offset Charge Response Comparison.....	71

Figure 59. 3-D Model w/Offset Charge Fluid Mesh Pressure Profiles.....	72
Figure 60. 3-D Model w/Offset Charge Shock Wave Propagation	74
Figure 61. 3-D Model w/Offset Charge Shock Wave Propagation (Continued).....	75
Figure 62. 3-D Model w/Charge Under Keel Damped Response Comparison.....	77
Figure 63. 3-D Model w/Charge Under Keel Damped Response Comparison.....	78
Figure 64. 3-D Model w/Charge Under Keel Damped Response Comparison.....	79
Figure 65. 3-D Model w/Charge Under Keel Damped Response Comparison.....	80
Figure 66. 3-D Model w/Charge Under Keel Damped Response Comparison.....	81
Figure 67. 3-D Model w/Charge Under Keel Damped Response Comparison.....	82
Figure 68. 3-D Model w/Charge Under Keel Damped Response Comparison.....	83
Figure 69. 3-D Model w/Charge Under Keel Damped Response Comparison.....	84
Figure 70. 3-D Model w/Charge Under Keel Damped Response Comparison.....	85
Figure 71. 3-D Model w/Charge Under Keel Damped Response Comparison.....	86
Figure 72. 3-D Model w/Charge Under Keel Damped Response Comparison.....	87
Figure 73. 3-D Model w/Charge Under Keel Damped Response Comparison.....	88
Figure 74. 3-D Model w/Charge Under Keel Damped Response Comparison.....	89
Figure 75. 3-D Model w/Charge Under Keel Damped Response Comparison.....	90

ACKNOWLEDGEMENTS

I would like to extend a warm thank you and much appreciation to Dr. Young S. Shin for his continued guidance, patience, and support through out the course of this research. The completion of this study would not have been possible without his advice and assistance. I would also like to thank all of those who offered their inputs and assistance along the way, especially Dr. John DeRuntz and Dr. Robert Rainsberger for their technical expertise and support. A special thanks also goes to Tom Christian for his technical assistance with all things computer oriented.

Finally, I would like to dedicate this work to my beautiful and loving wife Susan and my wonderful daughter Maggie for their love, support, and understanding during our time at the Naval Postgraduate School, especially during the completion of this project.

I. INTRODUCTION

A. BACKGROUND

An underwater explosion event, such as that created by a mine, creates a pressure pulse or shock wave. This shock wave, upon impacting a surface ship's hull, can cause severe structural and equipment damage, as well as personnel casualties. As a defensive measure against underwater explosions, shipboard systems must be shock hardened to a certain level to ensure combat survivability of both personnel and equipment. The Navy, since the Second World War, has developed guidelines and specifications for the shock testing and hardening of shipboard equipment and systems. NAVSEA 0908-LP-000-3010A [Ref. 1] and MIL-S-901D [Ref. 2] are examples of such guidance. The total ship system design is then validated through shock trials as required in OPNAVINST 9072.2 [Ref. 3]. Shock trials are the only means of testing the ship and its systems under combat-like conditions short of an actual conflict. These trials are required for the lead ship of each new construction shock hardened ship class.

Shock trials, however, require extensive planning and coordination. The shock trials of the USS John Paul Jones (DDG-53) provide a recent example. Planning for the test began four years prior to the test date and involved over 50 government agencies and a shock team of 300 personnel. The trials were subsequently delayed three months due to a lawsuit brought against the Navy by concerned environmentalist groups. When testing occurred in June 1994, only two of the four planned tests could be carried out due to inclement weather and post-delivery schedule considerations. [Ref. 4]

Finite element modeling and simulation provides a viable, cost effective alternative to live fire testing. A finite element model of sufficient fidelity is required to achieve good results from the simulation. Sufficient fidelity means the model must be of enough refinement to accurately capture the overall gross response of the ship caused by the impact of the shock wave. One important aspect of model refinement is the inclusion of the surrounding fluid. The fluid mesh must be constructed to mate exactly with the finite element mesh of the structure model and must be of sufficient size to capture the

bulk cavitation zone. Advances in computer technology and finite element codes enables ship shock simulation and modeling, with the inclusion of the fluid mesh, to be carried out with greater precision and speed than previously possible.

B. SCOPE OF RESEARCH

This thesis investigates the effect of bulk and local cavitation on a three-dimensional ship-like box model¹. The ship-like box model used in the simulations includes two bulkheads, a keel, and beam stiffeners (simulating the structure of a typical ship). The model response without the fluid mesh will be used as the baseline for comparison purposes. Fluid mesh size will be varied in order to study its effect on the response. Rayleigh damping will also be included in the model. Viable results from these ship shock simulations will validate the fluid modeling and simulation method used and provide the basis for further investigation into the use of fluid modeling in underwater explosion simulation, specifically for the simulation of the USS John Paul Jones shock trials.

II. UNDERWATER EXPLOSIONS

A. SEQUENCE OF EVENTS

An underwater explosion (UNDEX) is a complex event. It begins with the detonation of a high explosive, such as TNT or HBX-1. Once the reaction is initiated, it propagates through the explosive material by means of a moving discontinuity in the form of a pressure wave. As this pressure wave advances through the explosive, it initiates chemical reactions that create more pressure waves. The detonation process converts the original explosive material from its original form (solid, liquid, or gas) into a gas at very high temperature and pressure (on the order of 3000° C and 50000 atm.) [Ref. 5]. The detonation process occurs rapidly (on the order of nanoseconds) due to the fact that the increase in pressure in the material results in wave velocities that will exceed the acoustic velocity in the explosive material. Therefore, a shock wave exists in the explosive material. The combination of high heat and high compressive pressure enables detonation to be a self-exerting process. This mass of hot, high-pressure gas will then affect the surrounding fluid.

Water, for UNDEX purposes, will be treated as a homogeneous fluid incapable of supporting shear stress, and because water is compressible, pressure applied at one area of the volume will be transmitted as a wave disturbance to other points in the fluid. The disturbance is assumed to propagate at the speed of sound in water, approximately 5000 ft/s [Ref. 6]. It is important to note that this value is a design approximation and the actual acoustic velocity is affected by such parameters as temperature, pressure, and salinity. The wave propagation velocity is several times the acoustic velocity in water near the charge, but it rapidly approaches the acoustic velocity [Ref. 5].

Once the pressure wave reaches the water boundary of the gas bubble, a strong pressure wave and subsequent outward motion of the water relieve it. This pressure is on the order of 2×10^6 lb/in² for TNT. The compressive wave created in the water is called the shock wave. The shock wave is a steep fronted wave because the pressure rise is discontinuous. The rise is then followed by an exponential decay and gradual broadening

of the shock wave as the wave propagates. Figure 1 shows an example a shock wave pressure profile for a TNT charge. [Ref. 5]

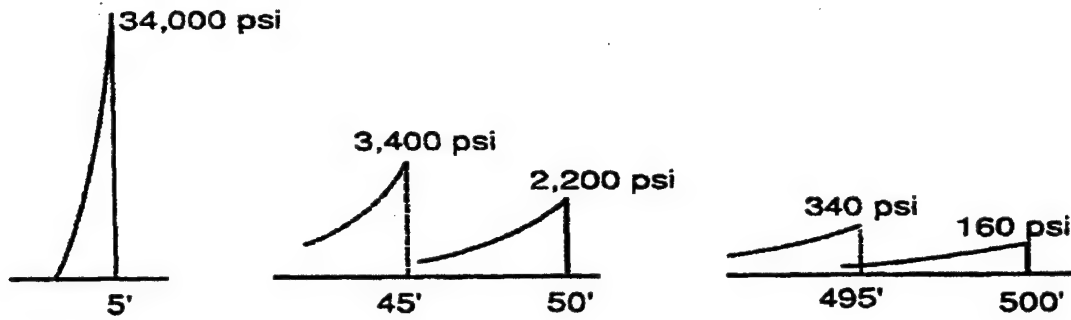


Figure 1. Shock Wave Profiles From a 300 lb. TNT Charge [Ref. 5]

Empirical relations have been derived to characterize the shock wave. These relations are fairly accurate for distances between 10 and 100 charge radii and for duration of one decay constant [Ref. 6]. These relations enable calculation of the pressure profile of the shock wave ($P(t)$), the maximum pressure of the wave (P_{\max}), the shock wave decay constant (θ), the bubble period (T), and the maximum bubble radius (A_{\max}).

$$P(t) = P_{\max} e^{-\frac{t-t_1}{\theta}} \quad (\text{psi}) \quad (2.1)$$

$$P_{\max} = K_1 \left(\frac{W^{\frac{1}{3}}}{R} \right)^{A_1} \quad (\text{psi}) \quad (2.2)$$

$$\theta = K_2 W^{\frac{1}{3}} \left(\frac{W^{\frac{1}{3}}}{R} \right)^{A_2} \quad (\text{msec}) \quad (2.3)$$

$$T = K_5 \frac{W^{\frac{1}{3}}}{(D+33)^{\frac{5}{6}}} \quad (\text{sec}) \quad (2.4)$$

$$A_{\max} = K_6 \frac{W^{\frac{1}{3}}}{(D+33)^{\frac{1}{3}}} \quad (\text{ft}) \quad (2.5)$$

The variables in Equations (2.1) through (2.5) are:

W = Charge weight in lbf

R = Standoff distance in ft

D = Charge depth in ft

t_1 = arrival time of shock wave in msec

t = time of interest in msec

$K_1, K_2, K_5, K_6, A_1, A_2$ = Shock wave parameters

From the above relations, it can be calculated that P_{\max} decreases by approximately one-third after one decay constant.

Subsequent pressure waves known as bubble pulses are generated by the oscillation of the gas bubble created by the UNDEX. The peak pressure in the first bubble pulse is about 10-20% of the shock wave, but is of greater duration so that the area under the two pressure curves are similar [Ref. 5]. The bubble will expand until dynamic equilibrium is reached. Dynamic equilibrium is at a slightly lower pressure than hydrostatic equilibrium due to the effect of the bubble inertia. The bubble will then contract until dynamic equilibrium is again reached; another expansion will then follow. This sequence of oscillation will continue until the energy of the reaction is dissipated or the bubble reaches the free surface or impacts the target.

Based on the location of the charge with respect to the sea floor and the free surface, a vessel may experience a combination of different pressure waves, due to different propagation paths. Free surface reflection, bottom reflection, and bottom refraction are possible. Figure 2 shows these path profiles (except for bottom refraction).

Bottom reflection and refraction effects are dependent on the sea floor type and depth of water under the vessel and the charge. In reasonably deep water, these paths are usually not an issue for surface vessels. Free surface reflection is very important however. This reflected wave is tensile in nature and contributes to the creation of bulk cavitation. This tensile, or rarefaction wave, will be discussed in greater detail below.

B. FLUID-STRUCTURE INTERACTION

The dynamic response of a linear elastic structure in a fluid can be expressed as

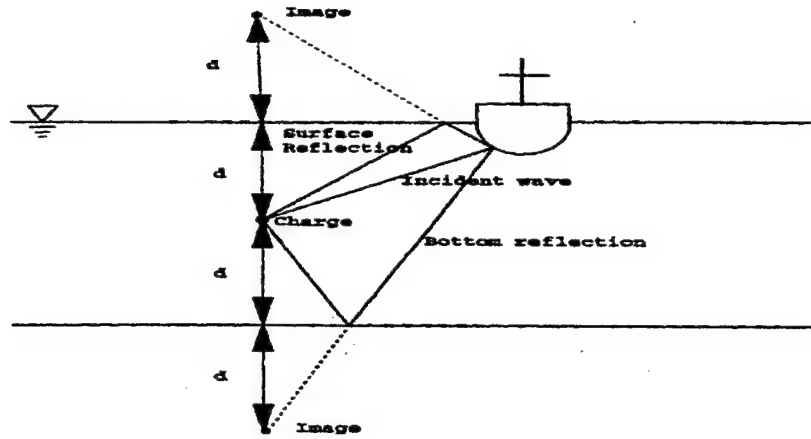


Figure 2. Pressure Wave Profiles [Ref. 7]

follows in Equation (2.6),

$$[M]\{\ddot{x}(t)\} + [C]\{\dot{x}(t)\} + [K]\{x(t)\} = \{f(t)\} \quad (2.6)$$

where $[M]$ = symmetrical structural mass matrix, $[C]$ = symmetrical damping matrix, $[K]$ = symmetrical stiffness matrix, $\{f(t)\}$ = applied external force, $\{x(t)\}$ = displacement vector and derivatives with respect to time. $[M]$ may or may not be diagonal. In the case of a submerged structure excited by an acoustic wave, $\{f(t)\}$ is given by

$$\{f(t)\} = -[G][A_f]\{\{p_I\} + \{p_s\}\} + \{f_D\} \quad (2.7)$$

where $[G]$ = transformation matrix relating structural and fluid nodal surface forces,

$[A_f]$ = diagonal area matrix for the fluid elements, $\{p_I\}$ = incident wave nodal pressure vector, and $\{p_s\}$ = scattered wave nodal pressure vector.

The fluid-structure interaction problem can then be solved using the DAA (Doubly Asymptotic Approximation) method [Ref. 8]. The DAA models the surrounding acoustic medium as a membrane on the surface of the wetted surface of the structure. The DAA may be written as [Ref. 9]

$$[M_f]\{\ddot{p}_s\} + \rho c[A_f]\{\dot{p}_s\} = \rho c[M_f]\{\dot{u}_s\} \quad (2.8)$$

where $[M_f]$ = symmetric fluid mass matrix for the wetted surface fluid mesh, ρ = fluid density, c = fluid acoustic velocity, and $\{u_s\}$ = scattered wave velocity vector. Other terms are as defined above. This relation is called "doubly asymptotic" because it is exact at both high and low frequencies (early and late time respectively) [Ref. 9]. Equation (2.8)

is known as the first order DAA or DAA₁. A second order DAA (DAA₂) exists and has improved accuracy over the DAA₁ at intermediate frequencies. The formulation of the DAA₂ will not be covered here. The DAA methods main advantage is that they model the interaction of the submerged portion of the structure in terms of the wet-surface response variables only.

The kinematic compatibility relation can then be applied to relate $\{u_s\}$ to the structural response,

$$[G]^T \dot{x} = \{u_I\} + \{u_s\} \quad (2.9)$$

The superscript "T" in the above equation denotes the matrix transpose. Equation (2.9) is an expression of the constraint that the normal fluid particle velocity must match the normal structural velocity on the structure wetted surface.

Equation (2.7) can be substituted into Equation (2.6) and Equation (2.9) can be substituted into Equation (2.8) to yield the following interaction equations,

$$[M]\{\ddot{x}\} + [C]\{\dot{x}\} + [K]\{x\} = -[G][A_f](\{p_I\} + \{p_s\}) \quad (2.10)$$

$$[M_f]\{\dot{p}_s\} + \rho c[A_f]\{p_s\} = \rho c[M_f]([G]^T \{\ddot{x}\} - \{\dot{u}_I\}) \quad (2.11)$$

These equations are solved simultaneously by the Underwater Shock Analysis (USA) code using an unconditionally stable staggered solution procedure [Ref. 9]. The solution to this system of equations will yield the displacement, velocity, and acceleration of the structure.

C. CAVITATION

Two types of cavitation can occur during an UNDEX event. "Local cavitation" occurs at the fluid-structure interface and "bulk cavitation" occurs near the free surface and can cover a relatively large area. Both forms of cavitation are discussed below.

1. Local Cavitation

Taylor flat theory is used to illustrate how local cavitation occurs. Figure 3 shows a Taylor flat plate subjected to a plane wave. The plate is considered to be an infinite, air-backed plate of mass per unit area, m . The plate is subjected to an incident plane shock

wave, $P_i(t)$. $P_r(t)$ is the reflected wave from the plate. Newton's second law of motion can then be applied, letting $v_p(t)$ be the velocity of the plate (Equation (2.1)).

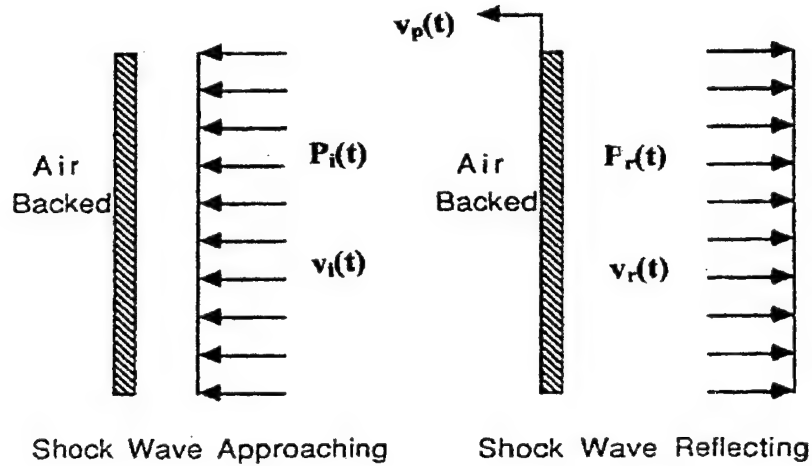


Figure 3. Taylor Plate Subjected to a Plane Wave [Ref. 7]

$$m \frac{dv_p(t)}{dt} = P_i(t) + P_r(t) \quad (2.12)$$

The fluid particle velocities behind the incident and reflection shock waves are $v_i(t)$ and $v_r(t)$, respectively. The plate velocity can then be written as

$$v_p(t) = v_i(t) - v_r(t) \quad (2.13)$$

For a one-dimensional wave, it can be shown using the D'Alembert solution to the wave equation and the reduced momentum equation for a fluid, that the pressure for the incident and reflected shock waves are defined as

$$P_i = \rho C v_i(t) \quad (2.14)$$

$$P_r = \rho C v_r(t) \quad (2.15)$$

where ρ = fluid density and C = acoustic velocity.

Equations (2.14) and (2.15), along with (2.1) can then be substituted into Equation (2.12). The reflected wave pressure, $P_r(t)$, can then be solved for:

$$P_r(t) = P_i(t) - \rho C v_p = P_{\max} e^{-\left(\frac{t}{\theta}\right)} - \rho C v_p \quad (2.16)$$

where t = the time after the arrival of the shock wave. The original equation of motion

(Equation 2.12 above) can now be rewritten as a first order linear differential equation using the above relations.

$$m \frac{dv_p}{dt} + \rho C v_p = 2P_{\max} e^{-\left(\frac{t}{\theta}\right)} \quad (2.17)$$

Equation (2.17) may then be solved for the plate velocity,

$$v_p = \frac{2P_{\max} \theta}{m(1-\beta)} \left[e^{-\left(\frac{\beta t}{\theta}\right)} - e^{-\left(\frac{t}{\theta}\right)} \right] \quad (2.18)$$

where $\beta = \rho C \theta / m$ and $t > 0$. The net pressure experienced by the moving plate can then be expressed as

$$P_i + P_r = P_{\max} \left[\frac{2}{1-\beta} e^{-\left(\frac{t}{\theta}\right)} - \frac{2\beta}{1-\beta} e^{-\left(\frac{\beta t}{\theta}\right)} \right] \quad (2.19)$$

As β becomes large (a lightweight plate), the total pressure in Equation (2.19) will become negative at a very early time. Since water cannot sustain tension (i.e. any significant negative pressure), cavitation will occur when the vapor pressure of water is reached. This is known as local cavitation. The plate is essentially separating from the fluid and the maximum velocity of the plate is attained.

A ship's hull can be easily generalized as a Taylor flat plate. Local cavitation is likely to occur along the hull where the pressure pulse from the UNDEX impinges with sufficient force and the hull plating β value is large enough to make the net pressure negative.

2. Bulk Cavitation

The incident shock wave is compressive in nature. A tensile or rarefaction wave is created when the shock wave is reflected from the free surface. Since water cannot sustain any significant tension, the fluid pressure is lowered and cavitation will occur when the pressure drops to zero or below. In actuality, water can sustain a small amount of tension (approximately three to four psi of negative pressure), but zero psi is typically used for design and calculation purposes [Ref. 6]. Upon cavitation, the water pressure rises to the vapor pressure of water, approximately 0.3 psi. This cavitated region created

by the rarefaction wave is known as the bulk cavitation zone. It consists of an upper and lower boundary and its extent is dependent on the charge size, type, and depth.

Figure 4 shows a typical bulk cavitation zone. The cavitation zone is symmetric about the y-axis in the figure; typically only one-half is shown due to the symmetry. The water particles behind the shock wave front at the time of cavitation have velocities depending on their location relative to the charge and the free surface. Water particles near the free surface, for example, will have a primarily vertical velocity at cavitation. As the reflected wave passes, the particles will be acted upon by gravity and atmospheric pressure.

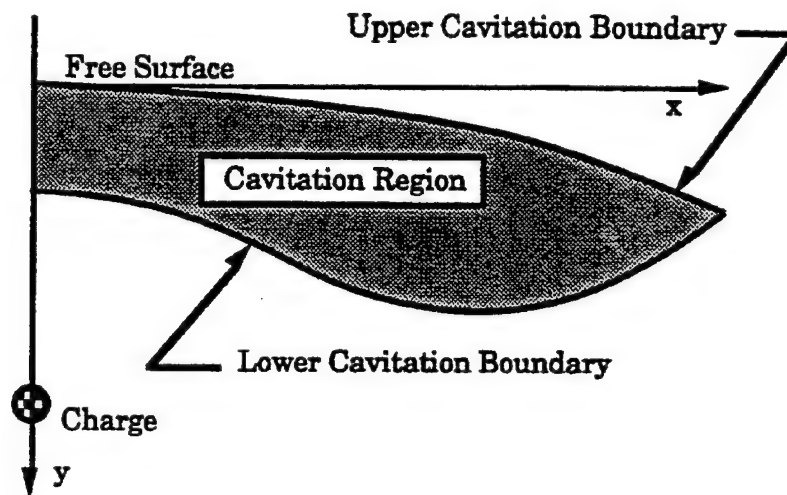


Figure 4. Bulk Cavitation Zone [Ref. 6]

The upper cavitation boundary is the set of points where the rarefaction wave passes and reduces the absolute pressure to zero or a negative value. The region will remain cavitated as long as the pressure remains below the vapor pressure. The total or absolute pressure which determines the upper boundary is a combination of atmospheric pressure, hydrostatic pressure, incident shock wave pressure, and rarefaction wave pressure.

The lower cavitation boundary is determined by equating the decay rate of the breaking pressure to the decay rate of the total absolute pressure. The breaking pressure is the rarefaction wave pressure that reduces a particular location of a fluid to the point of

cavitation pressure, or zero psi.

The upper and lower cavitation boundaries can be calculated from Equations (2.20) and (2.21), respectively [Ref. 10]. Any point which satisfies $F(x,y)$ and $G(x,y) = 0$ determines the bulk cavitation boundary.

$$F(x,y) = K_1 \left(\frac{W^{\frac{1}{3}}}{r_1} \right)^{A_1} e^{\frac{(r_2-r_1)}{\theta}} + P_A + \gamma y - K_1 \left(\frac{W^{\frac{1}{3}}}{r_2} \right)^{A_1} \quad (2.20)$$

$$G(x,y) = -\frac{P_i}{C\theta} \left\{ 1 + \left[\frac{r_2 - 2D \left(\frac{D+y}{r_2} \right)}{r_1} \right] \left[\frac{A_2 r_2}{r_1} - A_2 - 1 \right] \right\} - \frac{A_1 P_i}{r_1^2} \left[r_2 - 2D \left(\frac{D+y}{r_2} \right) \right] + \gamma \left(\frac{D+y}{r_2} \right) + \frac{A_1}{r_2} (P_i + P_a + \gamma y) \quad (2.21)$$

The variables in Equations (2.20) and (2.21) are:

$$r_1 = \sqrt{(D-y)^2 + x^2}$$

$$r_2 = \sqrt{(D+y)^2 + x^2}$$

x, y = horizontal range and vertical depth of the point

r_1 = standoff distance from the charge to the point

r_2 = standoff distance from the image charge to the point

C = acoustic velocity in the water

D = charge depth

θ = decay constant

γ = weight density of water

P_A = atmospheric pressure

W = charge weight

$P_i = P(t)$, Equation (2.1)

θ = Equation (2.3)

K_1, A_1 = shock wave parameters

Figure 5 shows the charge geometry for the above two equations.

Appendix A provides a MATLAB m-file [Ref. 11] that calculates and plots the bulk cavitation zone for a user supplied charge weight (of HBX-1) and depth by solving Equations (2.20) and (2.21). Figure 6 provides an example of cavitation curves generated using the program for two different charge weights at three different depths.

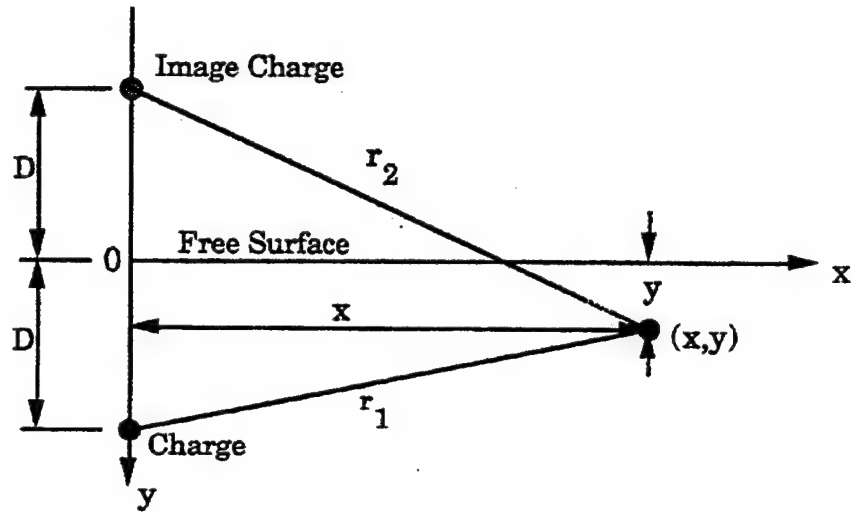


Figure 5. Charge Geometry for Bulk Cavitation Equations [Ref. 6]

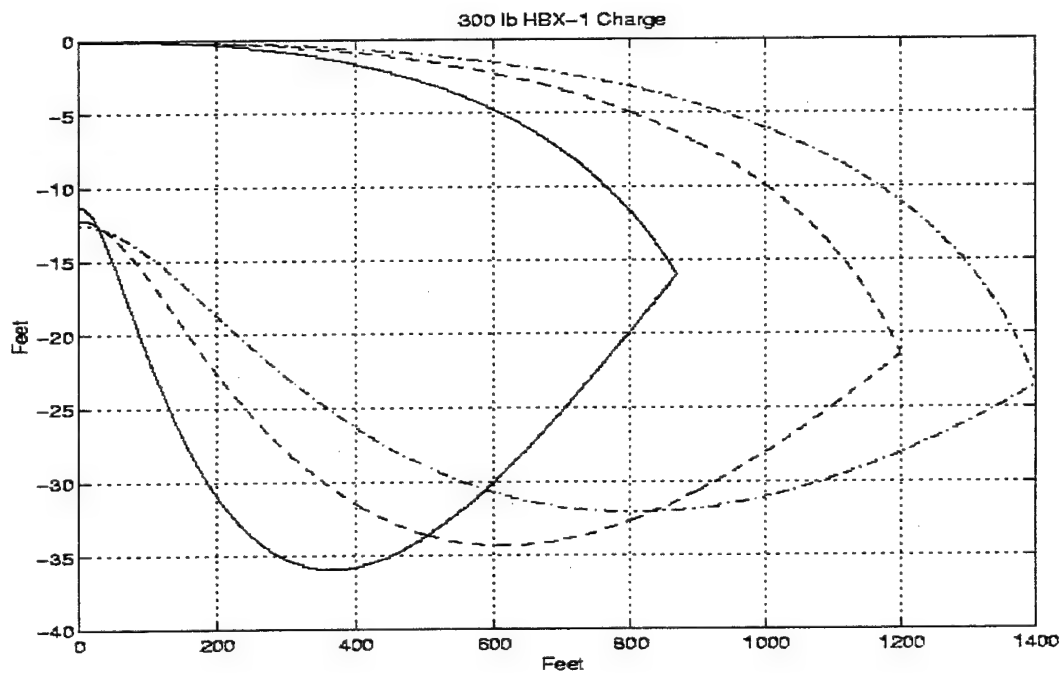
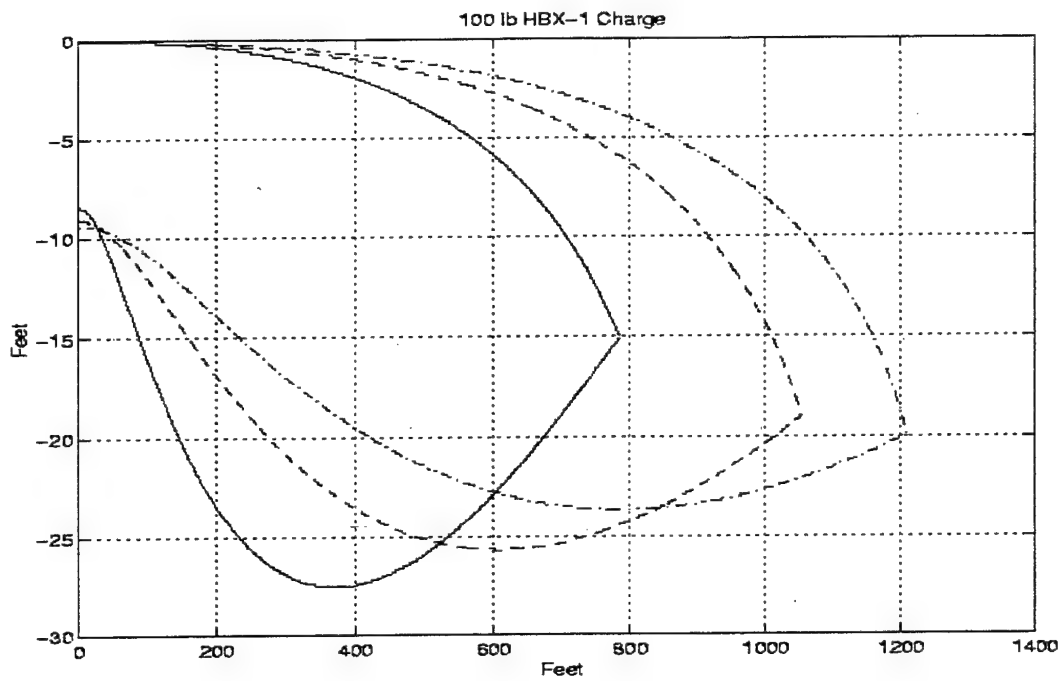


Figure 6. Bulk Cavitation Zones for HBX-1 Charges at the Following Depths:
- 50ft, - 100ft, -. 150ft

III. MODELING AND SIMULATION

The modeling and simulation process involves model construction, pre-processing, analysis and solution, and finally post-processing of the results. Figure 7 shows a flowchart of the procedure and the computer codes utilized.

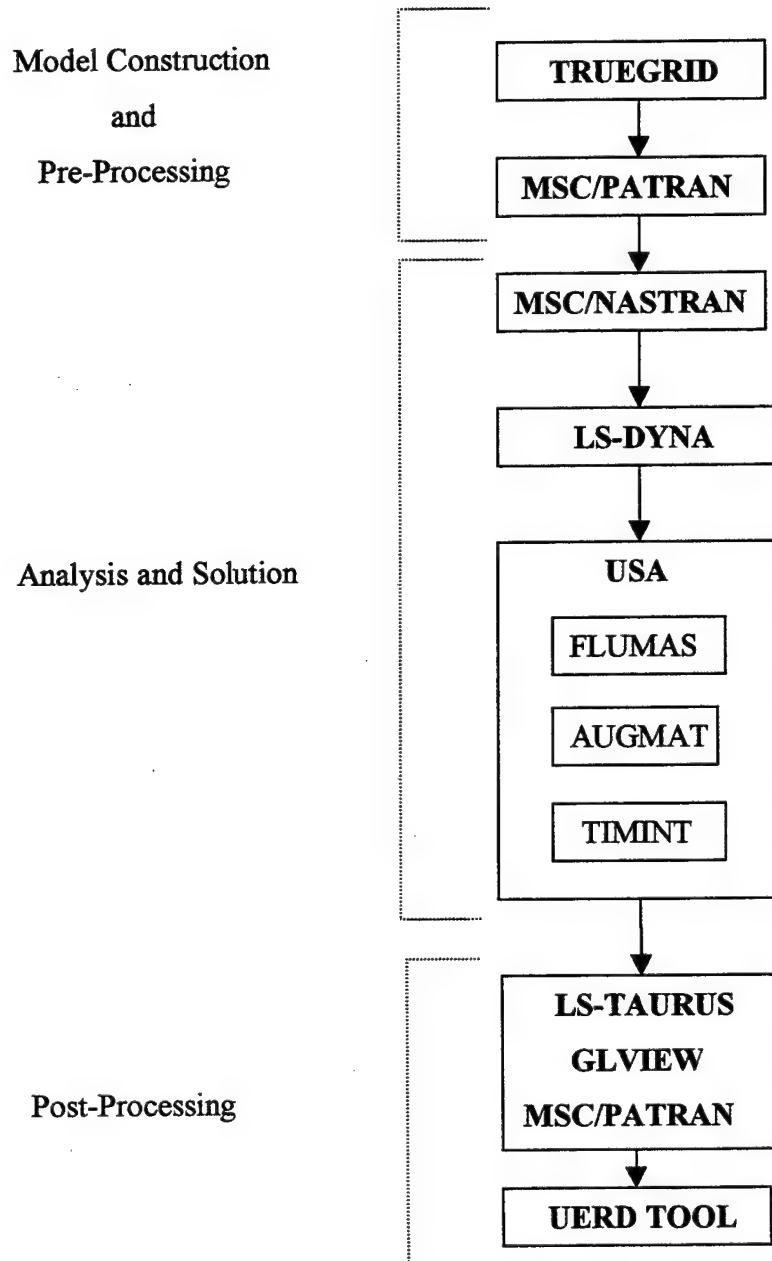


Figure 7. Modeling and Simulation Flow Chart

A. MODEL CONSTRUCTION AND PRE-PROCESSING

1. Three Dimensional Structural Model

The ship-like box model used for the ship shock simulation was constructed using a finite element mesh generation program called TrueGrid [Ref. 12]. The model is based on one used in a previous study [Ref. 13].

The model constructed simulates the structure of a typical ship, albeit on a smaller scale. The model consists of two bulkheads, a fully "stiffened" mesh, and a keel. The model is 120-in long, 24-in wide, and 24-in deep. The model was weighted with four lumped masses ($0.138\text{-lbf s}^2/\text{in}^4$) evenly spaced (to ensure the center of gravity remained on the centerline) along the keel to place the waterline at 12-in (halfway up the side). The shell plating was constructed of $\frac{1}{4}$ -in steel having a weight density of 0.284 lbf/in^3 , a Young's Modulus of 30×10^6 psi, and a Poisson's ratio of 0.3. The stiffeners and keel were constructed of the same material. The stiffeners and keel were added to increase the plating rigidity. These beams are of rectangular cross section. The stiffeners are each 0.125-in wide by 2-in high and the keel is 0.25-in wide by 6-in high. The overall finite element mesh consists of 386 nodes, 378 quadrilateral (4-noded) shell elements, 615 beam elements, and four point elements (used placement of the lumped masses). Table 1 and Figure 8 summarize the model particulars. Figure 9 shows the overall finite element model and Figure 10 shows the beam elements.

After the structural finite element mesh was generated in TrueGrid, it was output in MSC/NASTRAN input file format [Ref. 14]. This format was then read into an MSC/PATRAN database. MSC/PATRAN is a finite element mesh generator and visualization program [Ref. 15]. PATRAN was used to set up the model for a normal modal analysis to be conducted using NASTRAN. The modal analysis is performed to ensure a correct dynamic response of the model and to obtain the natural frequencies of the structure to be used later for addition of Rayleigh Damping to the model. The modal response also provides a useful tool for predicting the model response due to an UNDEX pressure wave. PATRAN was then used for three-dimensional visualization of the modal

analysis response. Appendix B details some help features in PATRAN for model manipulation.

Length	120-in
Beam	24-in
Depth	24-in
Design Waterline	12-in
Plating/Stiffener Material	Steel
Plating Thickness	1/4-in
Stiffener Dimensions	0.125-in x 2-in
Keel Dimensions	0.25-in x 6-in
Nodes	386
Shell Elements	378
Beam Elements	615
Point Elements	4

Table 1. Model Specifications

2. Three-Dimensional Fluid Modeling

The next step in the model construction process was the design of the fluid mesh. TrueGrid's element extrusion feature was utilized to build this mesh. Appendix C describes the extrusion feature in detail. The fluid mesh consists of 8-noded solid elements. LS-DYNA's Material Type 90 (acoustic pressure element) is used to model the pressure wave transmission properties of water [Ref. 16]. Figure 11 shows the fluid mesh designed for model. The extent (in the x and y directions) of this fluid mesh was set to five times the width of the model (120-in) and the depth of the mesh (under the keel) was set to twice the depth of the computed bulk cavitation zone, 140-in. (to be discussed later). This mesh contains 75344 8-noded elements and 81448 nodes. This fluid mesh shows how large and complex the mesh can be even for a relatively small structural model such as this one. Computational power is a must to run a ship shock simulation involving a fluid mesh.

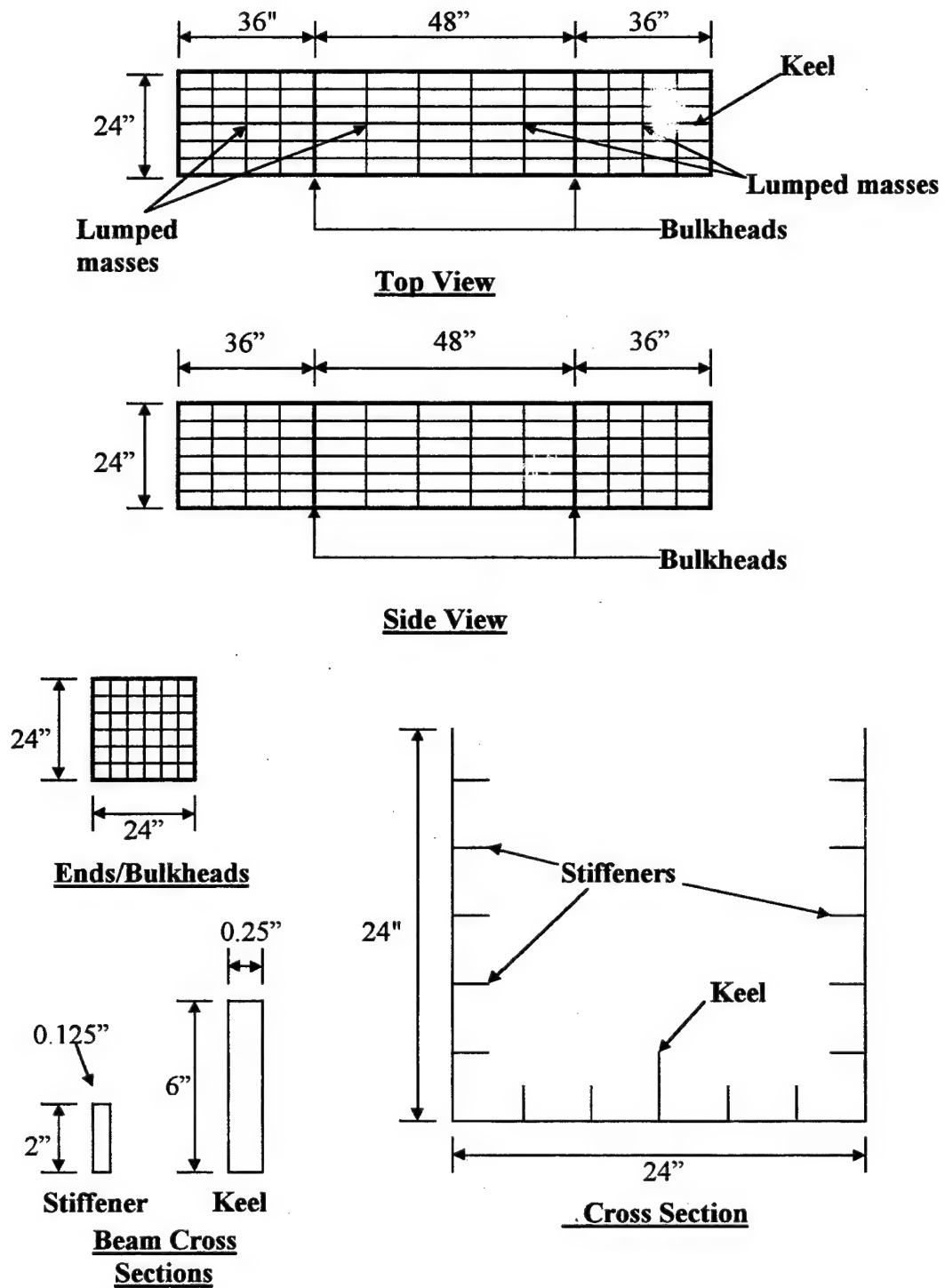


Figure 8. Model Specifications

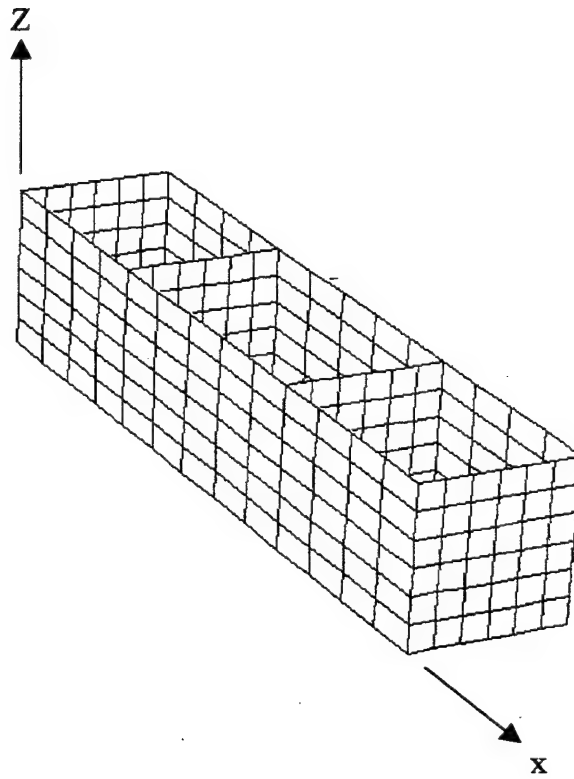


Figure 9. Finite Element Mesh

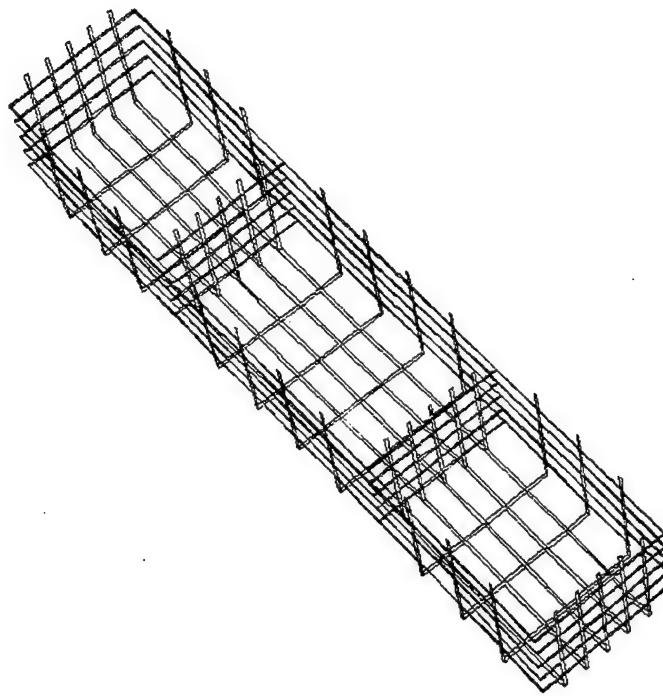


Figure 10. Beam Elements

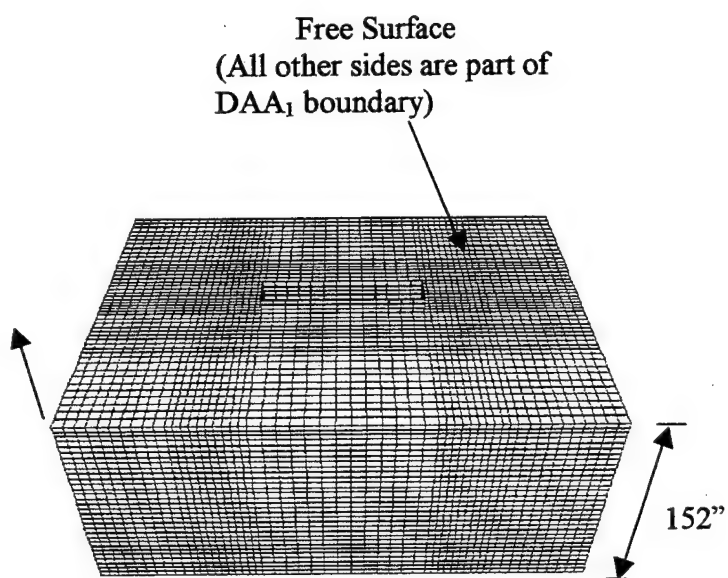
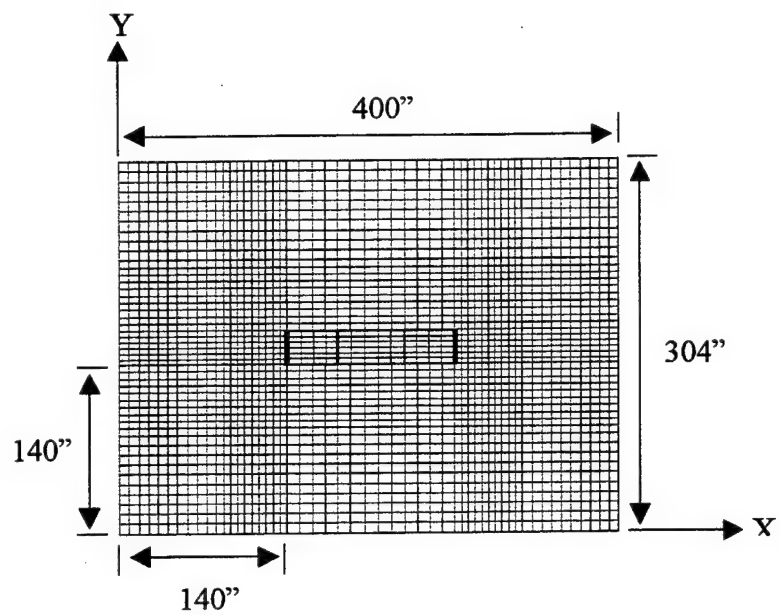


Figure 11. Three-Dimensional Fluid Mesh

An important feature of the fluid mesh is the element size next to the structural mesh. For the cavitation analysis using the USA code, the critical element size is determined by the following equation [Ref. 17]:

$$\frac{2\rho D}{\rho_s t_s} \leq 5 \quad (3.1)$$

where ρ = density of water, D = thickness of the fluid element in the direction normal to the wetted surface of the structure, ρ_s = density of the submerged structure, and t_s = thickness of the submerged structure. It can be shown for the ship-like box model that the critical element thickness, D , is 5 inches (using $\rho_s/\rho = 8$). The first ten element rows adjacent to the structural model were set equal to this value in thickness.

3. Two-Dimensional Model

From the above three-dimensional model, a two-dimensional model was created to perform the initial analysis work on and to verify correct behavior of the shock wave in the fluid mesh. The two-dimensional model basically consists of the "midships" section from the three dimensional model. The structural portion of the model contains only shell elements and the appropriate boundary conditions were applied to the axis of symmetry (the z-axis) to simulate the attachment of the rest of the model.

Figure 12 shows a two-dimensional model; here the lateral extent of the fluid mesh was set to ten times the width of the model (240-in) and the depth is 152-in. This model consists of approximately 4100 nodes and 1900 eight-noded elements.

B. ANALYSIS AND SOLUTION

The finite element model must be translated into LS-DYNA keyword format in order to perform the analysis since LS-DYNA/USA code is used. These two codes are coupled together. The USA code performs the bulk of the work (formulation of the fluid-structure interaction matrices) and LS-DYNA is utilized in performing the time integration solution for the structure. LS-DYNA is a non-linear three-dimensional structural analysis code [Ref. 16]. The USA code itself consists of three main modules: FLUMAS, AUGMAT, and TIMINT.

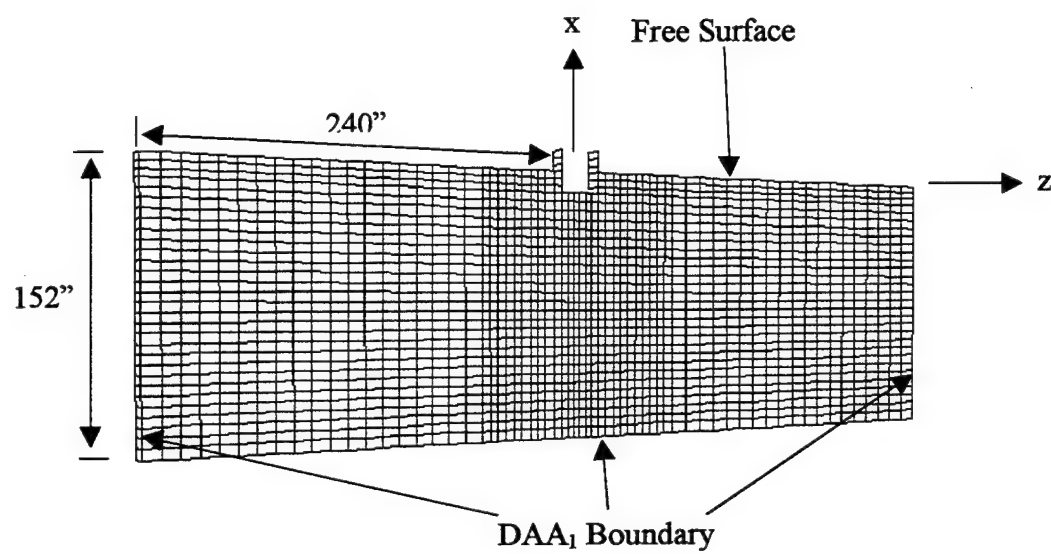


Figure 12. Two-Dimensional Model

FLUMAS is the first USA module to be run. FLUMAS generates the fluid mass matrix for the submerged portion of the structure [Ref. 18]. The fluid mesh data, as well as the transformation coefficients that relate both the structural and fluid degrees of freedom on the wetted surface are generated, including the nodal weights for the fluid element pressure forces and the direction cosines for the normal pressure force. The fluid area matrix is diagonal and the fluid mass matrix is fully symmetric.

AUGMAT is run second. This module takes the data generated by FLUMAS and LS-DYNA to construct the specific constants and arrays utilized in the staggered solution procedure for the actual transient response analysis [Ref. 18]. The augmented interaction equations are formed from Equations (2.10) and (2.11). These two equations may be solved simultaneously at each time step, but this solution method can be very computationally expensive. The USA code uses a staggered solution procedure to achieve an efficient solution. The staggered solution procedure is implemented as follows [Ref. 9]. First, it is assumed that $[M]$ is nonsingular. Equation (2.10) is partitioned to obtain $[G]^T \{\ddot{x}\}$, which is then substituted into Equation (2.11). This result is then pre-multiplied by $[A_f][M_f]^{-1}$ to yield

$$[A_f]\{\dot{p}_s\} + ([D_{f1}] + [D_s])\{p_s\} = -\rho c[A_f][G]^T[M]^{-1}([C]\{\dot{x}\} + [K]\{x\}) - [D_s]\{p_1\} - \rho c[A_f]\{\dot{u}_f\} \quad (3.2)$$

where

$$[D_{f1}] = \rho c[A_f][M_f]^{-1}[A_f]$$

$$[D_s] = \rho c[A_f][G]^T[M]^{-1}[G][A_f]$$

The above process is known as augmentation and achieves unconditional stability (for the fluid governing equation solution) without making any approximations to the coupled system equations [Ref. 9]. Equation (2.10) and (3.2) are known as the augmented interaction equations. The fluid mass matrix inverse is in lower triangular form and the structural mass matrix inverse is in lower skyline form. Within this module is where the type of DAA to be used is specified. If the DAA boundary is to be on the wetted surface of the structural model, then a DAA₁ or a DAA₂ may be used. If fluid volume elements are utilized, then only a DAA₁ may be used.

TIMINT performs the direct numerical time integration and also handles the computation of the UNDEX parameters, such as the shock wave pressure profile. The structural response and fluid response equations are solved separately at each time step through the extrapolation of the coupling terms for the two systems. LS-DYNA is used to solve the structural equations and TIMINT handles the fluid equations. A result of using the aforementioned staggered solution procedure is that LS-DYNA and TIMINT can each have a different time step assigned. Although in practice it is best to set the LS-DYNA and TIMINT timesteps to the same value or at least within an order of magnitude of one another. Despite using an unconditionally stable solution scheme, the TIMINT timestep must be set small enough to accurately capture the fluid system response. It should also be noted that LS-DYNA uses a central difference integration method that is conditionally stable. The LS-DYNA timestep must be set equal to or less than the critical timestep for the structural finite element mesh or numerical instability will result. Overall, this step of the solution procedure is the most time consuming and computationally expensive.

Appendix D provides example input decks for each of the three USA modules for both the DAA on the wetted surface and on the fluid mesh for the two and three dimensional models, as well as example LS-DYNA KEYWORD input decks.

1. Test Description

Two different attack geometries were used in the shock simulations run during this study. The main factor in determining the test geometry was a "reasonably" sized (with respect to depth) bulk cavitation zone. Reasonable here means as compared to the model size.

A charge consisting of 20 lb. HBX-1 was decided upon to meet the above requirement. In one attack geometry the charge was placed offset from the center of the model's length (60-in.). The offset distance is 8.37-ft and the charge depth is 15.50-ft. The standoff distance is 16.75-ft and the angle of attack is 30°.

Figure 13 shows this attack geometry and Table 2 summarizes the UNDEX parameters of the explosion. The bulk cavitation zone was computed using the MATLAB

program in Appendix A and is included as Figure 14. The second attack geometry consisted of the same weight charge placed directly under the model at the same standoff distance (resulting in a charge depth of 17.75-ft). Figure 15 shows this geometry and Figure 16 shows the bulk cavitation zone for this configuration. The same parameters given in Table 2 for P_{\max} and θ apply since the standoff distance is the same. The bubble period and the maximum radius are also approximately the same (0.49 sec and 10.37-ft respectively).

C. POST-PROCESSING

The solution data is output in two main forms from the analysis: binary and ASCII. The binary data files created from the LS-DYNA/USA run contain the model's finite element response information. LS-TAURUS [Ref. 16] and Glview [Ref. 19] can both be used for three-dimensional response visualization. Both programs are quite powerful post-processors and have their individual advantages and disadvantages. Both Glview and TAURUS provide both powerful animation and image generation features; TAURUS has the added capability of extracting the ASCII solution data for a particular node for a particular component, such as x-velocity data, and writing it to a separate ASCII file. Appendix E provides some useful TAURUS commands for model post-processing.

This ASCII data can then be plotted and manipulated using UERD (Underwater Explosion Research Division) Tool. This program is a PC based plotting tool. It not only plots ASCII input files and provides standard graphing functions, but also provides a variety of data manipulation features, such as curve integration and derivation of shock spectra.

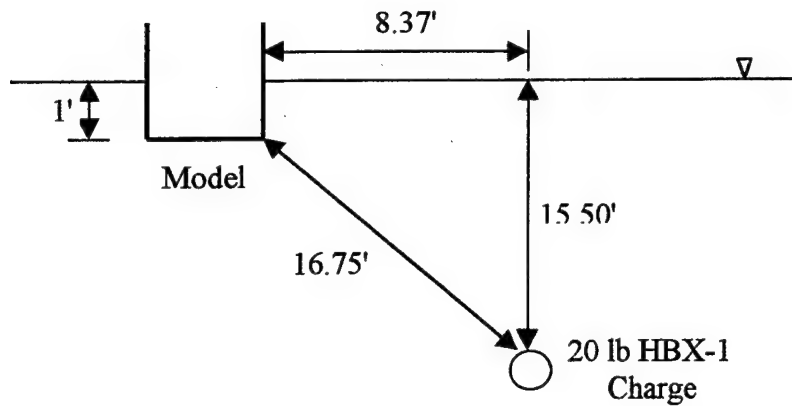


Figure 13. Offset Charge Test Geometry

P_{max}	2787 psi
θ	0.2383 msec
T	0.5 sec
A_{max}	10.52 ft

Table 2. UNDEX Parameters for Offset Charge

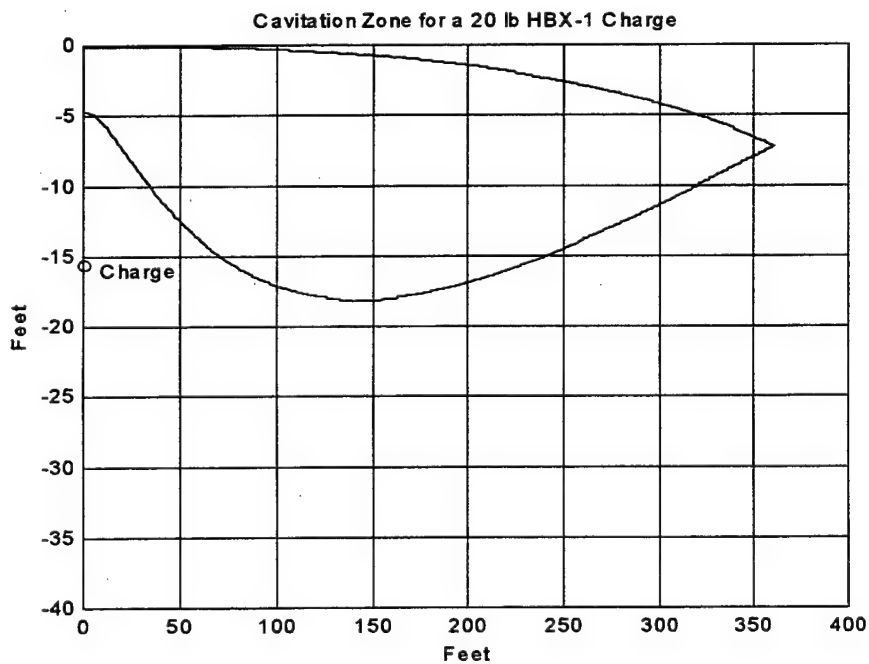


Figure 14. Bulk Cavitation Zone for 20 lb. Charge at 15.50-ft

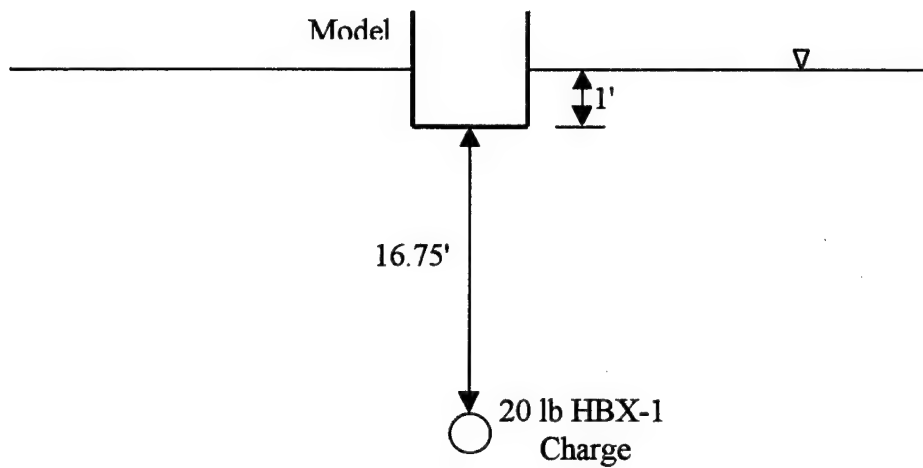


Figure 15. Charge Under Keel Test Geometry

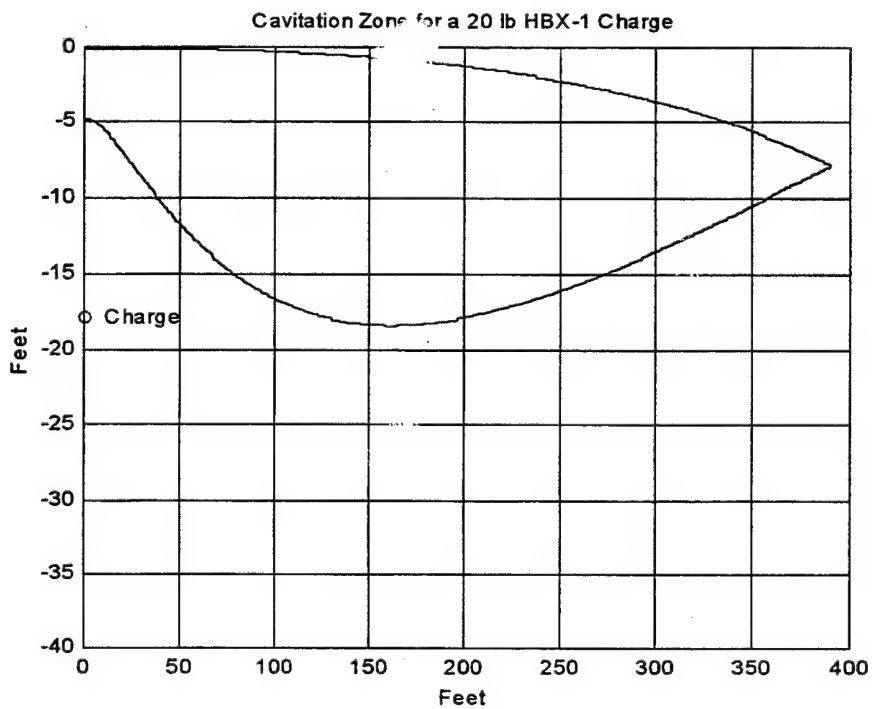


Figure 16. Bulk Cavitation Zone for a 20-lb. Charge at 17.75-ft

IV. SHOCK SIMULATION RESULTS

All of the ship shock simulations run using LS-DYNA/USA were made on an SGI Octane with two 195 MHz processors, 1.344 Gbytes of RAM, and 23 Gbytes of hard drive storage capacity. LS-DYNA version 940.1a and USA+ version 4 were the simulation codes.

A set of common node points was used for comparison between the different models used in the simulation. The velocity response was analyzed at these nodes. For the two-dimensional model, two nodes were selected for the response analysis: one on the centerline and one at the corner of the cross section. These nodes and their ID numbers are shown in Figure 17. For the three-dimensional model, a set of seven different nodes was analyzed. These nodes were located on the keel, sides, and on one bulkhead of the ship-like box model. Since the model is symmetric and the charge location is at the center of the model length, only the responses in one-half of the model need to be considered. Figure 18 provides a top view of the model with the keel output nodes labeled with their respective node ID numbers. Figure 19 is a side view of the model with the side output nodes identified. This is the starboard side, the same side as the charge. Figure 20 is a view of the bulkhead output node.

A. MODAL ANALYSIS

Prior to starting the underwater shock simulation analysis, a normal mode analysis was performed on the three-dimensional structural finite element model using MSC/NASTRAN. The modal analysis was performed in order to determine the mode shapes and corresponding frequencies of the model. Knowledge of the modal response enables predictions of the model response under a shock loading. The modal frequency values aid in determining how long the shock simulation must be run for in order to ensure the appropriate response frequency content is captured. Also, knowledge of the modal frequencies is crucial for determining Rayleigh Damping coefficients.

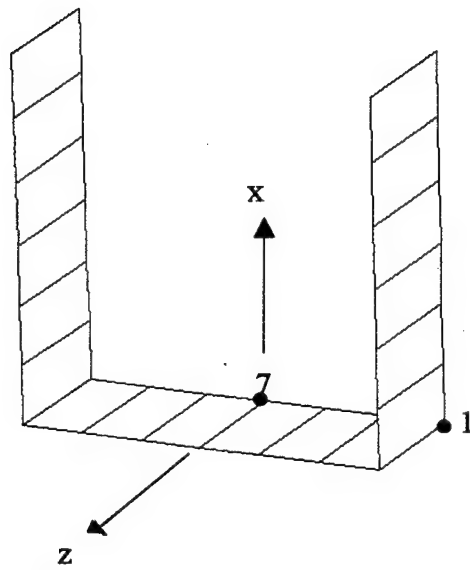


Figure 17. Two-Dimensional Model Output Nodes

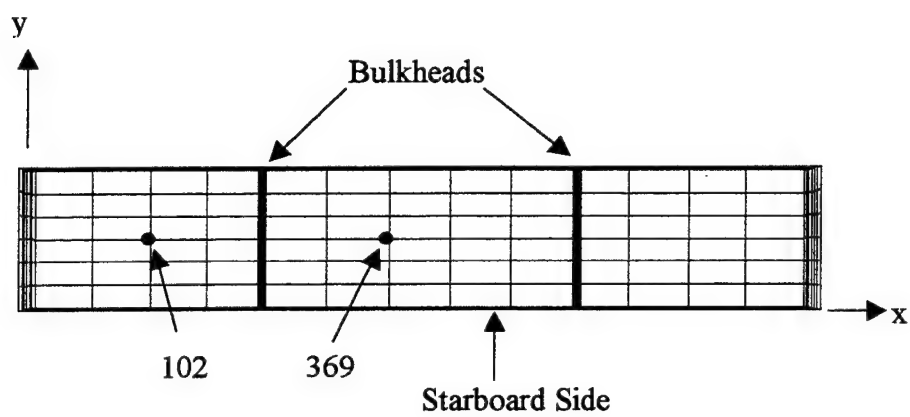


Figure 18. Keel Output Nodes (Top View)

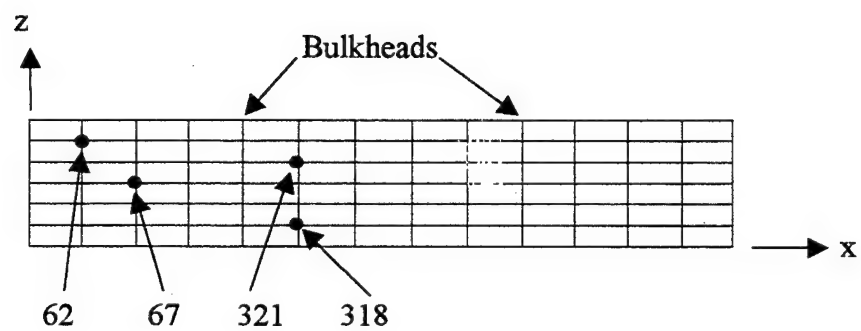


Figure 19. Side Output Nodes (Starboard Side)

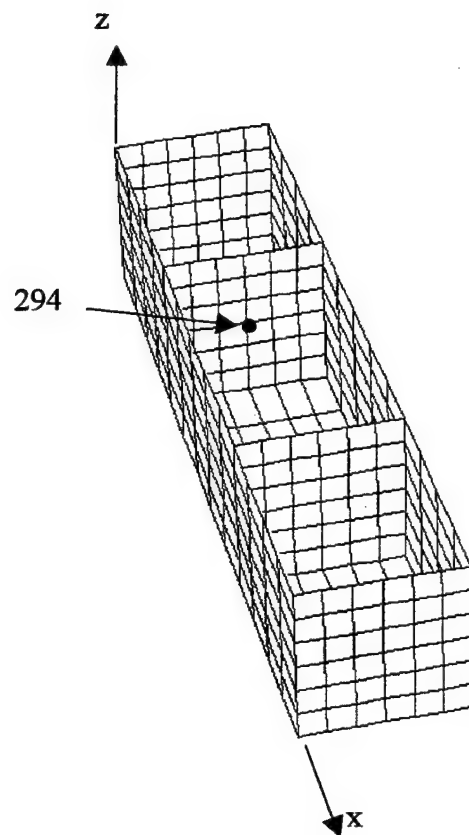


Figure 20. Bulkhead Output Node

For this model, it was determined that modes 7 through 11 were the dominant modes (the first six modes being rigid body modes). Mode 7 had a frequency of 48.317 Hz. Based on this value, it was determined that shock simulation runs of 30 ms should be sufficient to capture the model response. The modal frequencies for modes 8 through 11 are as follows (all values in Hz): 114.598, 132.71, 179.63, and 190.353. Figure 21 shows modes 7 through 11.

B. TWO-DIMENSIONAL MODEL

1. Charge Under Keel

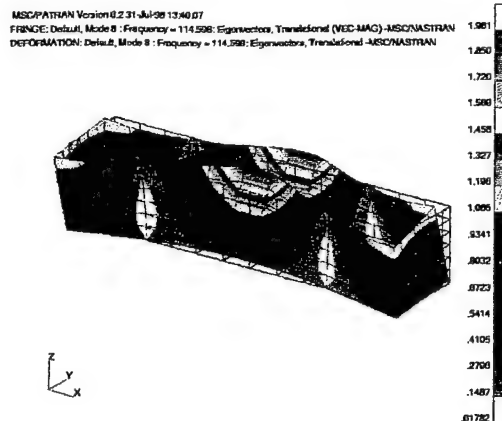
The DAA on the wetted surface case was examined first for this charge geometry. It must be emphasized that the DAA on the wet surface models is an ideal case and no cavitation effect can be taken into account. For output considerations, node 7 was examined. This node, as shown in Figure 17, is on the centerline of the structure. Vertical velocity was examined. As Figure 22 illustrates, the calculated response is as expected from the physics of the situation; the velocity increases rapidly to a peak value and then rapidly decreases and settles out quickly. The response will not and does not settle out at zero due to the rigid body motion of the structure.

The reason for the behavior of the structure is from the fact that the incident shock wave impacts the structure with a very high pressure (close to 2800 psi) at time zero and forces the structure rapidly upward. The structure is then quickly pulled back down as the shock wave reaches the free surface and a tensile reflected wave is generated. This wave causes the DAA boundary pressure to decrease rapidly, even going negative (the fluid pressure is allowed to go negative since no cavitation can be taken into account). This rapid decrease in pressure serves a type of vacuum to pull the structure back down, since the structure is coupled to the fluid through the DAA boundary. The DAA boundary simulates the mass of the surrounding fluid. The DAA pressure returns to zero once the reflected wave passes and the excitation of the structure ceases.

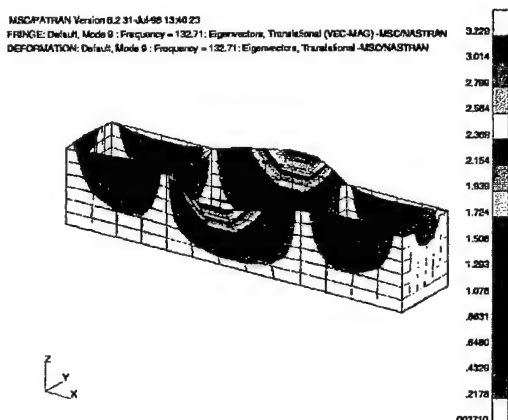
The effect of varying the axial width of the two-dimensional model was investigated next. The "basic" model started with an axial width of 9.6-inches. This is the



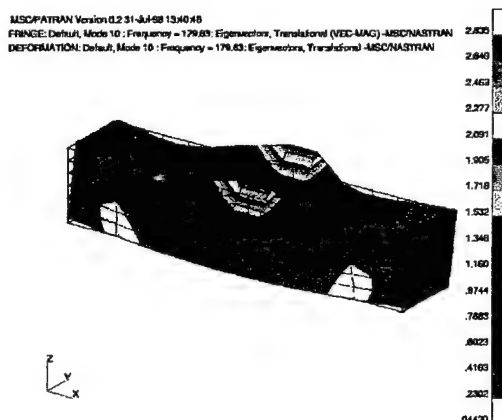
Mode 7



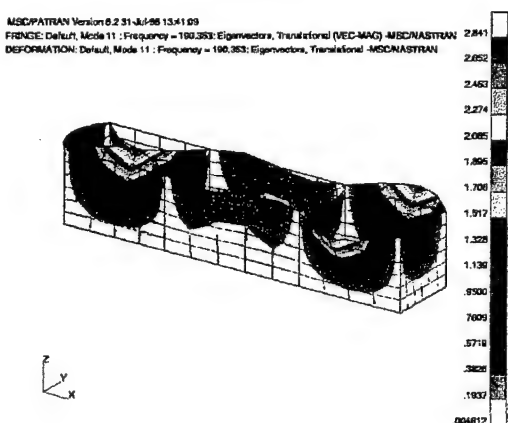
Mode 8



Mode 9



Mode 10



Mode 11

Mode	Frequency (Hz)
1 ~ 6	0 (Rigid Body)
7	48.317
8	114.598
9	132.71
10	179.63
11	190.353

Figure 21. Modes 7 Through 11

length of a midships section element from the three-dimensional model. The width was decreased to 0.1-inches and 0.01-inches to see if this thickness made a difference in the response. The reason for performing this study was based on experience with the infinite cylinder problem, where a thinner width yields more accurate results [Ref. 18]. The results showed that the responses had little variance between them. Due to timestep considerations, discussed below, the original 9.6-inch width was decided as being optimal for the case of the DAA on the wet surface. Figure 23 shows the comparison between the 9.6-inch width and the 0.1-inch width, and Figure 24 shows the comparison between the 0.1 and 0.01-inch widths. As can be seen on these two figures, the thinner shell width caused more high frequency content to show up in the velocity waveforms.

Decreasing the axial width also has the adverse effect of decreasing the LS-DYNA critical timestep size. The original mesh has a critical timestep size of approximately 10^{-5} . At a width of 0.1-inches the critical timestep is on the order of 10^{-7} and on the order of 10^{-8} for 0.01-inches of width. A decrease in critical timestep has an adverse effect on the computational time required for the solution.

The next parameter varied was the Geers modal coefficient (DAA2M in the AUGMAT input deck). This scalar coefficient is needed when using the modal form of the second order DAA formulation. This coefficient has a value between zero and one; there are no set guidelines for its application, only experience. It is known that a value of 0.5 works the best for an infinite cylinder and a value of 1 works best for a spherical shell. A value of zero reduces the solution to a first order DAA problem. It is known that this parameter does have a relationship with the diagonal local curvature matrix of the fluid. [Ref. 18]

Two values were investigated in this study, 0.5 and 0.68. The effect of varying this coefficient was found to be minimal on this particular problem. A value of 0.5 was used for all subsequent simulations and unless otherwise noted, all DAA on the wet surface simulations use this value.

Shock simulations were carried out next with the fluid mesh surrounding the structure. The mesh used is shown in Figure 12. The fluid mesh depth was set to a value

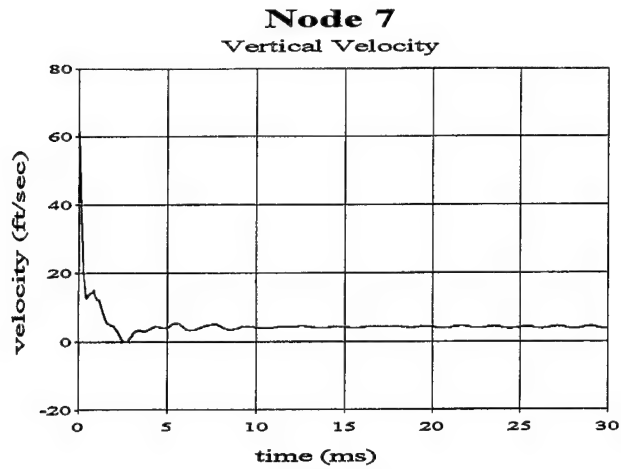


Figure 22. 2-D Model w/Charge Under Keel (DAA on Wet Surface)

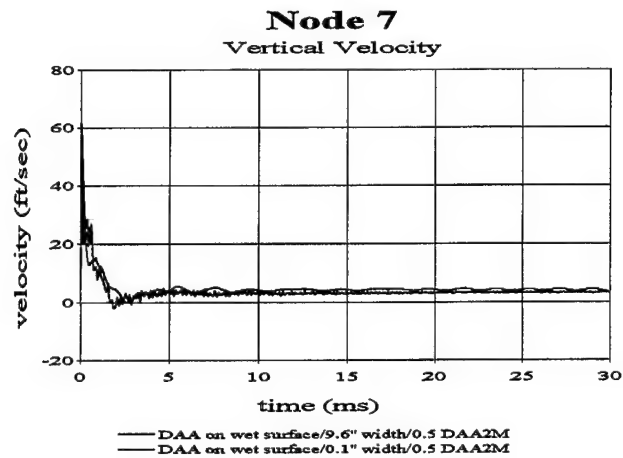


Figure 23. 2-D Model w/Charge Under Keel (DAA on Wet Surface)

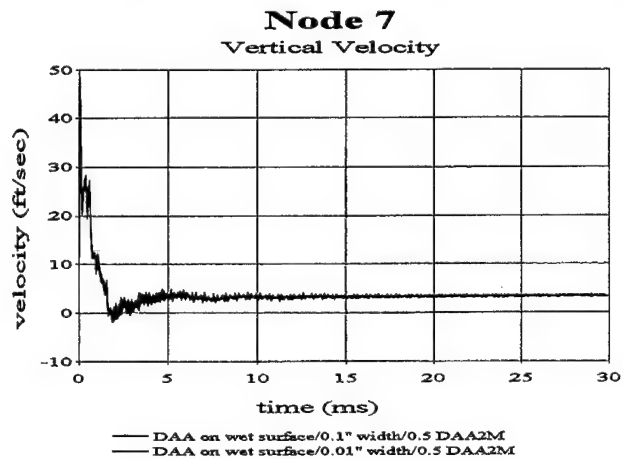


Figure 24. 2-D Model w/Charge Under Keel (DAA on Wet Surface)

of approximately twice the cavitation depth calculated. This is because the calculated depth is based on empirical equations and the actual depth will vary from this ideal value. It is not desirable to have the cavitation "hit" the lower DAA boundary; this could lead to inaccurate results from the simulation. The first order DAA boundary is placed on the exterior sides of the fluid mesh (except for the free surface). The terminology used henceforth to refer to this boundary is: DAA on the fluid mesh.

The LS-DYNA acoustic pressure element has a damping value that can be set. This value is an artificial viscosity and ranges in value from 0.1 to 1. It is used to smooth out discontinuities in the pressure waveform but it does not alter the characteristics of the wave. A value of 0.5 was used in all simulations.

Cavitation may be turned on and off by toggling a flag on the acoustic element card. If the flag is off, cavitation will not occur and the element pressure is allowed to go negative. If the flag is on, the pressure will be cut-off at zero. When the pressure goes to zero, this is a sign of cavitation occurring. This must be used with caution and a realization of the physics of the situation (i.e. time of zero pressure and location of the element considered). The element pressure may go to zero due to the pressure merely decaying away. A sharp drop in the pressure to zero is usually a sign of cavitation.

The same parametric study conducted on the DAA on the wet surface case was conducted on the DAA on the fluid case (with the exception of the modal coefficient, which does not apply to a first order DAA boundary). Figure 26 and Figure 27 apply. It was found here also that the 9.6-inch axial width was the best. The velocity response waveform exhibits better decay with this width than with the 0.1 or 0.01-inch widths. These studies were done with the cavitation flag off. There is also very little difference between the 0.1 and 0.01-inch widths (as was found early with the structure only).

The DAA on the fluid mesh results, with the cavitation flag off (cav off in the figure legends), were compared with the DAA on the wetted surface case. Figure 28 shows this comparison. The basic physics explained for the DAA on the wet surface case still apply, except the response is different due to the fluid mass being different from what the DAA on the wet surface calculates. The results seem to correlate fairly well in that the trend is the same. The resulting waveform is more oscillatory in nature, but it

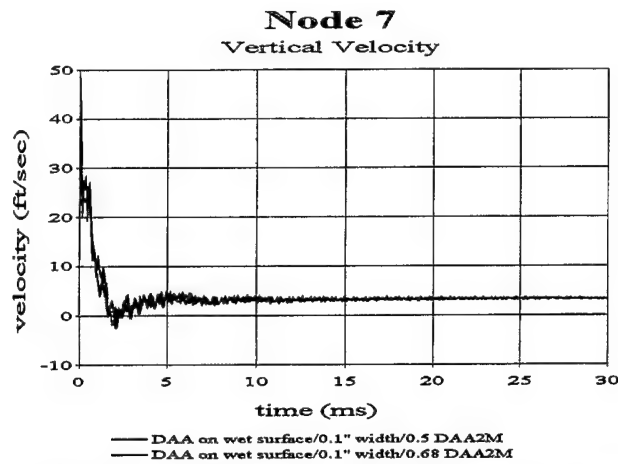


Figure 25. 2-D Model w/Charge Under Keel (DAA on Wet Surface)

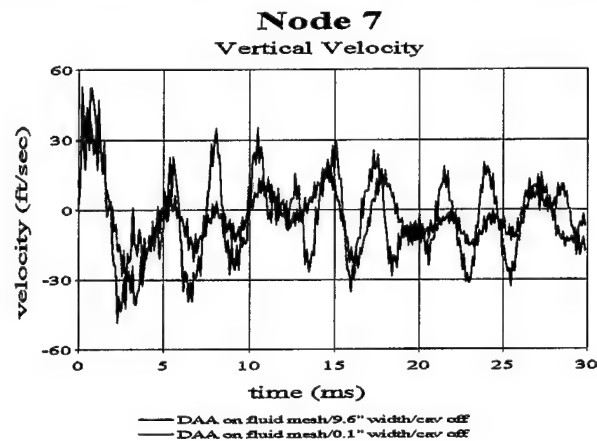


Figure 26. 2-D Model w/Charge Under Keel (DAA on Fluid Mesh)

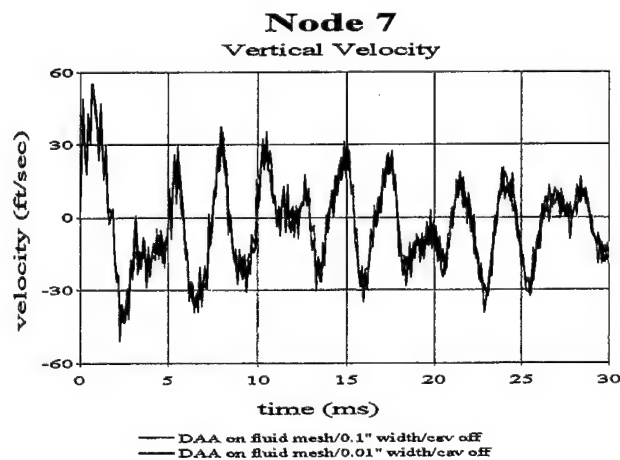


Figure 27. 2-D Model w/Charge Under Keel (DAA on Fluid Mesh)

does decay over the time of the simulation. The DAA on fluid mesh velocity waveform also has a much higher frequency content. This high frequency content can be removed by means of a low-pass filter, however one must be careful not to destroy the original shape of the response by over-filtering. The slope of the initial velocity peak matches very well with the DAA on the wetted surface case; the initial peak is at a slightly lower value however.

Once the cavitation flag is turned on (cav on in the figure legends), the response of the model is much different, as shown in Figure 29. Cavitation has a very significant effect on the response for the two-dimensional model. The initial slope is the same as the DAA on the fluid mesh/cavitation off case, but the velocity continues to increase and stays positive much longer than the previous cases. The reason for this trend is that the cavitation of the fluid allows the structure to "break free" of the fluid due to the lowered pressure region (the surface tension of the fluid goes to zero during the cavitation). This changes the entire response of the structure.

The pressure of the top, middle, and bottom of the fluid mesh underneath of the structural model was examined (with cavitation flag on). These pressure plots are included in Figure 30 and are element pressures taken directly below the structure. Cavitation can be seen to occur almost immediately underneath of the model (top of fluid mesh). It occurs later, and only for a few intermittent times, in the middle and not at all at the bottom of the mesh (as is desired). The pressure decay to zero between one and two milliseconds at the bottom of the mesh is not cavitation. This is because the rarefaction wave could not have reached the bottom of the mesh at this early time. Based on the distance traveled it arrives after 2 ms. This extent of the cavitation zone agrees with the predicted zone shown in Figure 16.

Figure 31 and Figure 32 show images of the shock wave propagation during the first two milliseconds of the simulation. The set-up of the initial shock wave can be observed and its subsequent propagation. The wave is initialized to be one fluid element away from the structure at time zero. The reflected wave can clearly be seen as can the subsequent formation of the cavitation zone. The DAA boundary shows no reflection of the pressure waves. These images were generated using LS-TAURUS.

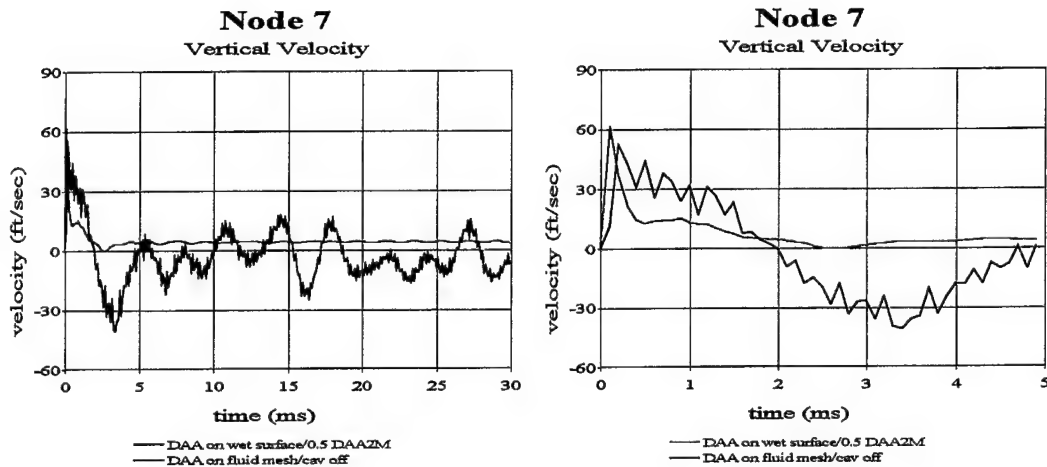


Figure 28. 2-D Model w/Charge Under Keel Response Comparison (Cavitation Off)

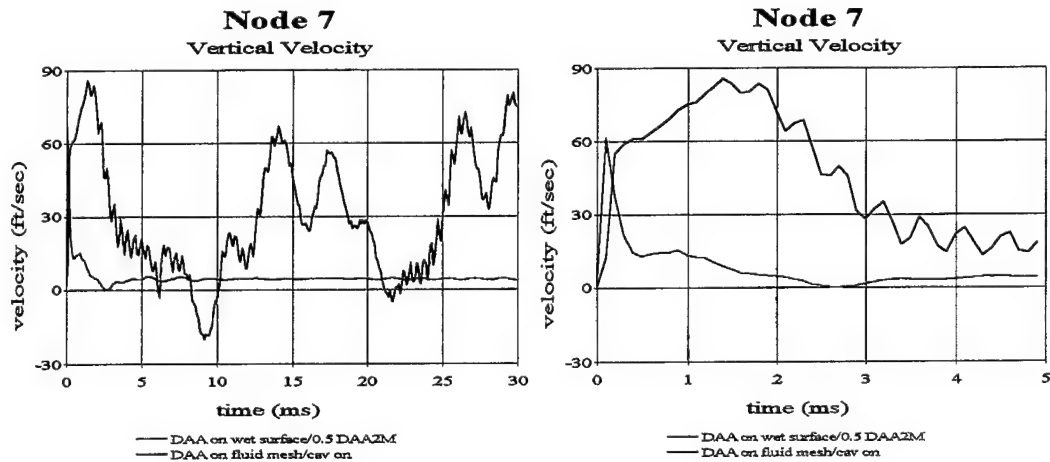


Figure 29. 2-D Model w/Charge Under Keel Response Comparison (Cavitation On)

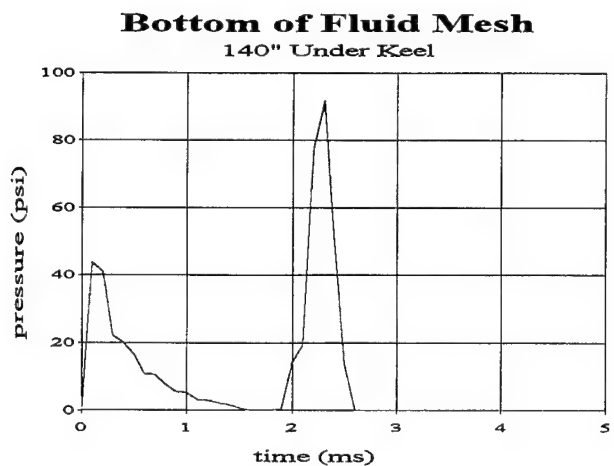
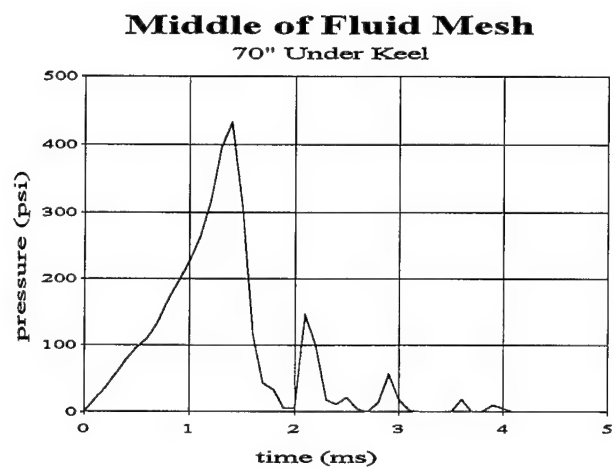
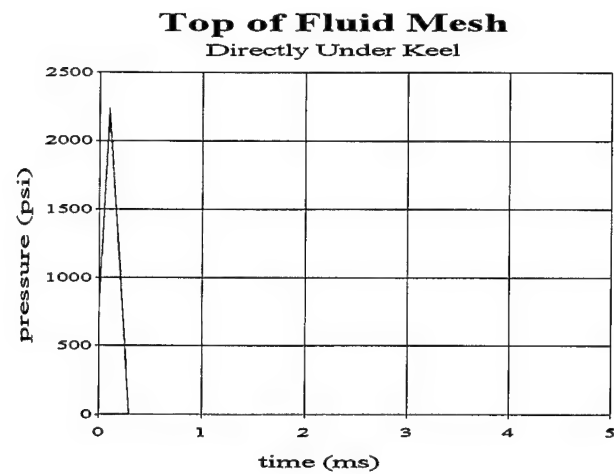
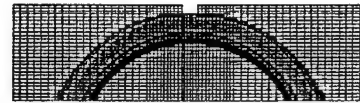


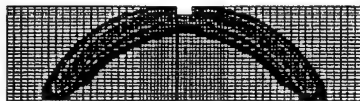
Figure 30. 2-D Model w/Charge Under Keel Fluid Mesh Pressure Profiles

Color Fringe Key
Pressure Magnitudes in psi

□	0
■	167
■	333
■	500
■	667
□	833
■	1000



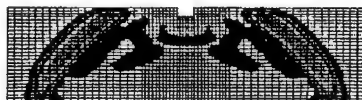
0 ms



0.25 ms



0.50 ms

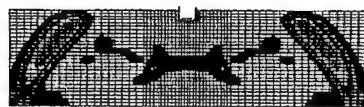


0.75 ms



1.0 ms

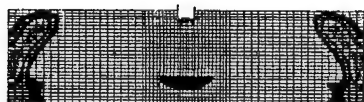
Figure 31. 2-D Model w/Charge Under Keel Shock Wave Propagation



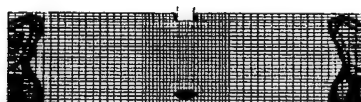
1.25 ms



1.50 ms



1.75 ms



2.0 ms

Figure 32. 2-D Model w/Charge Under Keel Shock Wave Propagation (Continued)

2. Charge Offset

Shock simulations were next conducted using the offset charge geometry shown in Figure 13. Since the parametric studies were previously conducted, they were not repeated for this case. The corner node of the structure (node 1) was considered in addition to the centerline or keel node. The vertical velocity was examined as before. Node 1 is the structural node closest to the charge (i.e. where the shock wave will impact the structure first).

For the case of the DAA on the wet surface, the response is as expected for both nodes 1 and 7; their response is basically the same as the charge under the keel case as shown in Figure 33 for node 1 and Figure 34 for node 7. With the addition the fluid mesh however, Node 1's response has significant differences however between the DAA on the wet surface and DAA on the fluid mesh as shown in Figure 35.

The response of node 7 with the fluid mesh included (cavitation off) follows that of the previous charge geometry (Figure 36). A major difference is the DAA on the fluid mesh peak velocity value is higher than the DAA on the wet surface case for this node. The fluid mesh velocity response also has less frequency content (less jaggging of waveform) than the charge under geometry. This is due to the structure acting as a filter on the pressure wave prior to it reaching this point in the structure.

The effect of cavitation is again very significant, with the peak nodal velocity increasing to almost double its previously calculated values as illustrated in Figure 37 and Figure 38. Node 1 experiences a very high frequency oscillation due to the cavitation. The pressure plots in Figure 39 show the development of cavitation. The formation of cavitation is immediate directly under the structure. The middle of the fluid does not experience much, if any, cavitation. Some cavitation may form briefly after 3 ms, but it disappears quickly. This extent of the observed cavitation zone agrees well with the extent predicted in Figure 14, although possibly somewhat shallower. Figure 40 and Figure 41 illustrate the shock wave propagation through the fluid mesh. The development of the cavitation zone is not quite as clear as the charge under keel geometry and a moderate pressure region is observed to form on the right side of the fluid mesh near the bottom boundary. This pressure region is observed to expand and interact with the

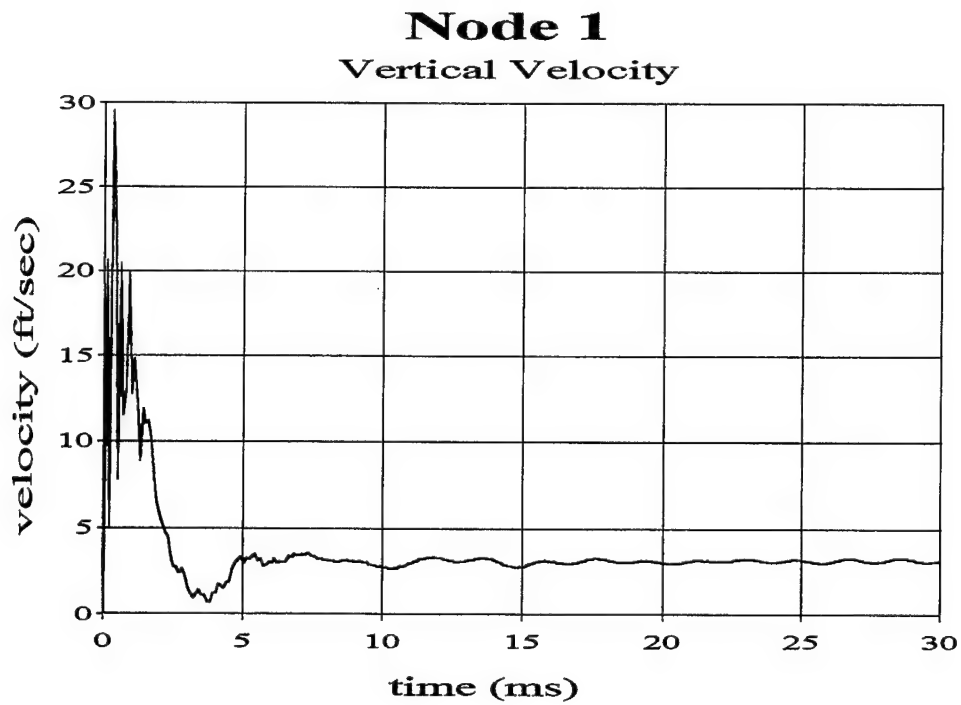


Figure 33. 2-D Model w/Offset Charge (DAA on Wet Surface)

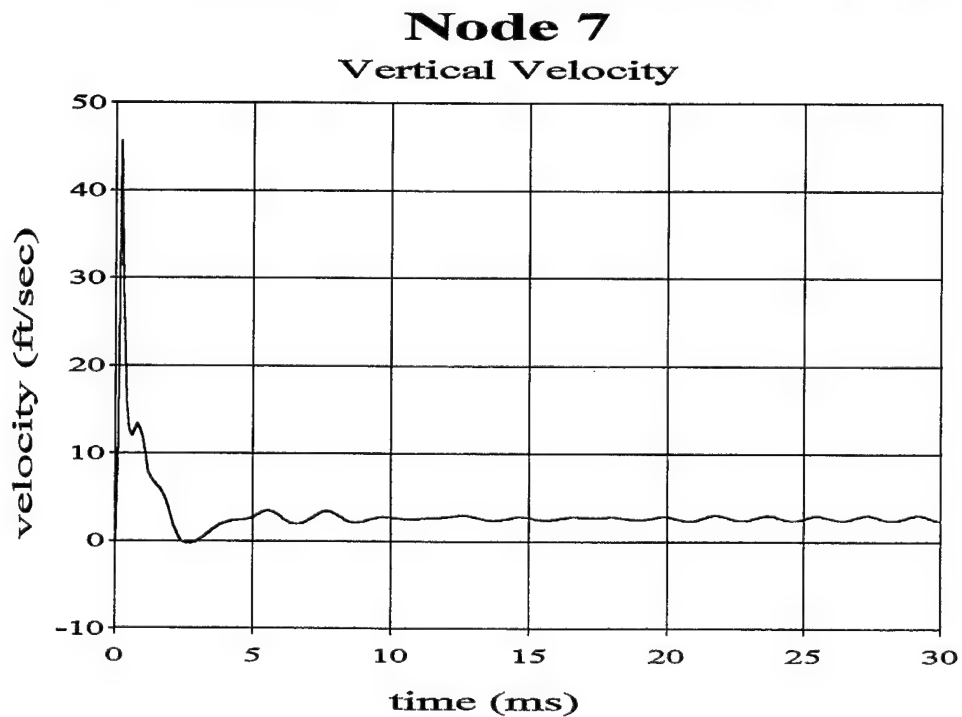


Figure 34. 2-D Model w/Offset Charge (DAA on Wet Surface)

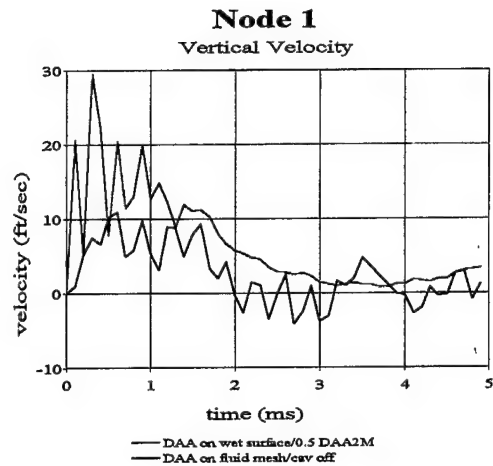
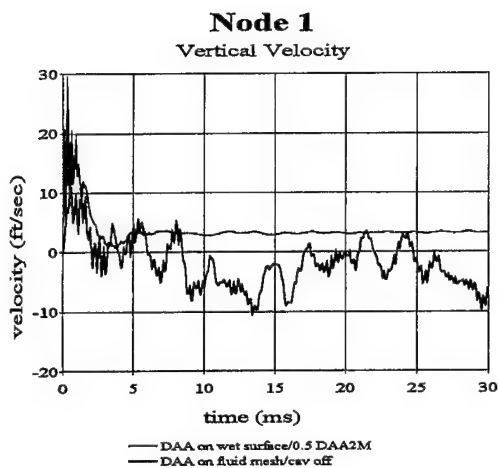


Figure 35. 2-D Model w/Offset Charge Response Comparison (Cavitation Off)

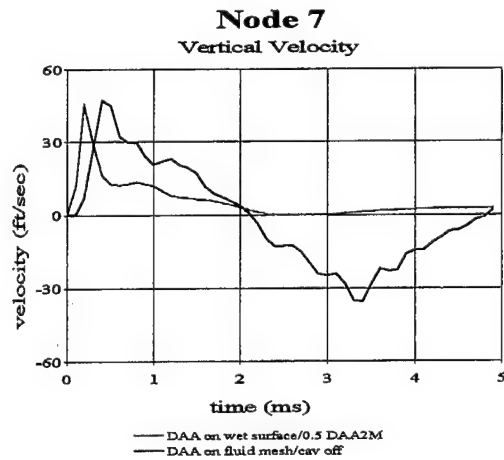
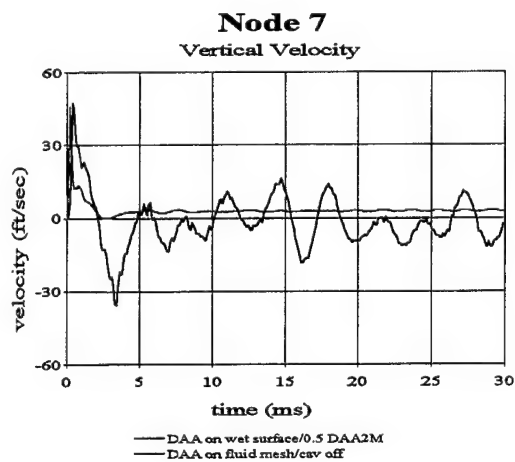


Figure 36. 2-D Model w/Offset Charge Response Comparison (Cavitation Off)

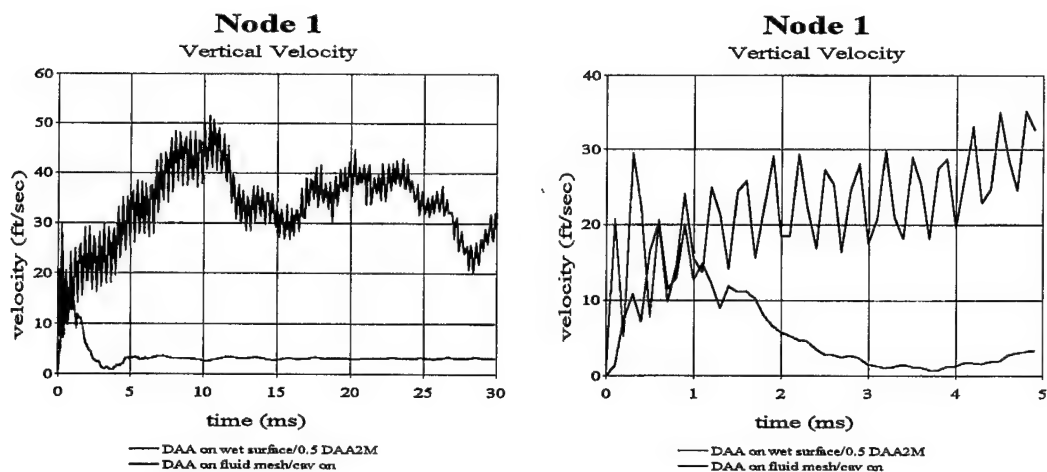


Figure 37. 2-D Model w/Offset Charge Response Comparison (Cavitation On)

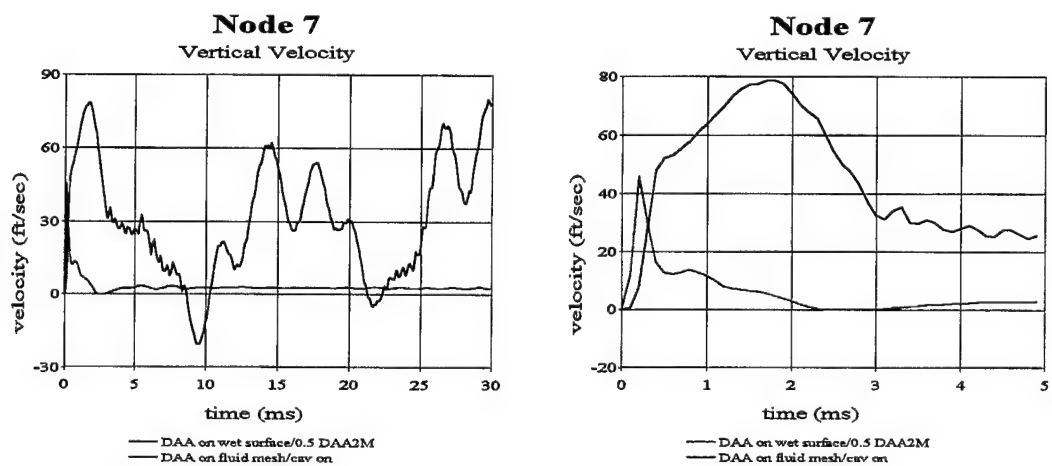


Figure 38. 2-D Model w/Offset Charge Response Comparison (Cavitation On)

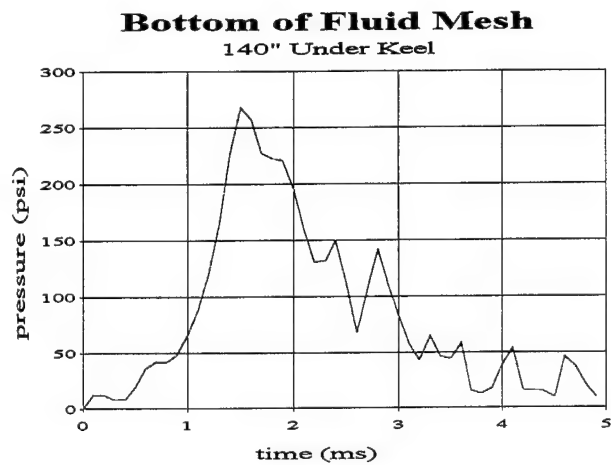
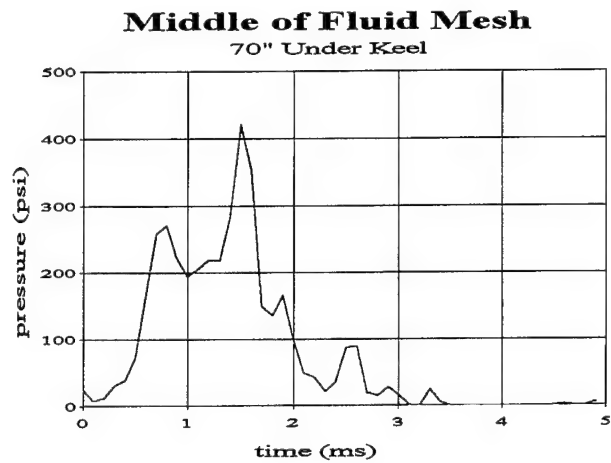
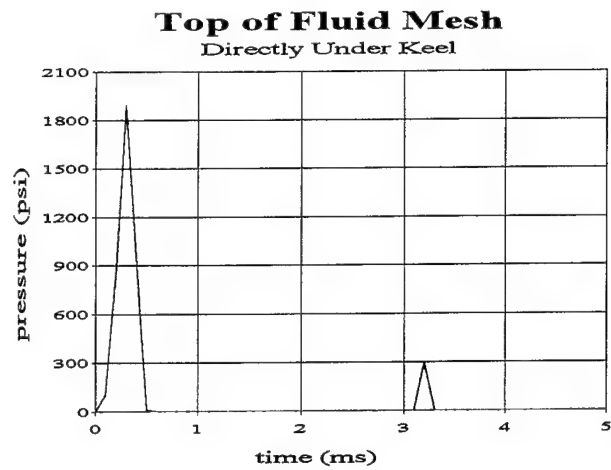


Figure 39. 2-D Model w/Offset Charge Fluid Mesh Pressure Profiles

Color Fringe Key
Pressure Magnitudes in psi

□	0
■	167
■	333
■	500
■	667
□	833
■	1000



0 ms



0.25 ms



0.50 ms



0.75 ms



1.0 ms

Figure 40. 2-D Model w/Offset Charge Shock Wave Propagation



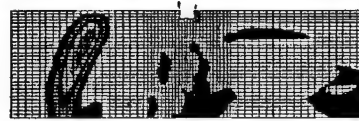
1.25 ms



1.50 ms



1.75 ms



2.0 ms

Figure 41. 2-D Model w/Offset Charge Shock Wave Propagation (Continued)

reflected wave. The reason for this pressure development and interaction is not understood. The gas bubble from the charge can be ruled out since the bubble grows at a very slow rate and its period is on the order of 500 ms for this charge geometry. This effect bears further investigation.

C. THREE-DIMENSIONAL MODEL

1. Charge Under Keel

The first case examined for the three-dimensional model was the charge under keel geometry. The same run sequence as the two-dimensional model was utilized; that is, the first case run was the DAA boundary on the structure wetted surface, then the DAA boundary on the exterior surface fluid mesh with the cavitation flag off was run, and finally the DAA on the fluid mesh with the cavitation flag on was simulated. The fluid model used for these simulations is shown in Figure 11. All three responses are plotted on one graph for ease of comparison. Figure 18, Figure 19, and Figure 20 apply for reference to the three-dimension model output node numbers and locations.

These simulations were run on the computer indicated at the beginning of this chapter. A total of 32 hours was required for FLUMAS to complete its computations. The TIMINT module took 12 hours to run (with a timestep of 10^{-5} utilized for both TIMINT and LS-DYNA; the simulations were run out to 30 ms). The AUGMAT module took only 35 seconds to run. The FLUMAS module is the most time consuming part of the simulation run. An increase or decrease in the size of the fluid mesh will impact this run time appropriately. The TIMINT time can be increased or decreased by a change in the timestep used (i.e. the DYNA critical timestep value).

The keel nodal responses (nodes 369 and 102) are plotted in Figure 42 and Figure 43. The case of the DAA on the wet surface response is very similar to that of the two-dimensional model (although a direct comparison cannot be made since the two-dimensional model is assumed to be infinite in the axis of symmetry directions). The point is the response follows correctly the physics of the situation as explained for the two-dimensional case. The response with the fluid mesh added (cavitation off case) is

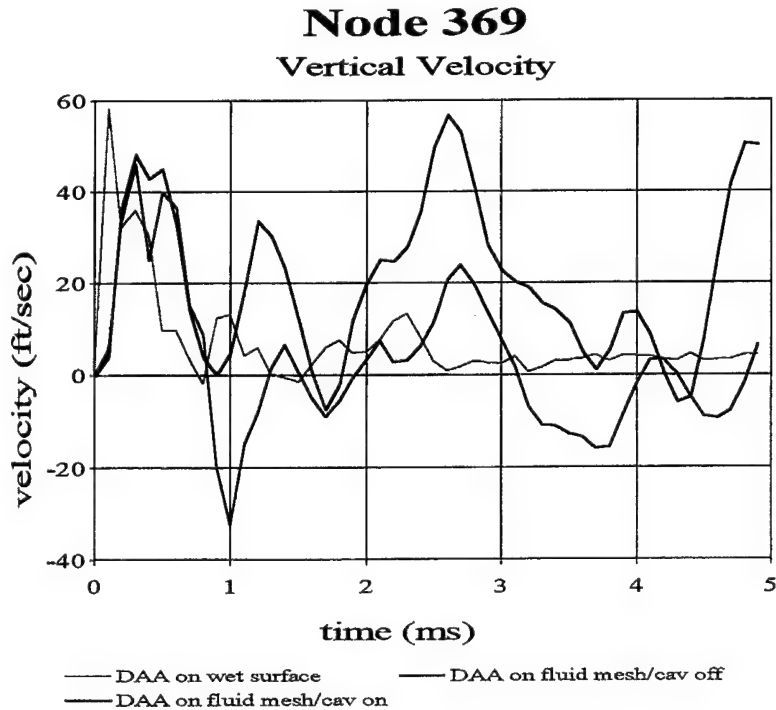
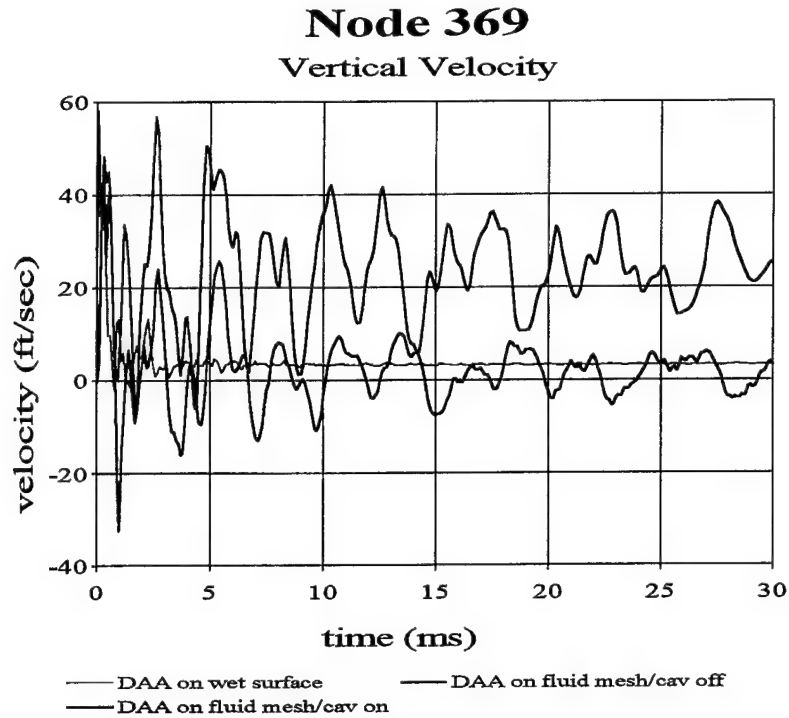


Figure 42. 3-D Model w/Charge Under Keel Response Comparison

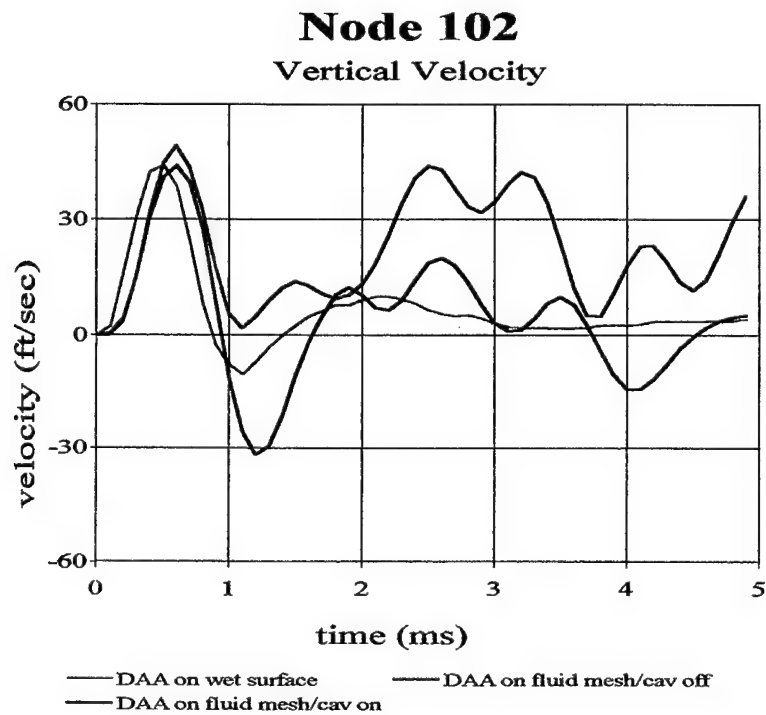
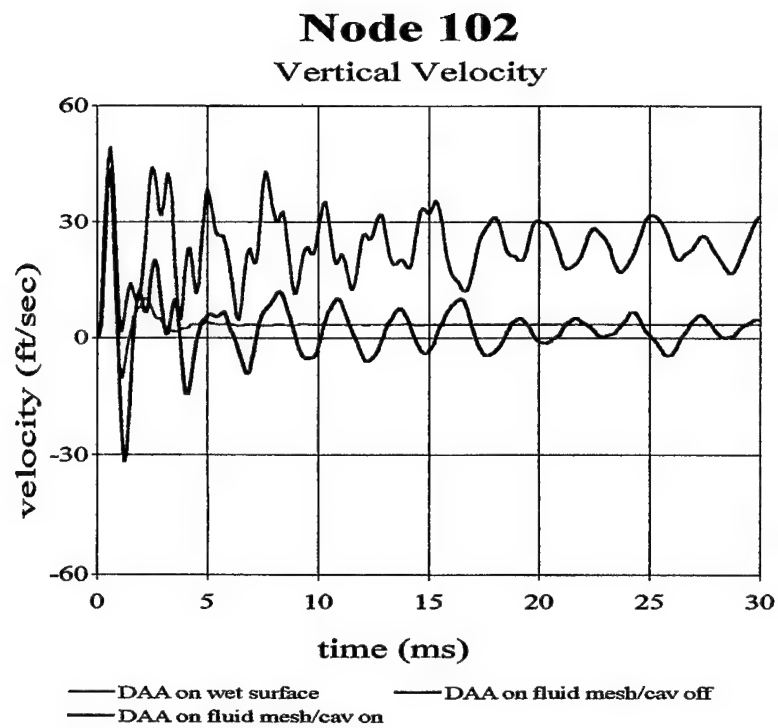


Figure 43. 3-D Model w/Charge Under Keel Response Comparison

very similar, although it does exhibit the oscillations typical of a fluid mesh problem. The oscillations can be observed to decrease in amplitude as time increases. This is as the response should be. The effect of cavitation is again significant, although not as significant as the effect observed on the two-dimensional model case. The peak velocity reached is only slightly higher than either the DAA on the wet surface case or the DAA on the fluid mesh case. The recorded velocity, however, does not go as far negative when cavitation is turned on, as compared to the two other cases. It should be noted also that the initial slope of the cavitation on and off fluid mesh curves matches exactly. This should happen since the cavitation zone has not formed when the wave initially impacts the structure.

Figure 44 shows the velocity response curves for node 294, which is in the center of a bulkhead. The effect of cavitation is not a great on the box model at this point. The cavitation off and on velocity profiles are very close. The DAA on the fluid mesh curves also show agreement with the DAA on the wet surface curve. The effect of cavitation is expected to be minimal at this point in the structure since the motion of the bulkhead is out of plane of the box model's induced motion from the shock wave impact.

Figure 45, Figure 46, Figure 47, and Figure 48 contain the velocity responses for the nodes on the side of the structure. The severity of the cavitation effect on the response depends on the node's location. A general comment can be made that the added effect of the fluid in general causes a much higher oscillatory response than the DAA on the wet surface case. The cavitation velocity response in general follows that of the cavitation off case, but with somewhat higher amplitudes. As can be observed from the node 67 response curves, the cavitation response is out of phase with the cavitation off case in some areas.

The pressure profiles for this charge case (with cavitation on) are included for the top and middle of the fluid mesh as Figure 49. The pressure profile for the bottom of the fluid mesh is not included, since the pressure remains at zero for the entire simulation. These pressure profiles are taken for elements directly below the structure. The formation of cavitation can be seen directly under the structure at the top of the fluid mesh. The middle of the fluid mesh (approximately 70 inches below the keel) does not exhibit any

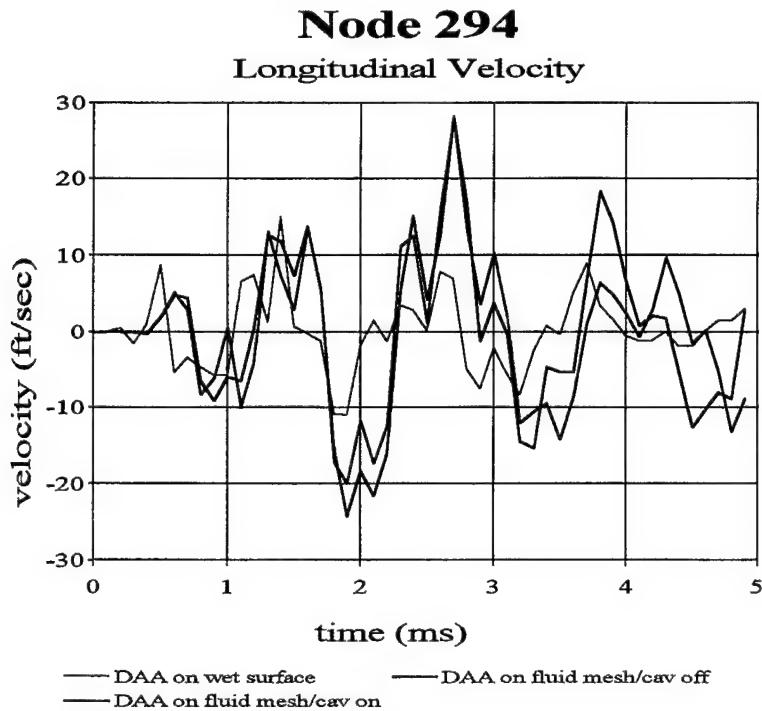
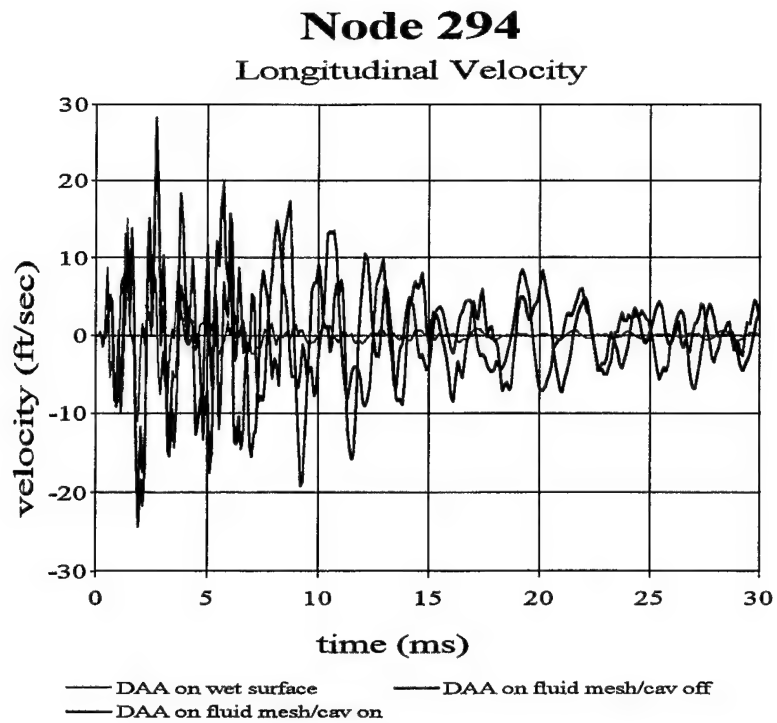


Figure 44. 3-D Model w/Charge Under Keel Response Comparison

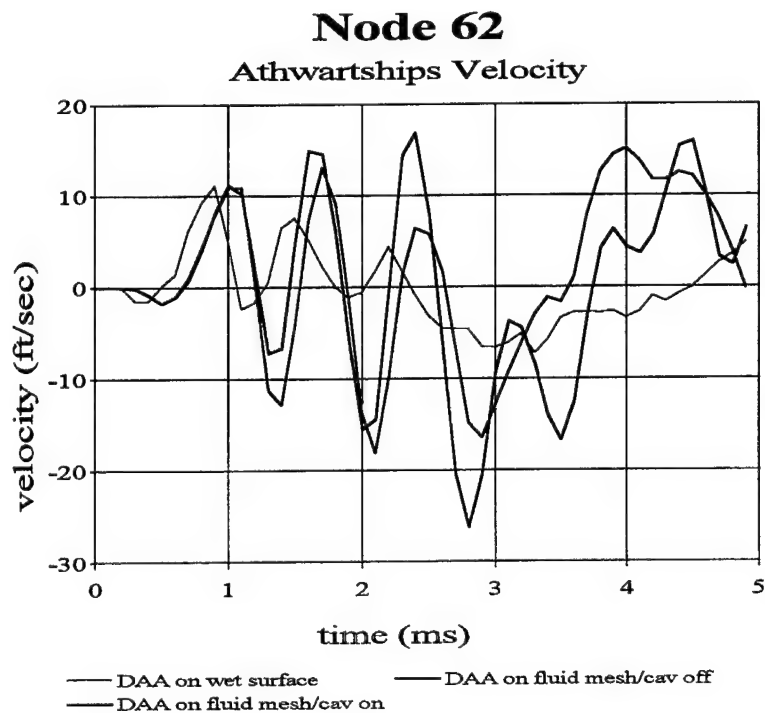
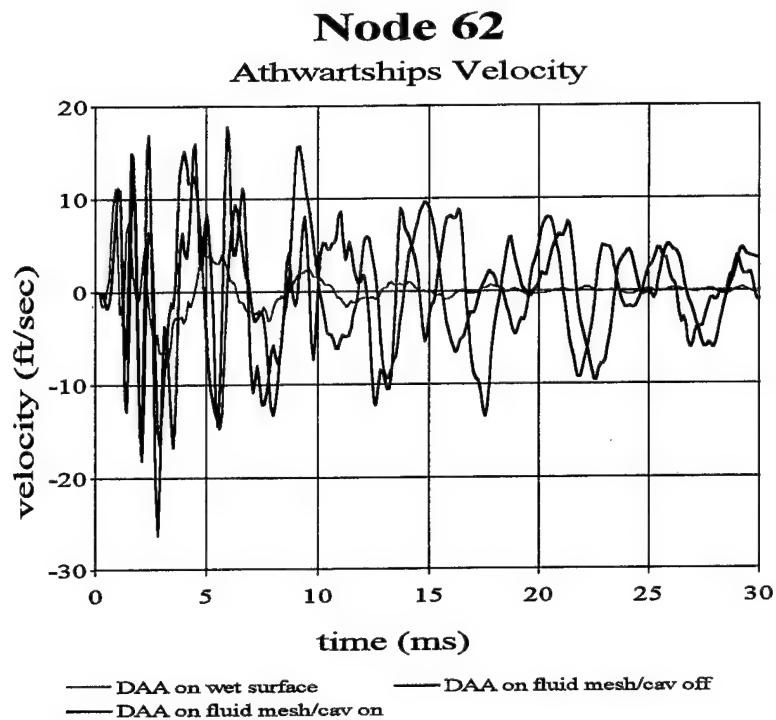


Figure 45. 3-D Model w/Charge Under Keel Response Comparison

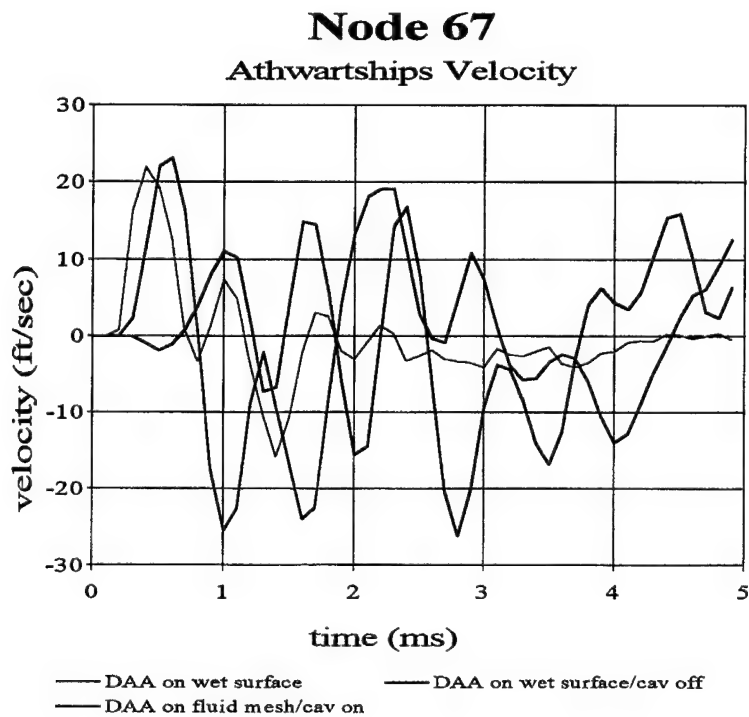
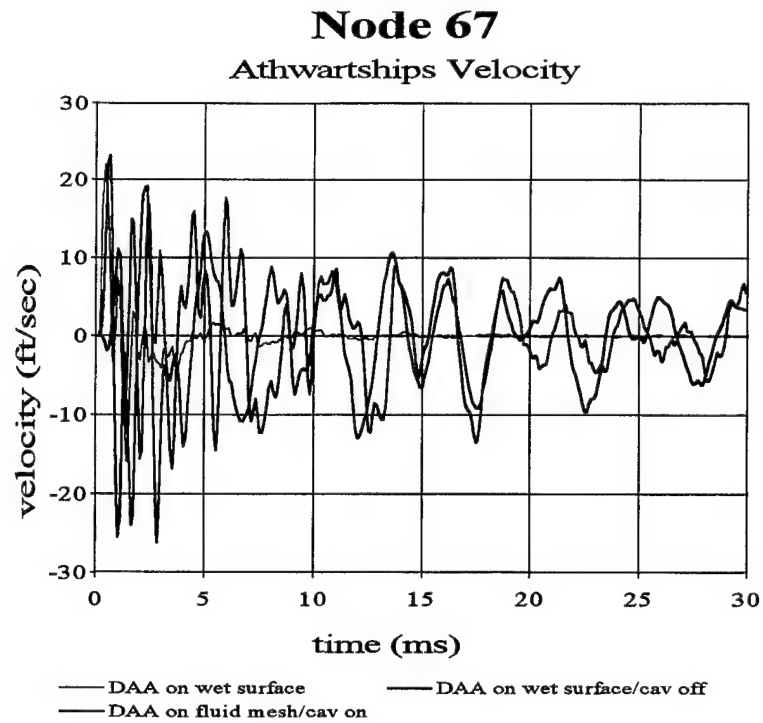


Figure 46. 3-D Model w/Charge Under Keel Response Comparison

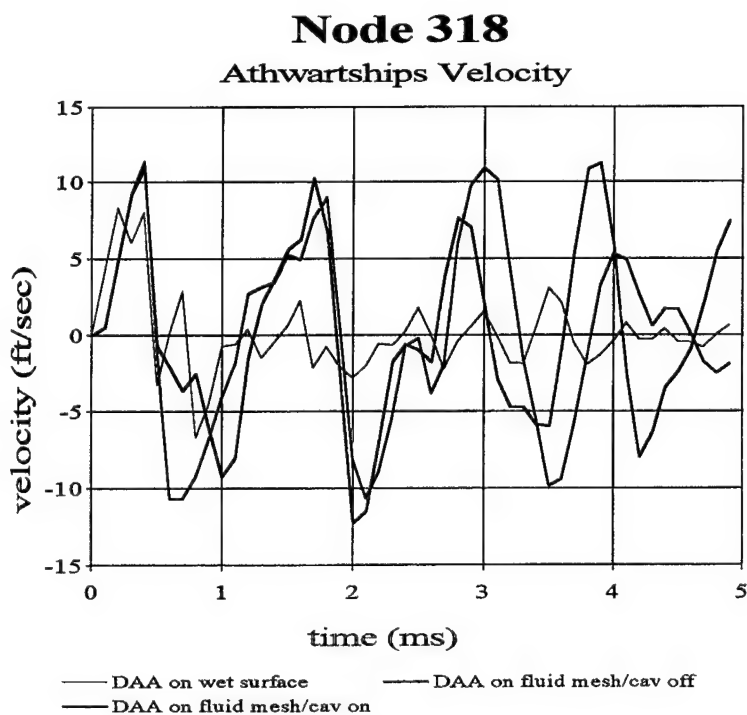
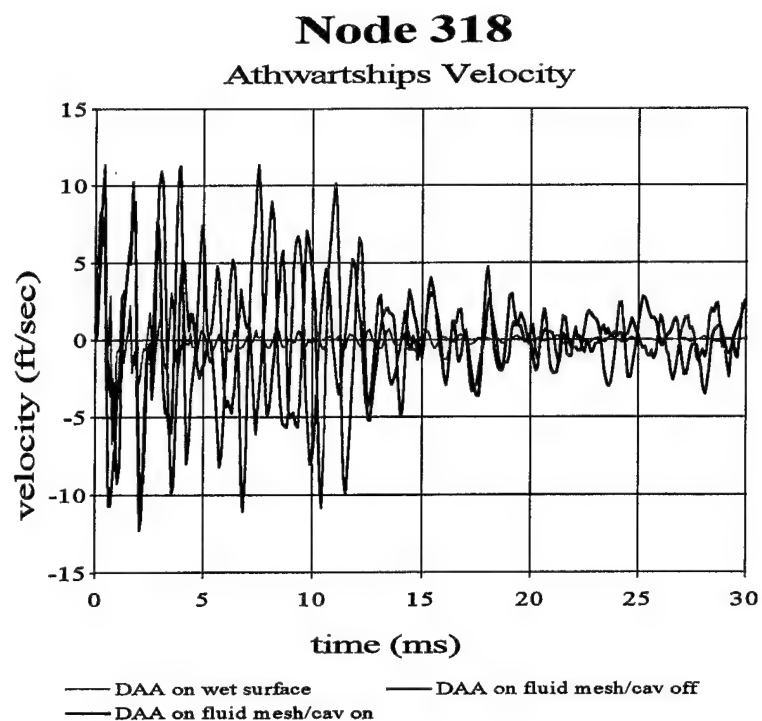


Figure 47. 3-D Model w/Charge Under Keel Response Comparison

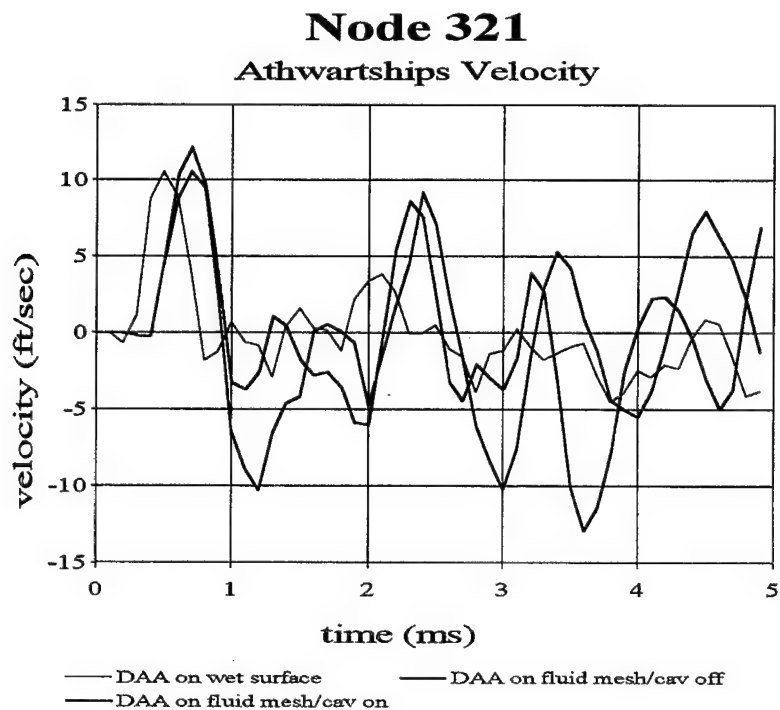
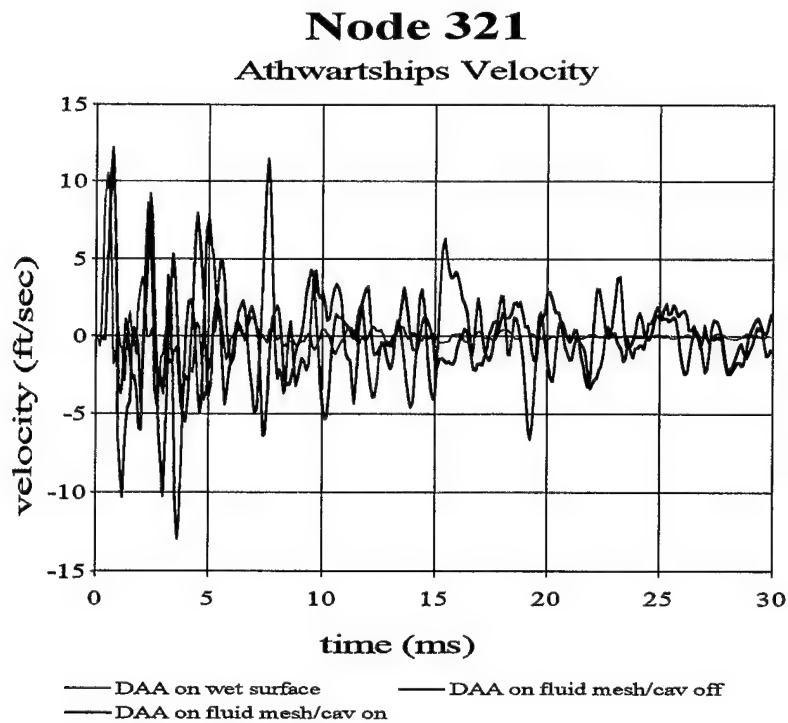
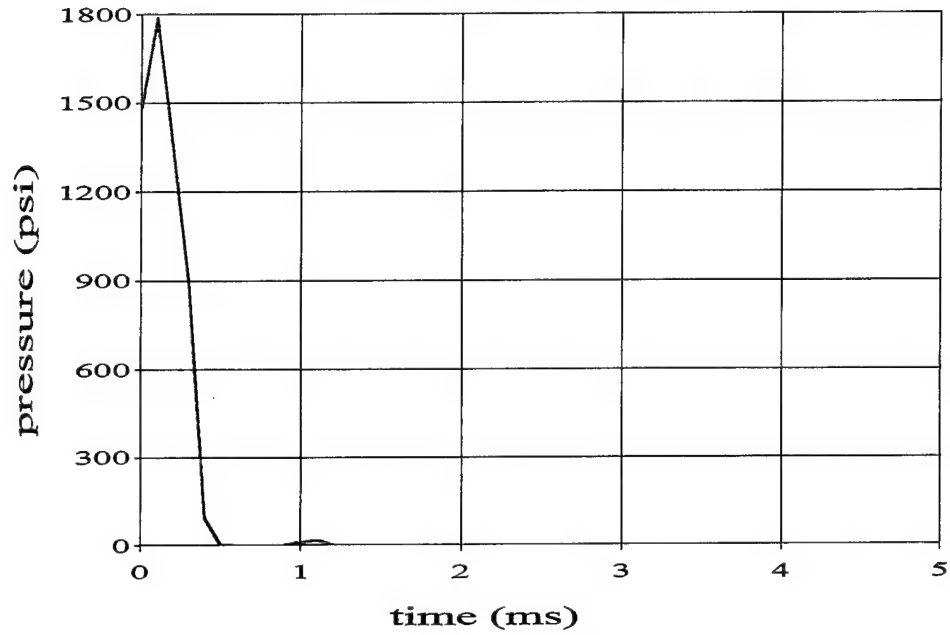


Figure 48. 3-D Model w/Charge Under Keel Response Comparison

Top of Fluid Mesh

Directly Under Keel



Middle of Fluid Mesh

70" Under Keel

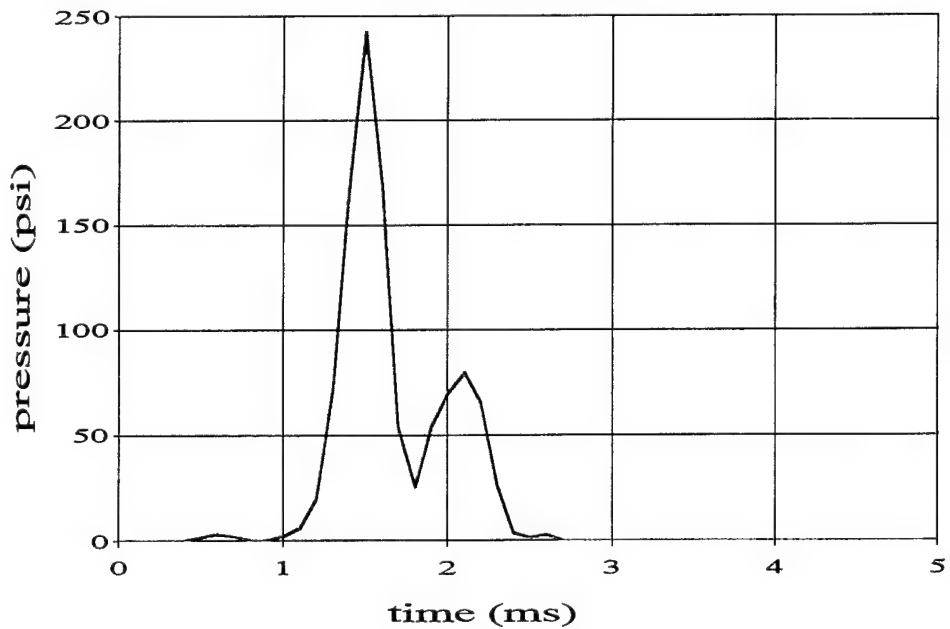


Figure 49. 3-D Model w/Charge Under Keel Fluid Mesh Pressure Profiles

cavitation. This indicates the cavitation zone ends prior to this point as predicted by the computed cavitation zone shown in Figure 16.

Three-dimensional visualization images generated by TAURUS as included as Figure 50 and Figure 51. The initial set-up of the shock wave at time zero can be seen. The true spherical shape of the shock wave is also evident. Cavitation forms immediately behind the reflected wave as predicted.

2. Offset Charge

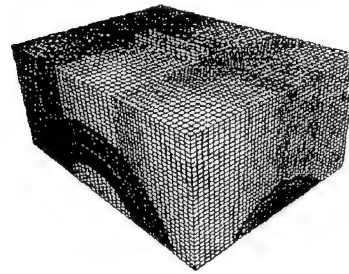
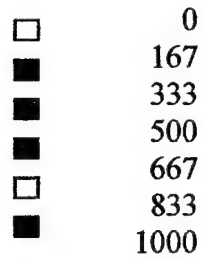
The three-dimensional shock simulations were next run for the offset charge geometry. The same combination of runs was conducted as for the charge under keel tests. The resultant observed responses are similar to those described above.

The keel node velocity profiles are plotted in Figure 52 and Figure 53. Once again the effect of cavitation is somewhat significant in changing the response from that observed in the DAA on the wet surface case and the cavitation off case for the DAA on the fluid mesh. The initial peak velocity is only somewhat higher than that of the two aforementioned cases. Comparing this charge geometry to the charge under keel case, the effect of cavitation can be said basically the same for the keel nodes.

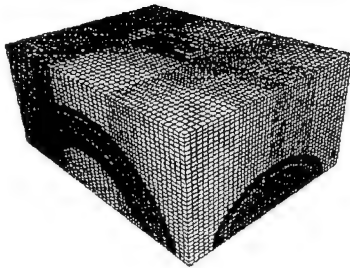
In Figure 54, the response of the bulkhead center node is plotted. As before, the general trend of the cavitation response is to follow that of the no cavitation case. The trends observed for the three test runs conducted for this charge geometry for the remaining nodes examined, all follow the same basic trends as observed for the charge under keel case. These remaining responses are plotted in Figure 55, Figure 56, Figure 57, and Figure 58.

The fluid mesh pressure profiles are shown in Figure 59. Cavitation clearly is formed directly under the structure. The middle of the fluid mesh does not experience any cavitation and this is consistent with the computed cavitation zone for this charge depth shown in Figure 14. The bottom of the fluid mesh, as expected, does not experience any cavitation.

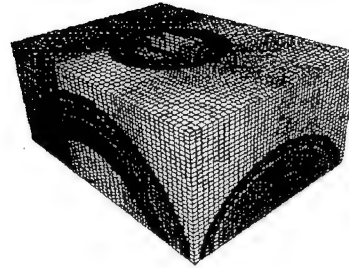
Color Fringe Key
Pressure Magnitudes in psi



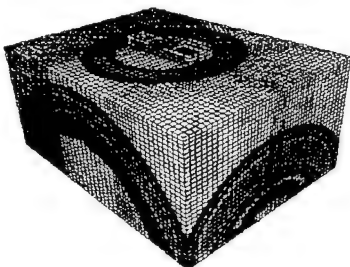
0 ms



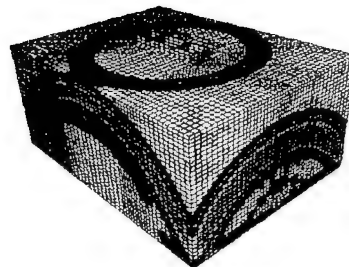
0.2 ms



0.4 ms

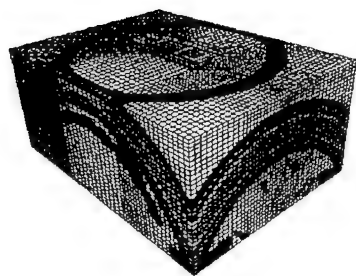


0.6 ms

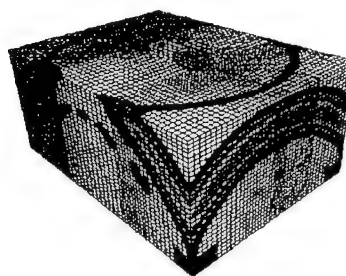


0.8 ms

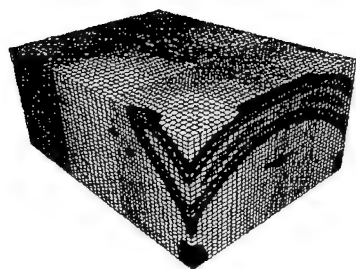
Figure 50. 3-D Model w/Charge Under Keel Shock Wave Propagation



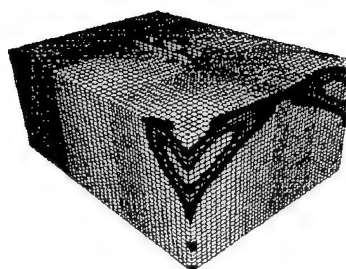
1.0 ms



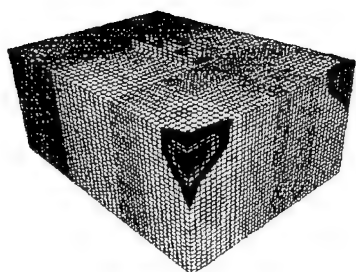
1.2 ms



1.4 ms



1.6 ms



1.8 MS

Figure 51. 3-D Model w/Charge Under Keel Shock Wave Propagation (Continued)

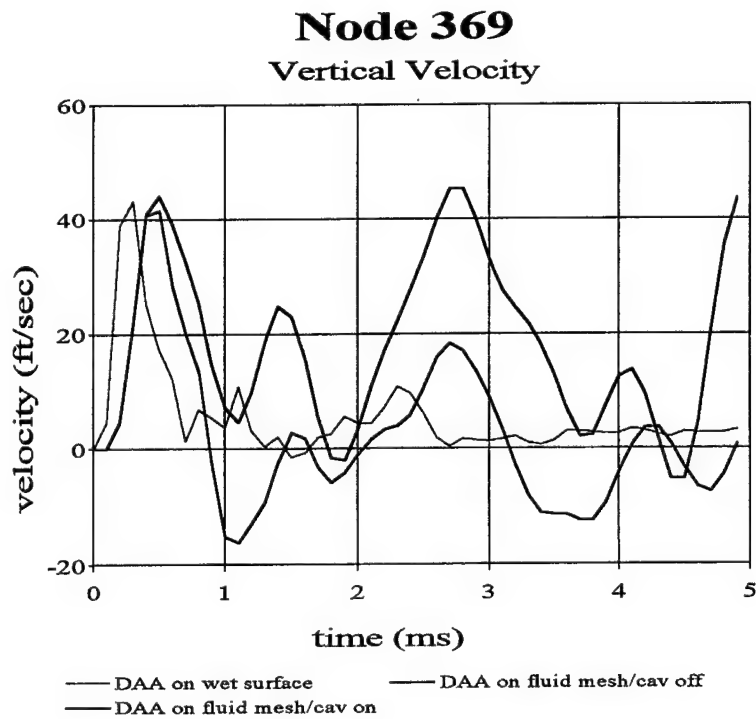
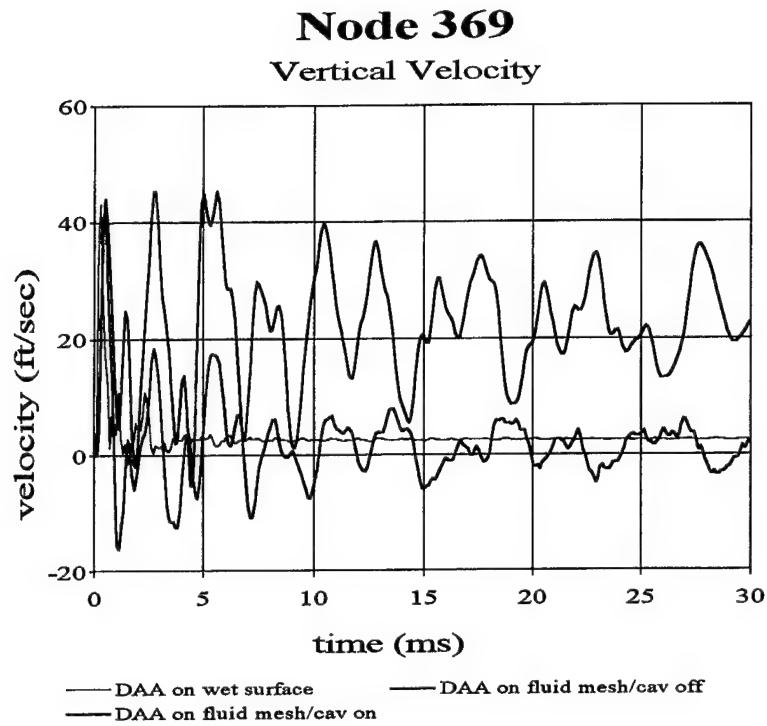


Figure 52. 3-D Model w/Offset Charge Response Comparison

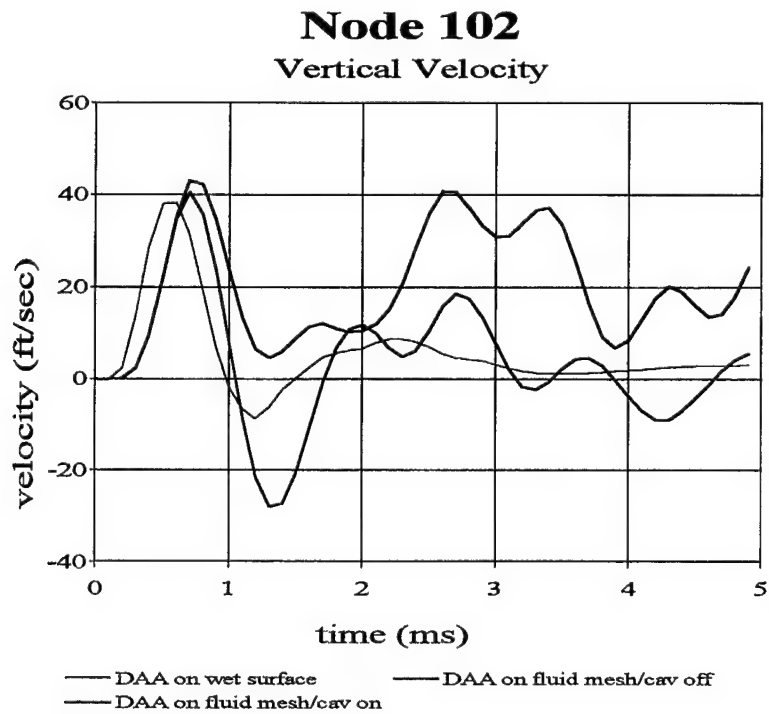
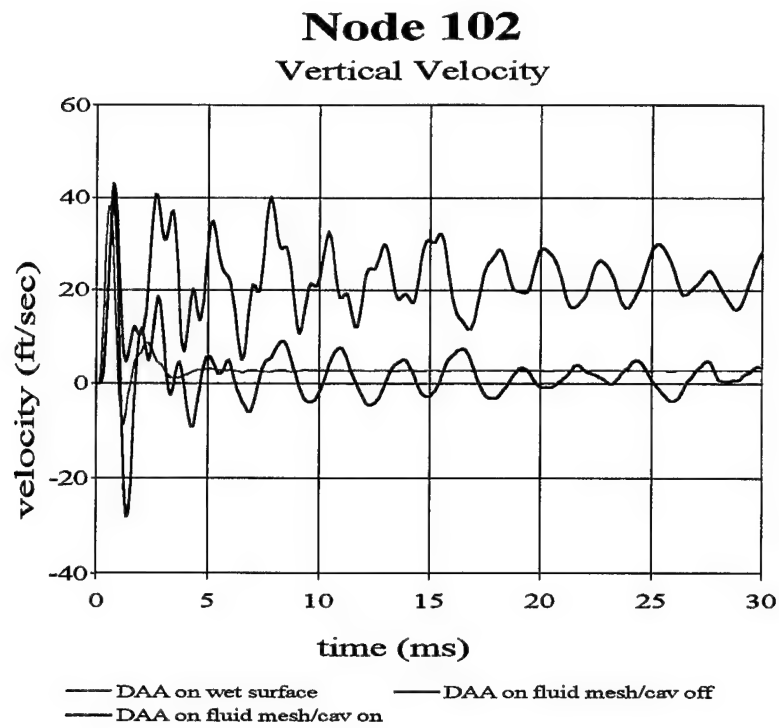


Figure 53. 3-D Model w/Charge Offset Response Comparison

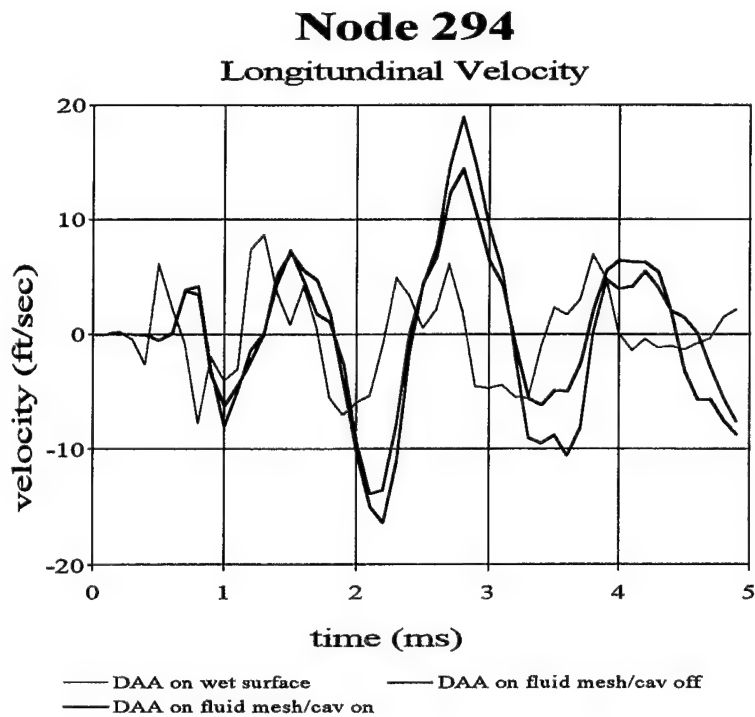
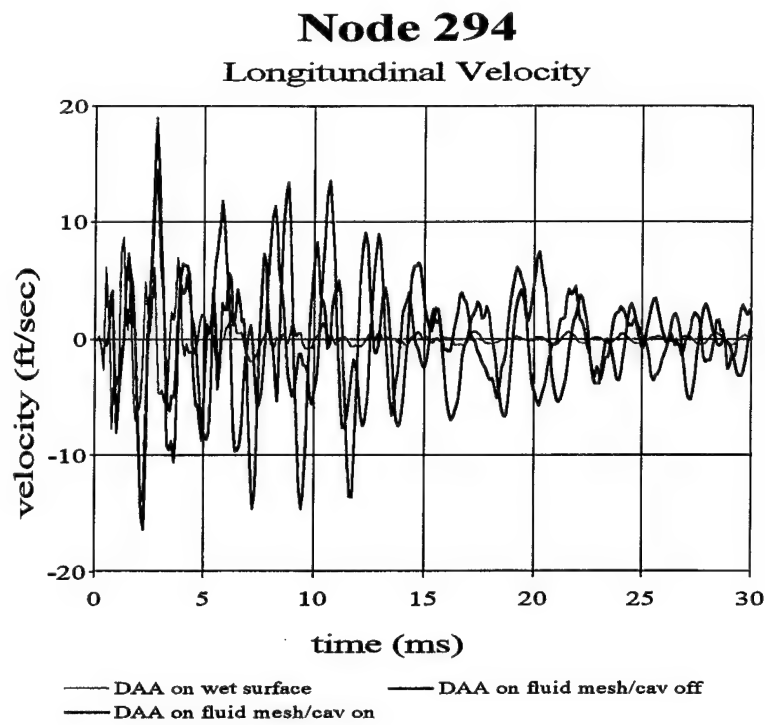


Figure 54. 3-D Model w/Offset Charge Response Comparison

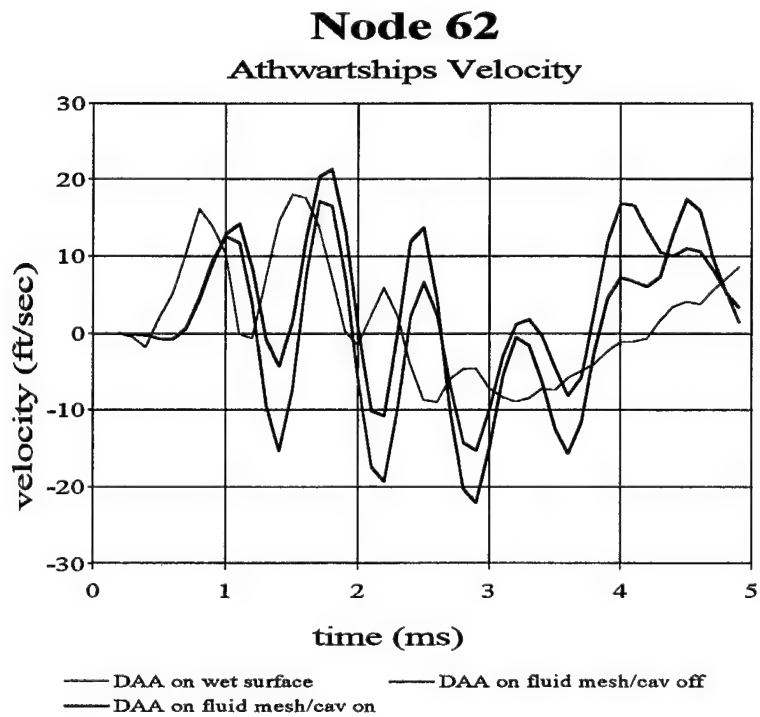
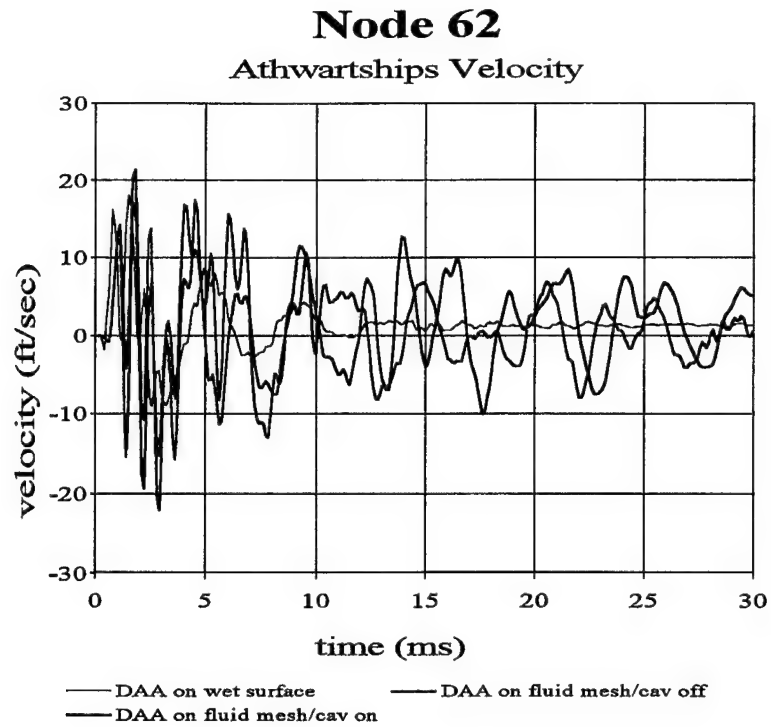


Figure 55. 3-D Model w/Offset Charge Response Comparison

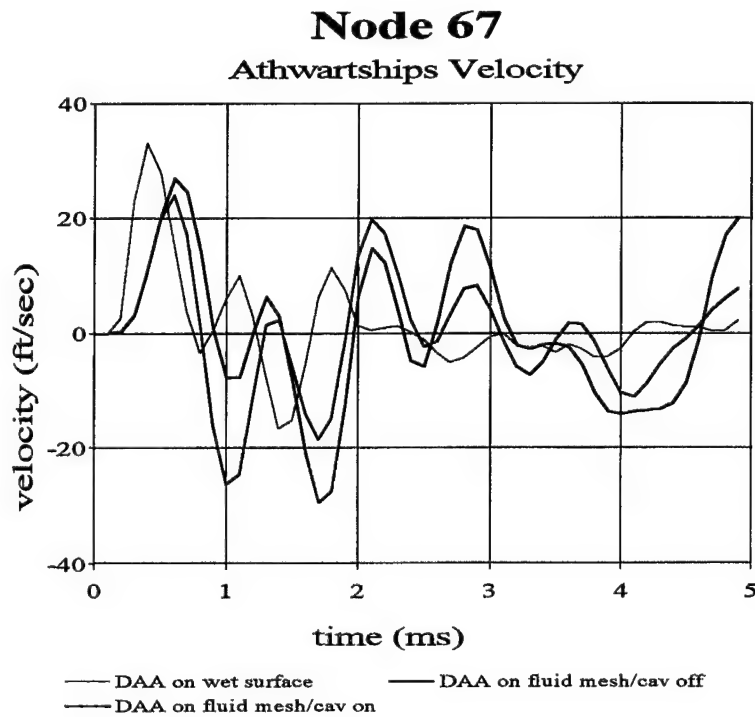
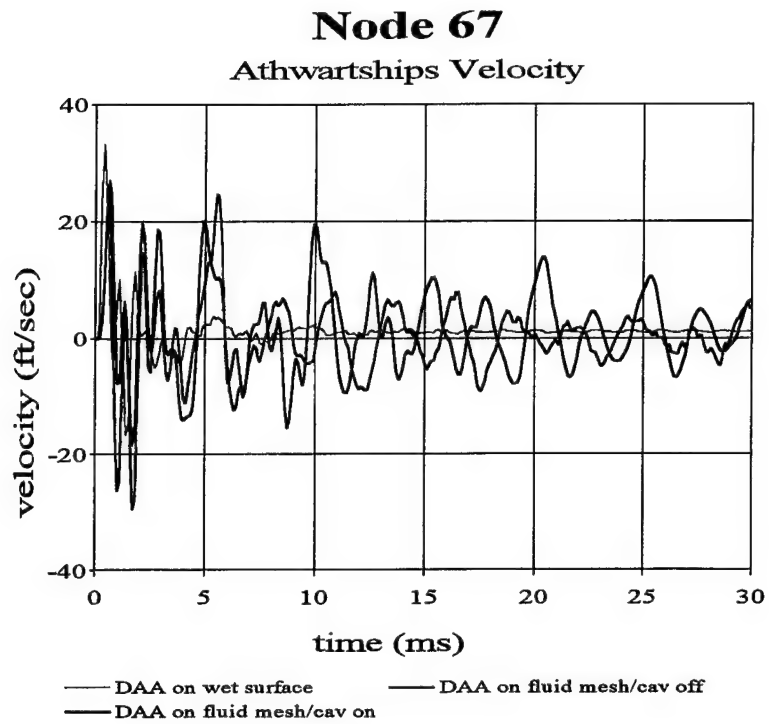


Figure 56. 3-D Model w/Offset Charge Response Comparison

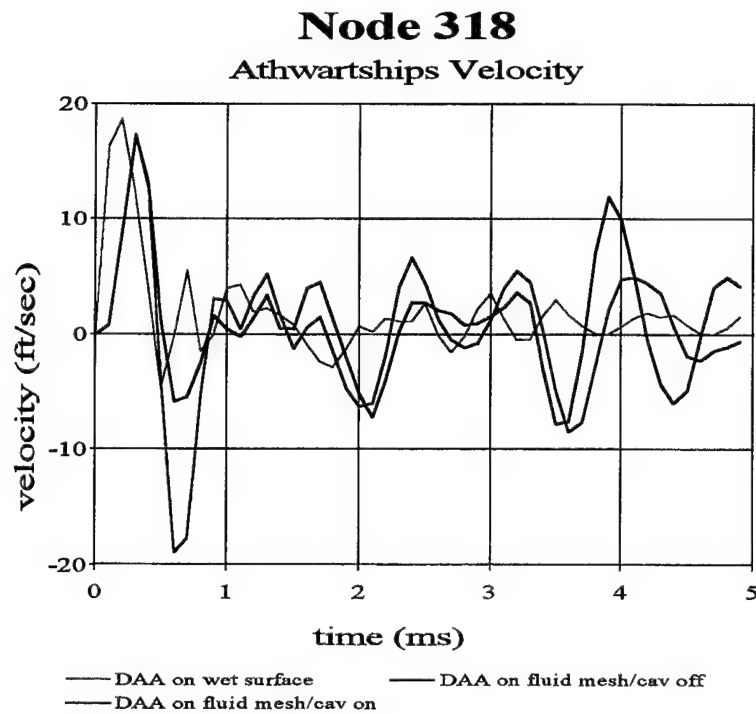
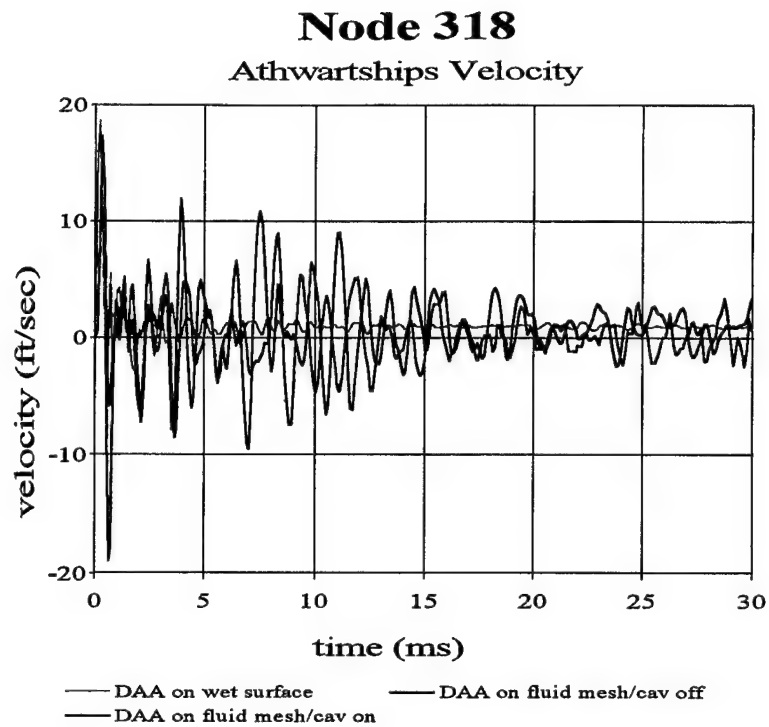


Figure 57. 3-D Model w/Offset Charge Response Comparison

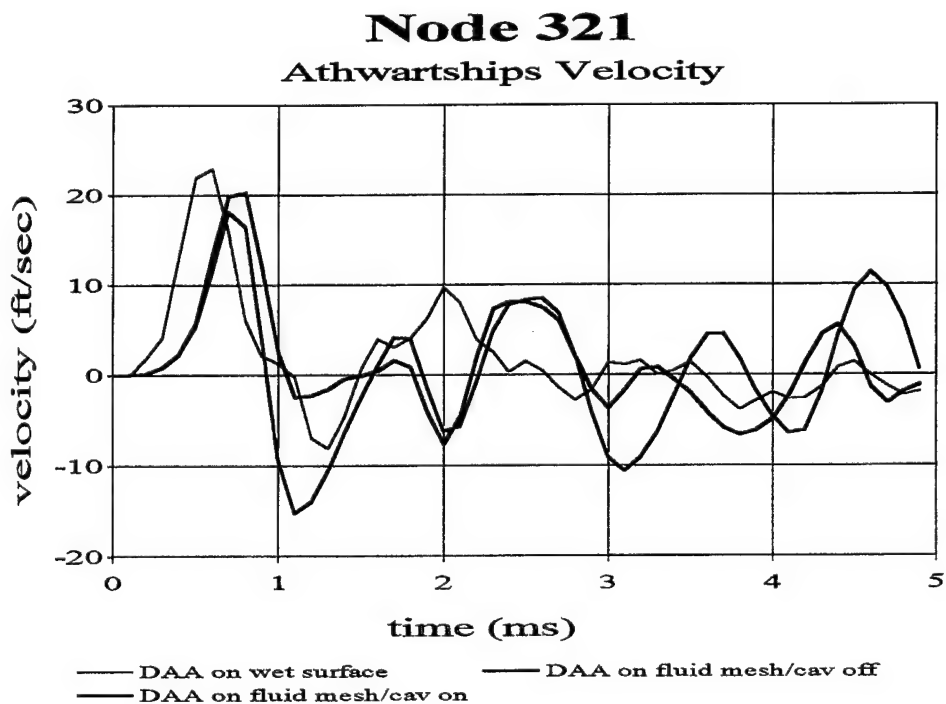
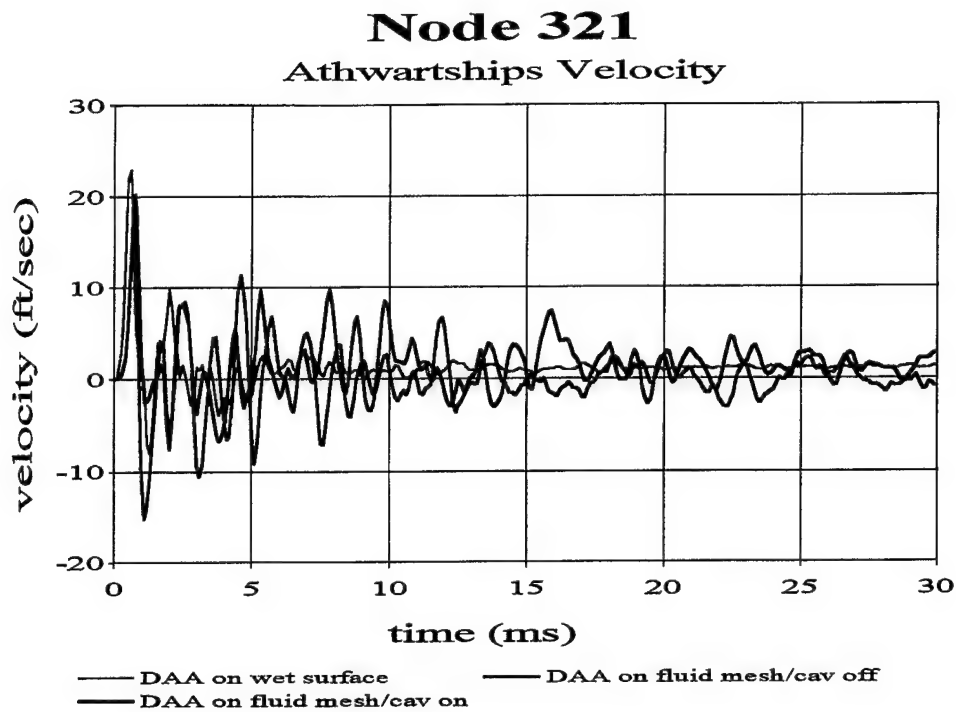


Figure 58. 3-D Model w/Offset Charge Response Comparison

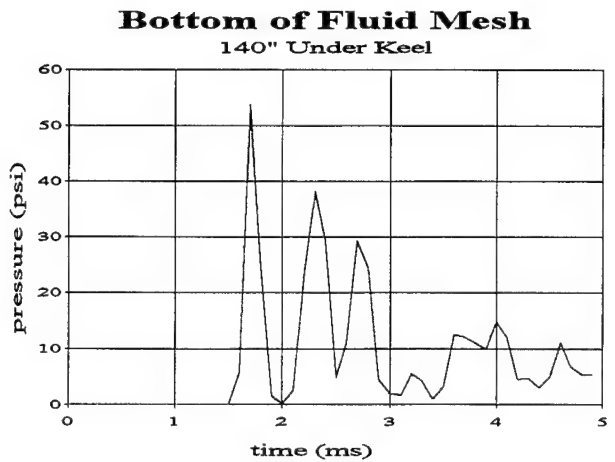
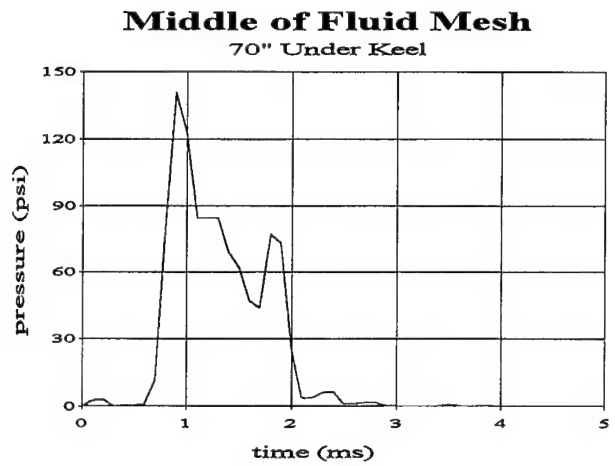
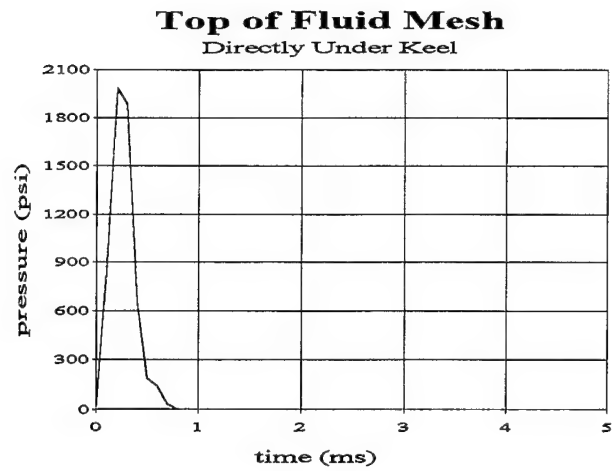


Figure 59. 3-D Model w/Offset Charge Fluid Mesh Pressure Profiles

The shock wave propagation is shown in Figure 60 and Figure 61. The differences in this charge geometry and the previous case can easily be noted. The formation of the cavitation zone can again be seen; the difference in its shape should be noted.

D. RAYLEIGH DAMPING

Rayleigh damping was added to the three-dimensional model to study its effect on the overall response for both the DAA on the wet surface case and the DAA on the fluid mesh (cavitation on) case. The charge under keel geometry was utilized.

Rayleigh damping is of the following form:

$$[C] = \alpha[M] + \beta[K] \quad (4.1)$$

Alternatively, the above equation can be written in the following form:

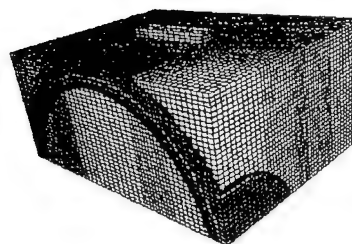
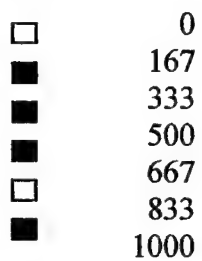
$$\alpha + \beta\omega_i^2 = 2\omega_i\xi_i \quad (4.2)$$

where $[C]$ = system damping matrix, $[M]$ = system mass matrix, $[K]$ = system stiffness matrix, α and β are the Rayleigh damping coefficients, ω_i is a frequency of interest, and ξ_i is the desired damping ratio for the i^{th} frequency. Typically, Rayleigh damping is utilized to provide damping over a frequency range. The damping coefficients can be easily determined given two frequencies of interest and the associated damping ratios for those those frequencies. A set of two equations with two unknowns can then be set up and solved. This is where knowledge of the structural modal frequencies and shapes is crucial for proper selection of the Rayleigh damping coefficients to achieve the desired effect.

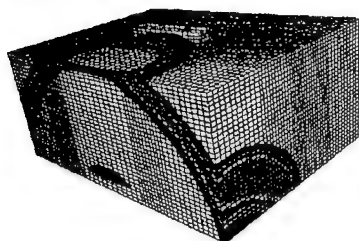
For this model the α value was chosen to be 2.464. The β value was set to 10^{-5} . For the ship-like box model, these Rayleigh coefficient values provide approximately 0.5% damping at 50 Hz and 0.7% damping at 200 Hz. While these values may not be physically realistic for this model, they provide the needed illustration of the effect of damping on the model for this conceptual study.

The effect of damping on the response of the DAA on the wetted surface case was examined. The velocity response for the output nodes is plotted in Figure 62, Figure 63,

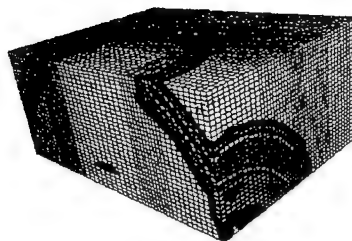
Color Fringe Key
Pressure Magnitudes in psi



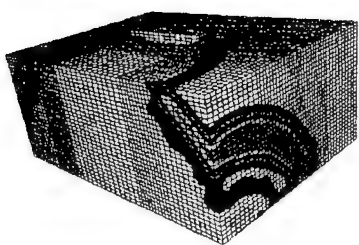
0 ms



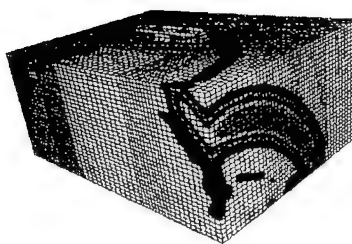
0.2 ms



0.4 ms

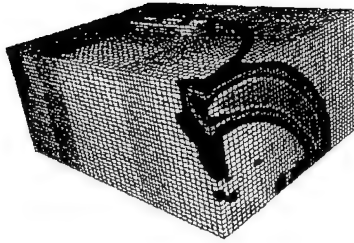


0.6 MS

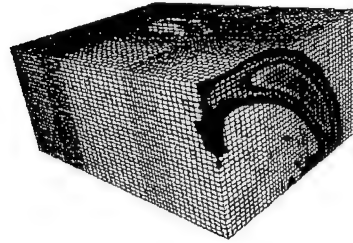


0.8 MS

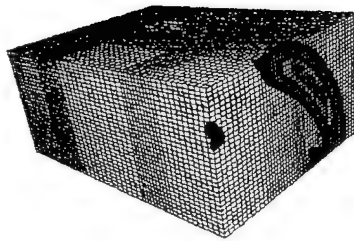
Figure 60. 3-D Model w/Offset Charge Shock Wave Propagation



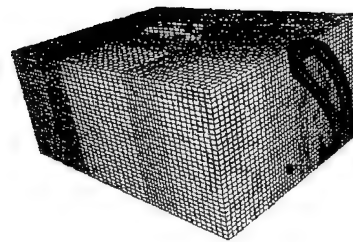
1.0 ms



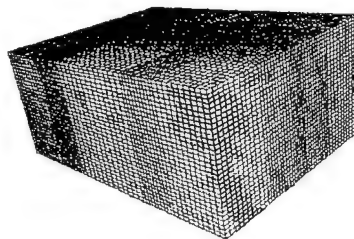
1.2 ms



1.4 ms



1.6 ms



1.8 ms

Figure 61. 3-D Model w/Offset Charge Shock Wave Propagation (Continued)

Figure 64, Figure 65, Figure 66, Figure 67, and Figure 68. While the undamped and damped responses are not dramatically different, the effects of damping can clearly be seen. The damping reduces the peak values of the response and in general has an overall “smoothing” effect on the response. The reason for this is that damping effects the resonant response of the model.

The effect of damping in the case of the DAA on the fluid mesh with the cavitation flag on was examined next. Figure 69, Figure 70, Figure 71, Figure 72, Figure 73, Figure 74, and Figure 75 show the nodal velocity response comparisons. Once again, the damping effect can be clearly seen in the response curves.

If the Rayleigh damping coefficients are accurately computed, the effect of damping can be significant. All structures have inherent damping present, and in order to accurately model the response of a particular structure, careful consideration of Rayleigh damping is a must.

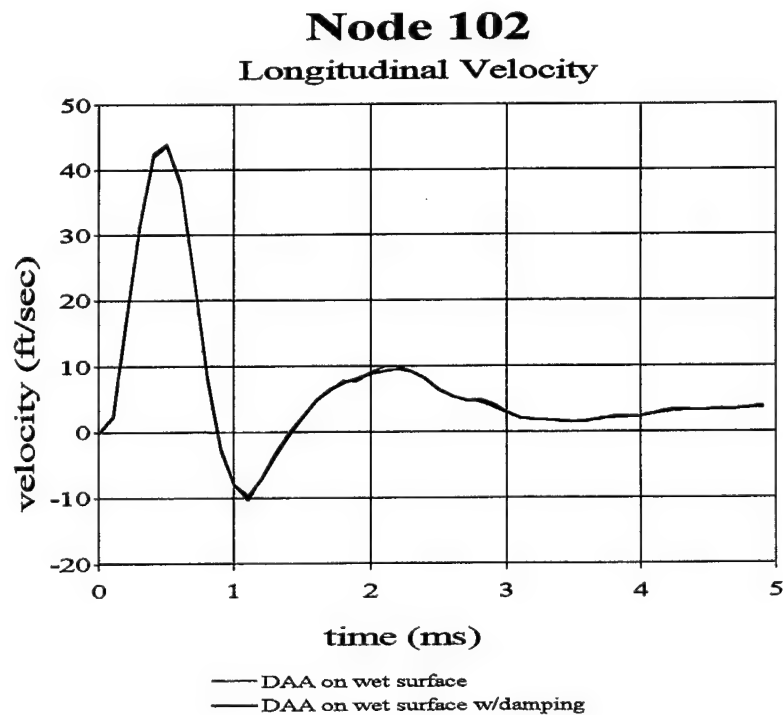
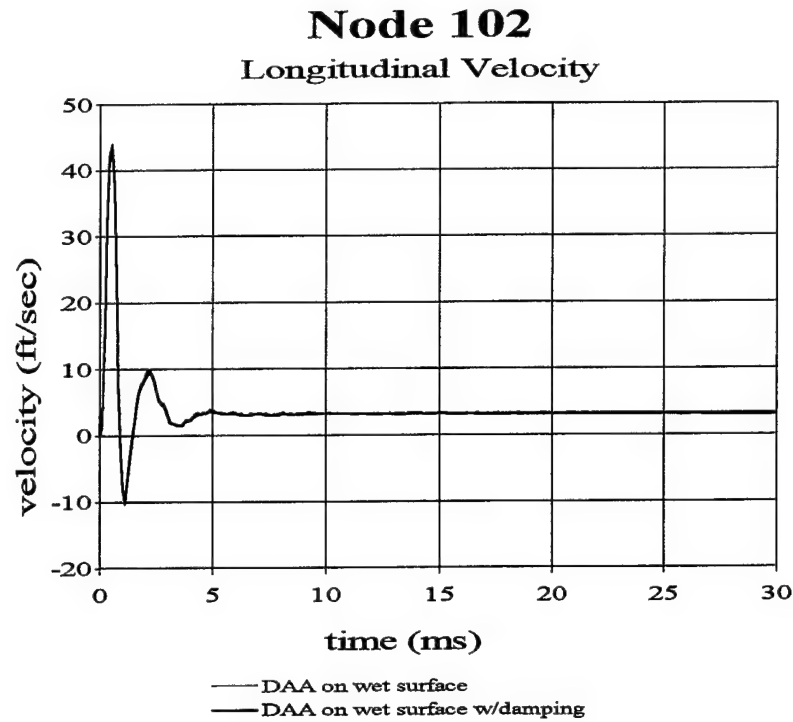


Figure 62. 3-D Model w/Charge Under Keel Damped Response Comparison

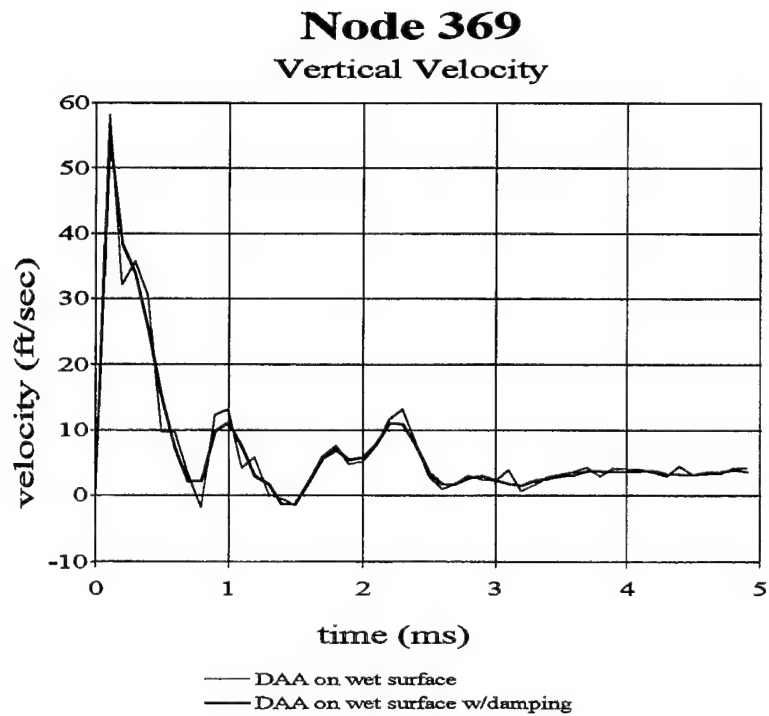
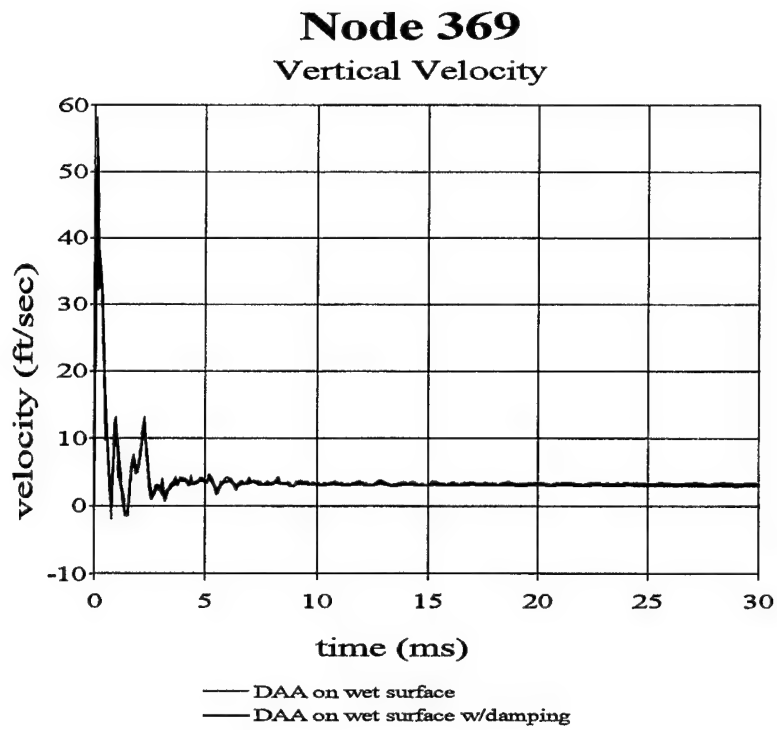


Figure 63. 3-D Model w/Charge Under Keel Damped Response Comparison

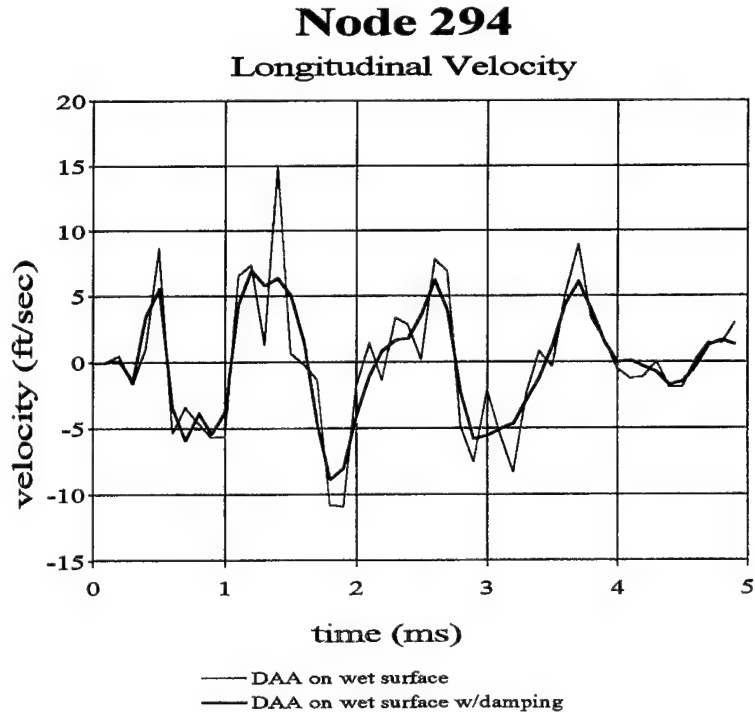
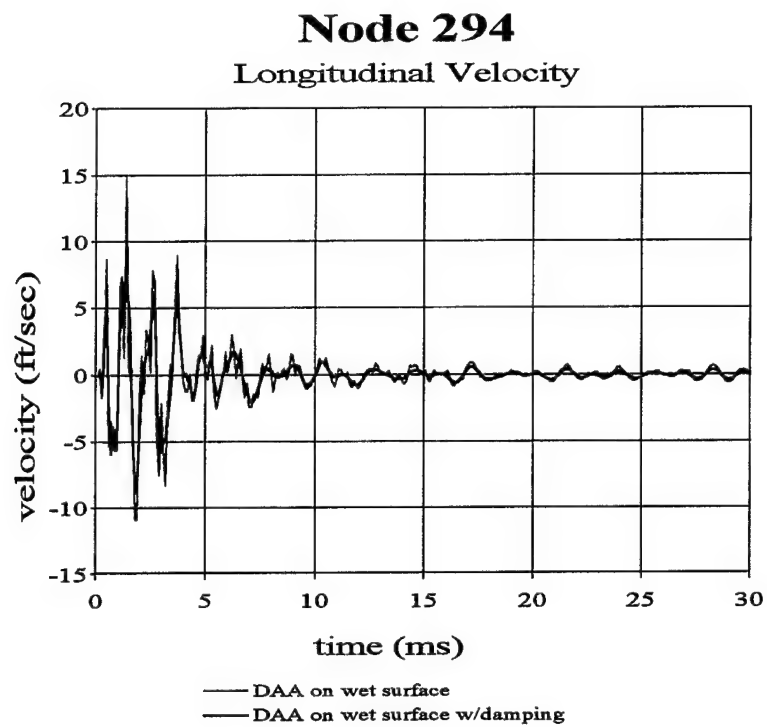


Figure 64. 3-D Model w/Charge Under Keel Damped Response Comparison

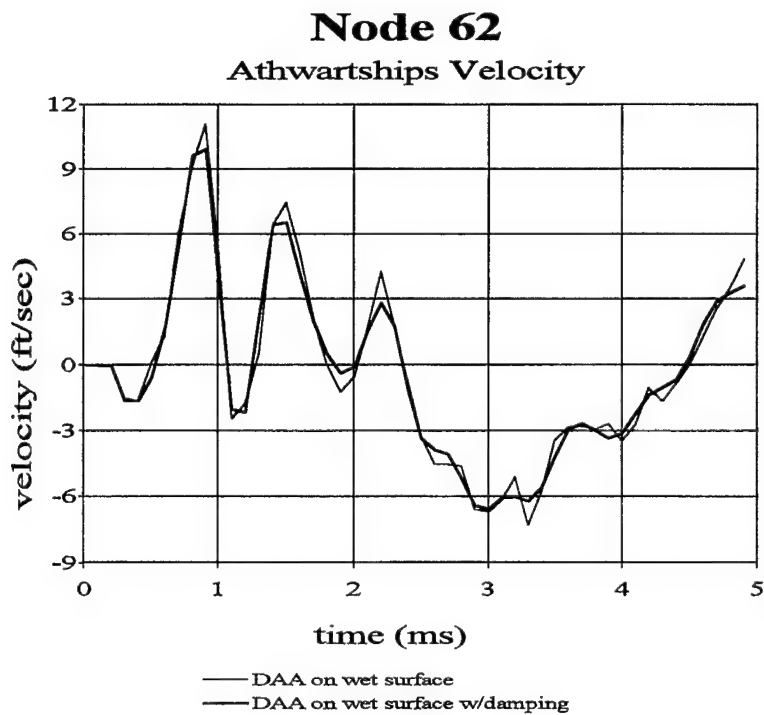
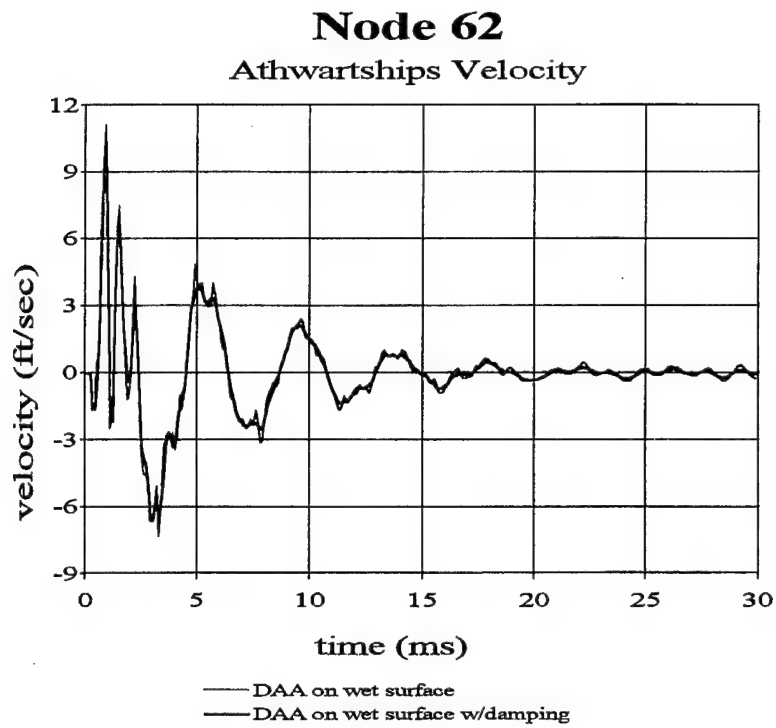


Figure 65. 3-D Model w/Charge Under Keel Damped Response Comparison

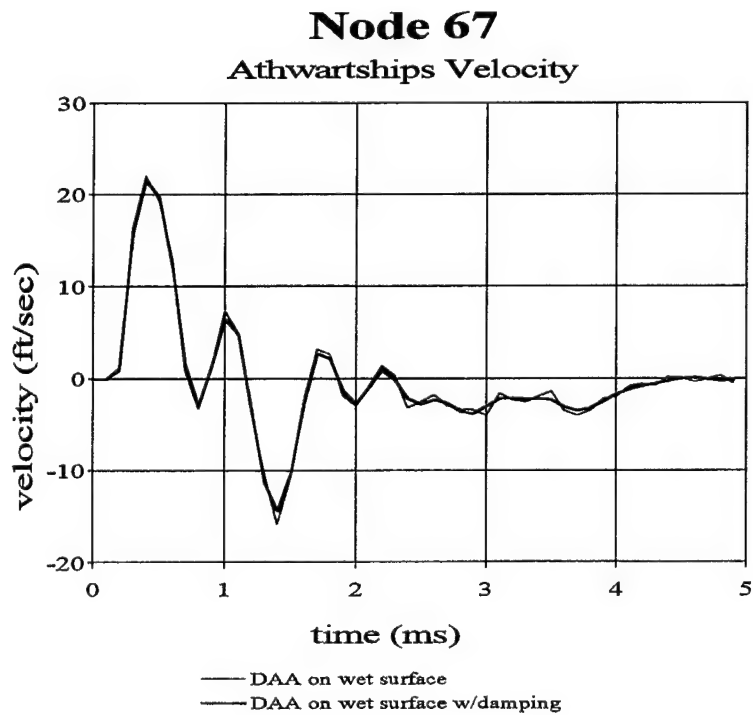
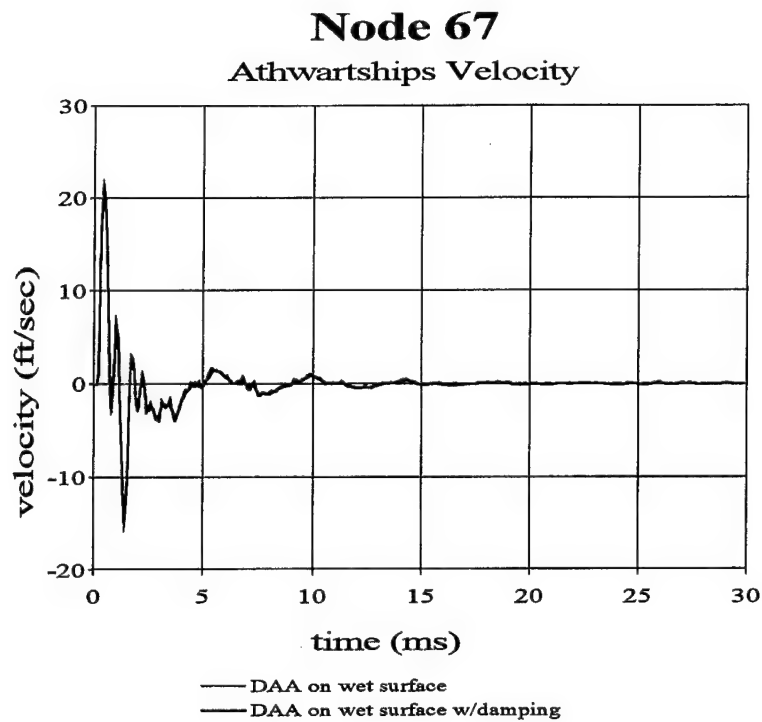


Figure 66. 3-D Model w/Charge Under Keel Damped Response Comparison

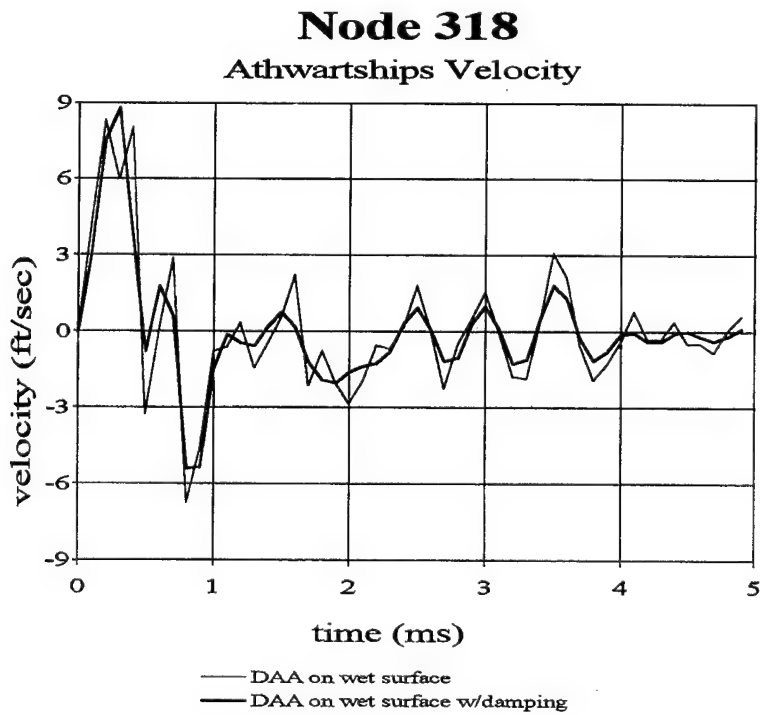
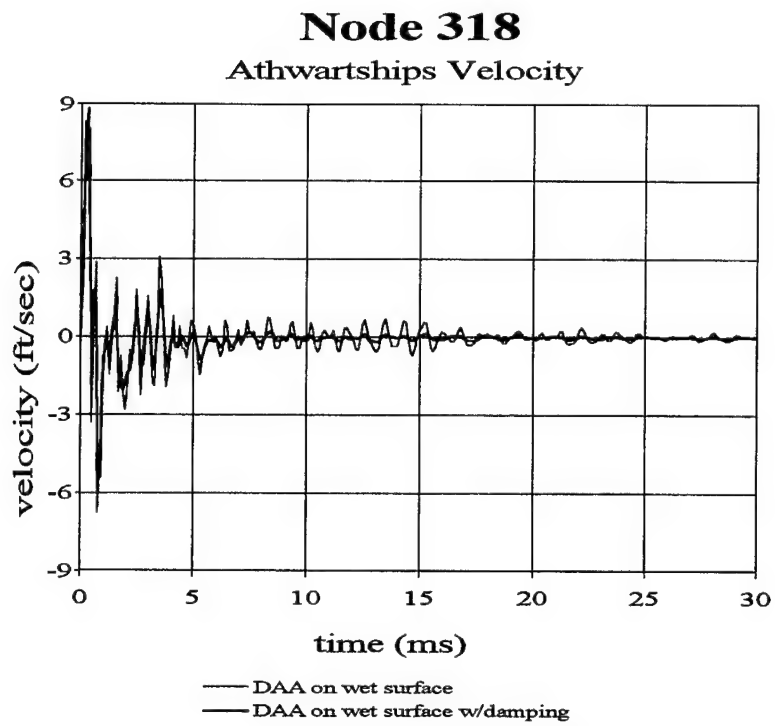


Figure 67. 3-D Model w/Charge Under Keel Damped Response Comparison

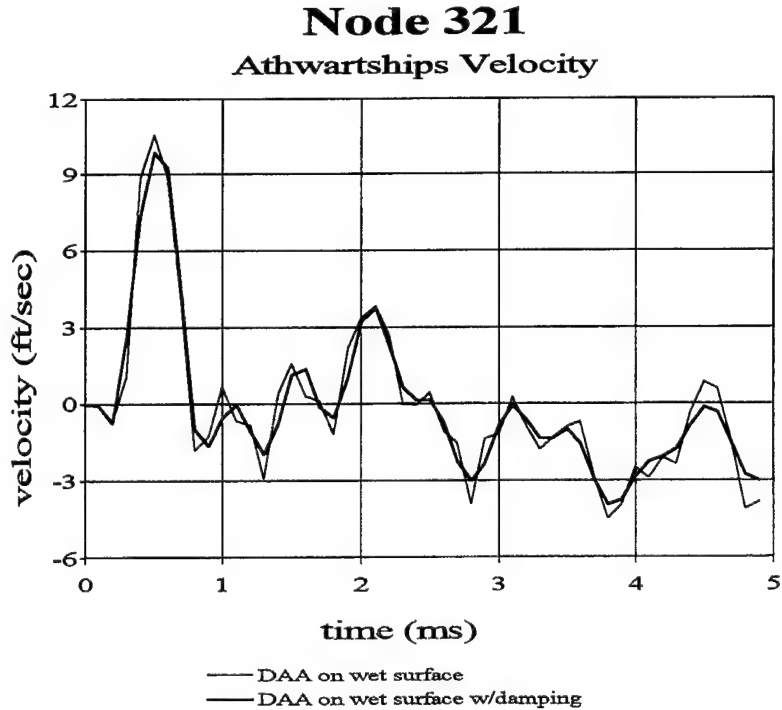
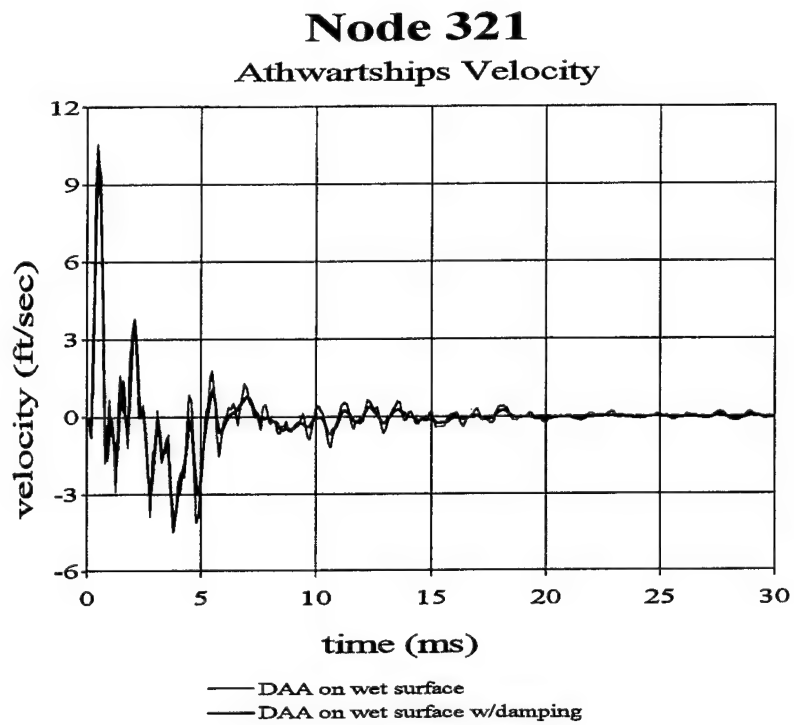


Figure 68. 3-D Model w/Charge Under Keel Damped Response Comparison

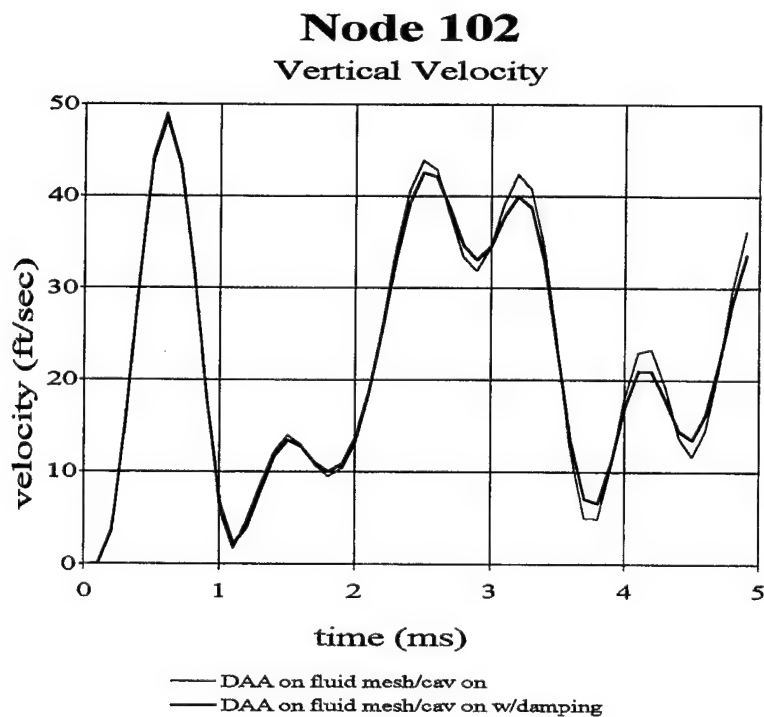
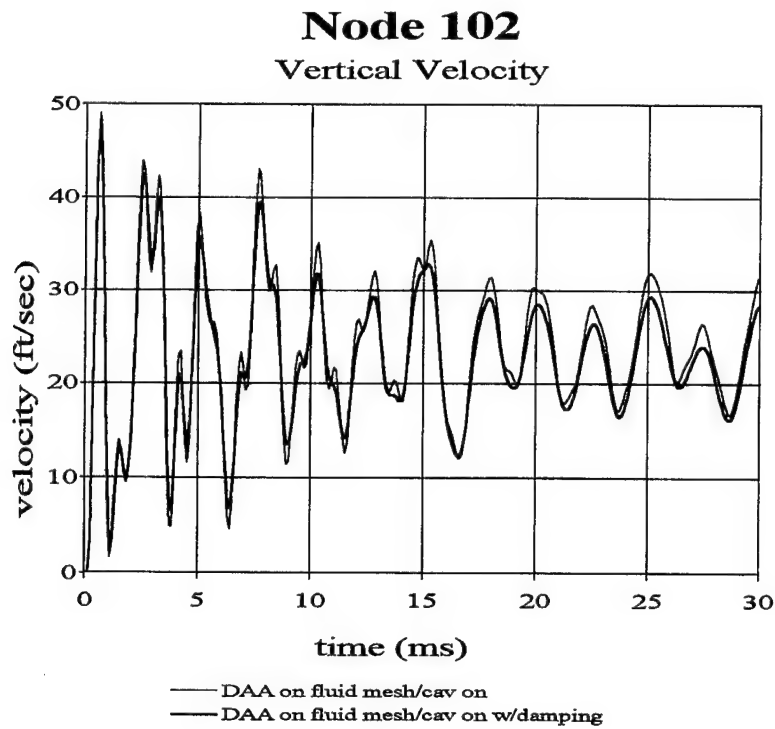


Figure 69. 3-D Model w/Charge Under Keel Damped Response Comparison

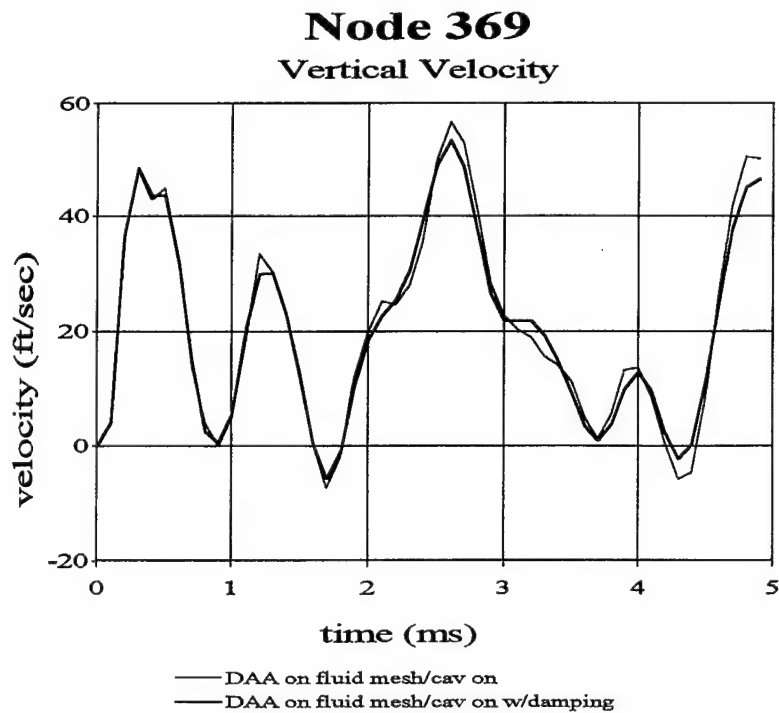
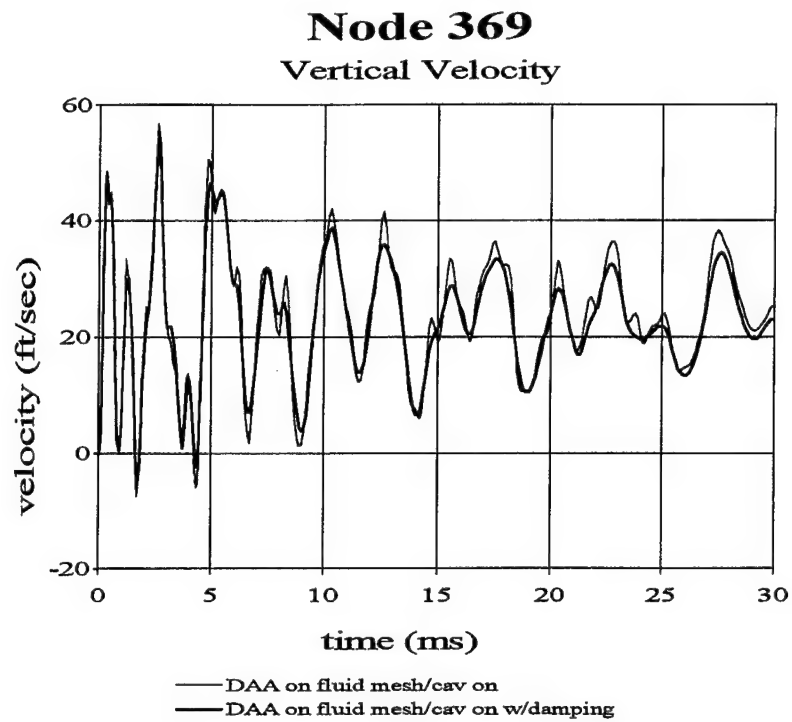


Figure 70. 3-D Model w/Charge Under Keel Damped Response Comparison

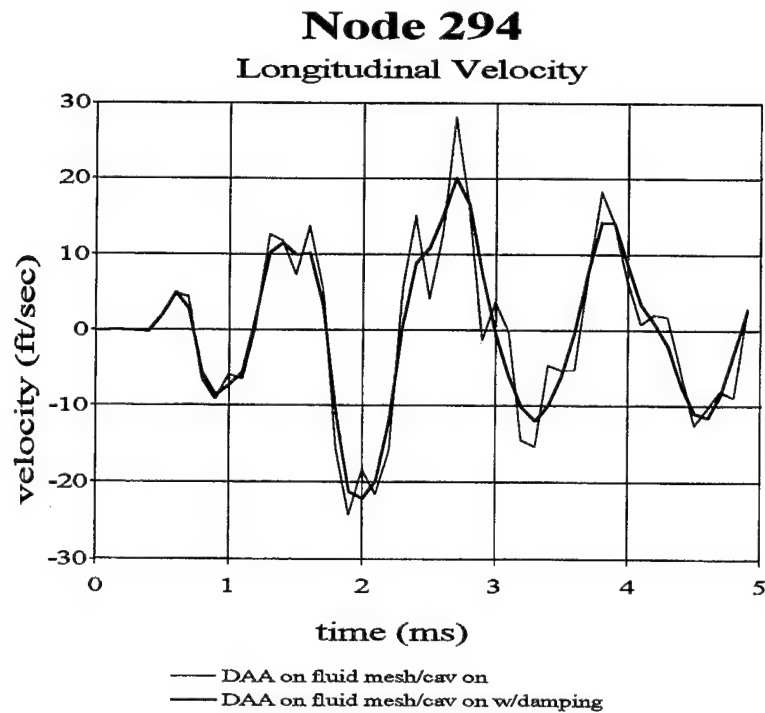
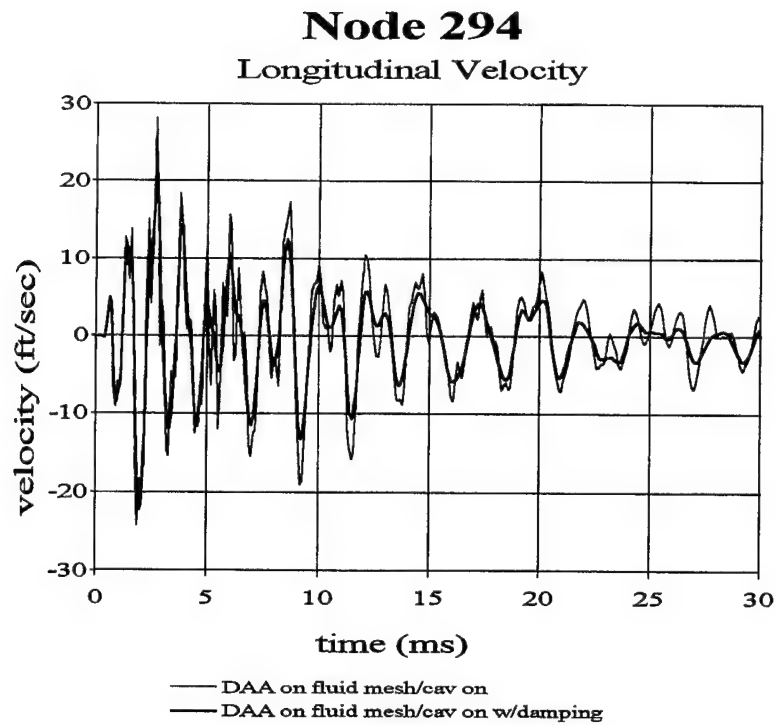


Figure 71. 3-D Model w/Charge Under Keel Damped Response Comparison

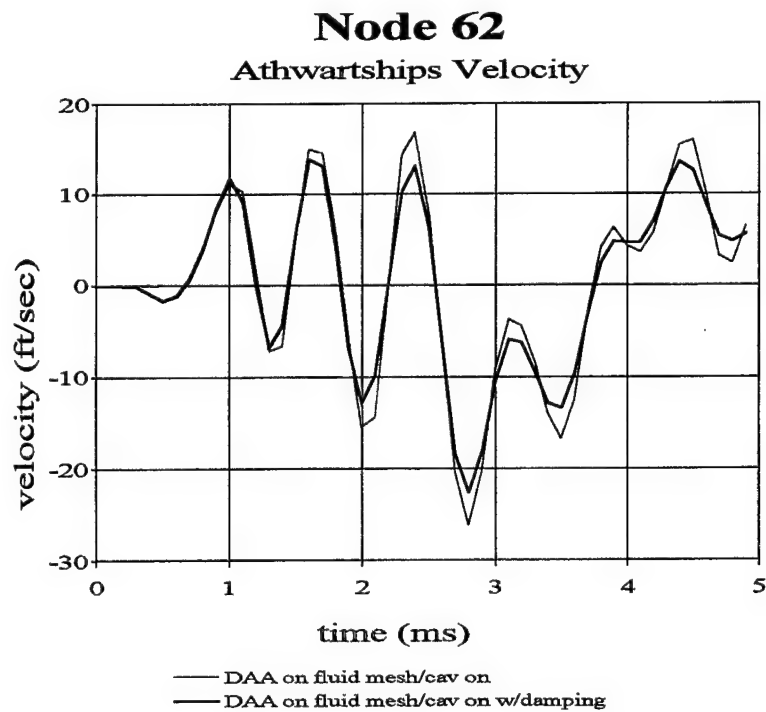
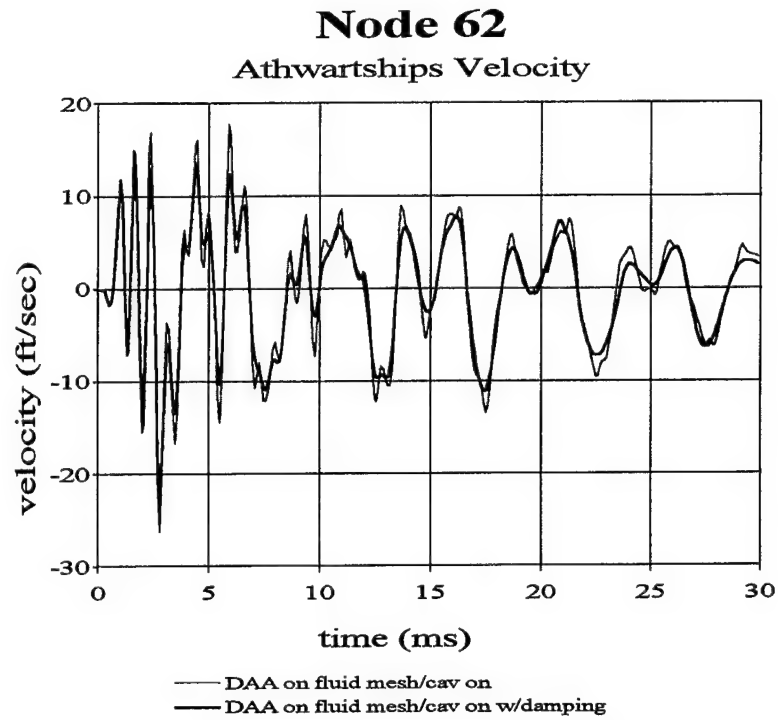


Figure 72. 3-D Model w/Charge Under Keel Damped Response Comparison

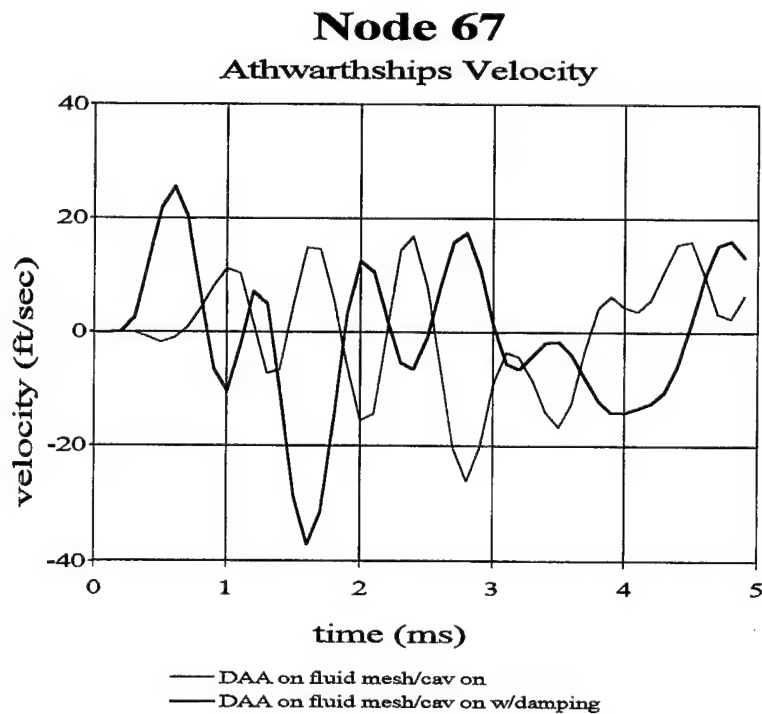
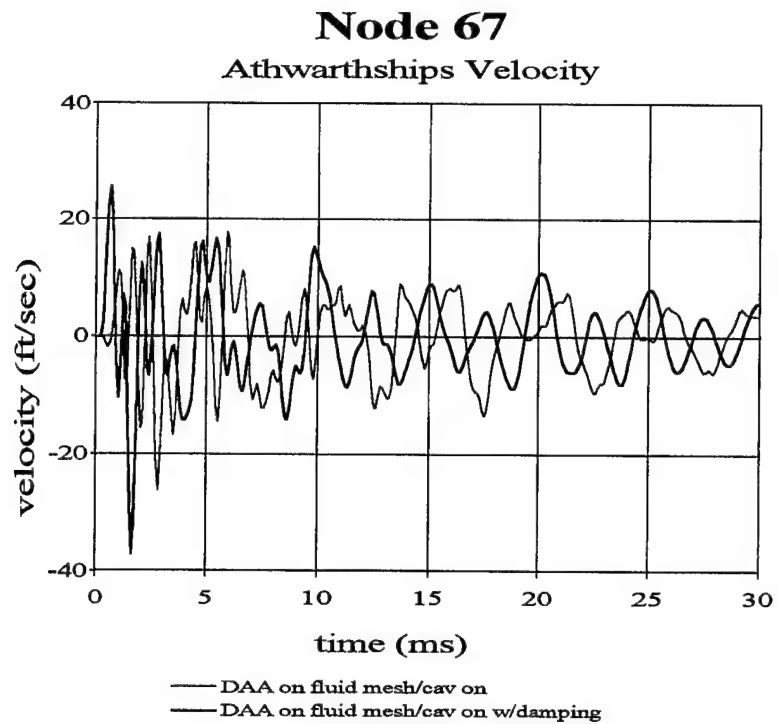


Figure 73. 3-D Model w/Charge Under Keel Damped Response Comparison

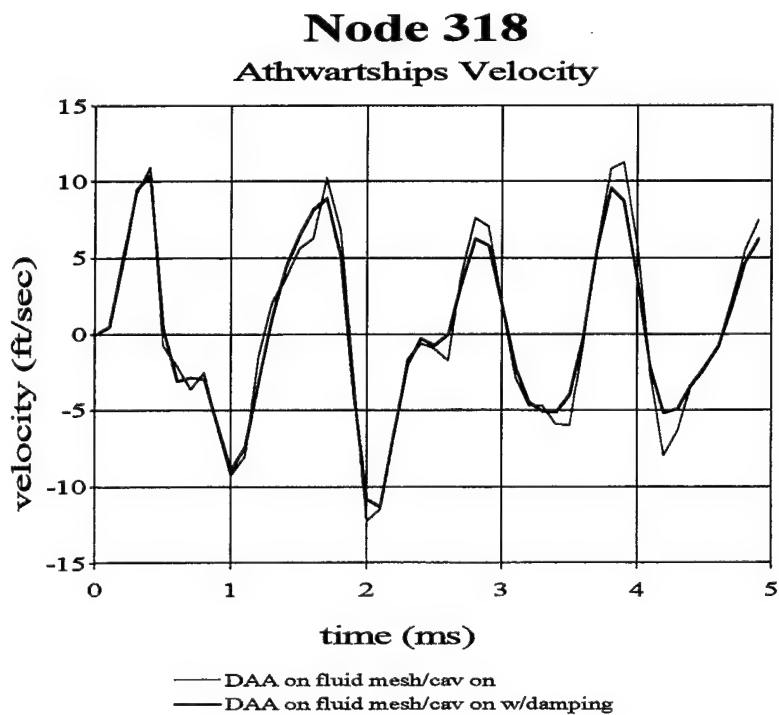
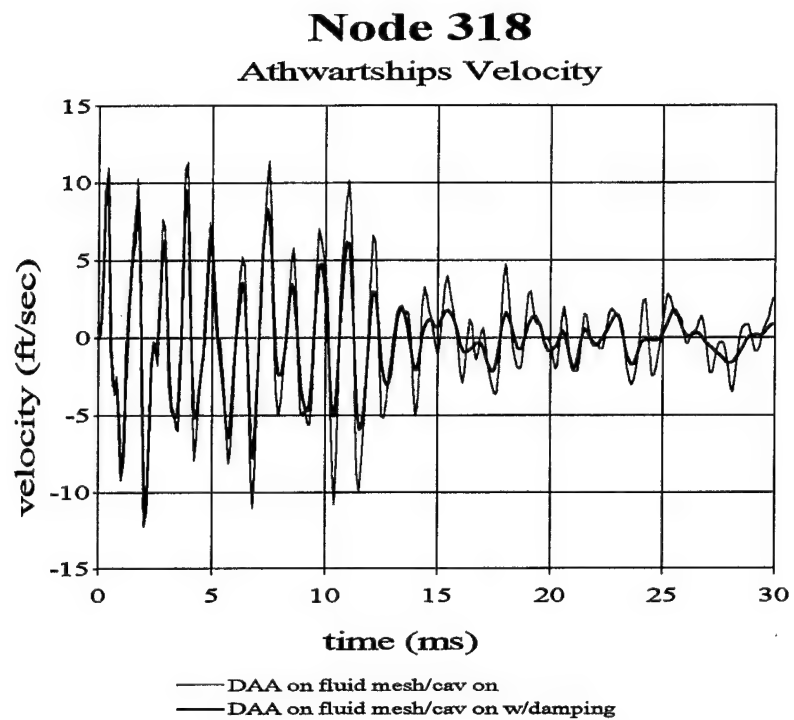


Figure 74. 3-D Model w/Charge Under Keel Damped Response Comparison

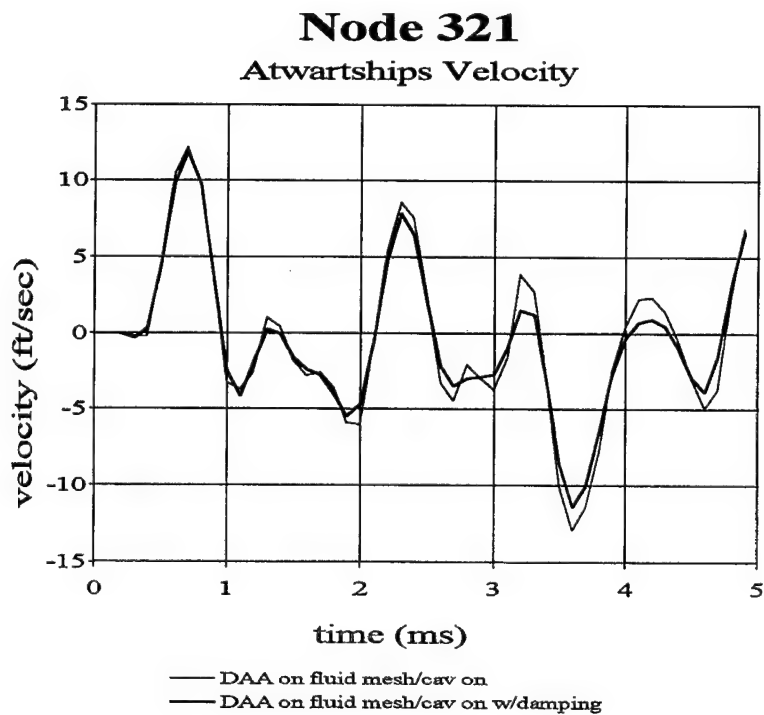
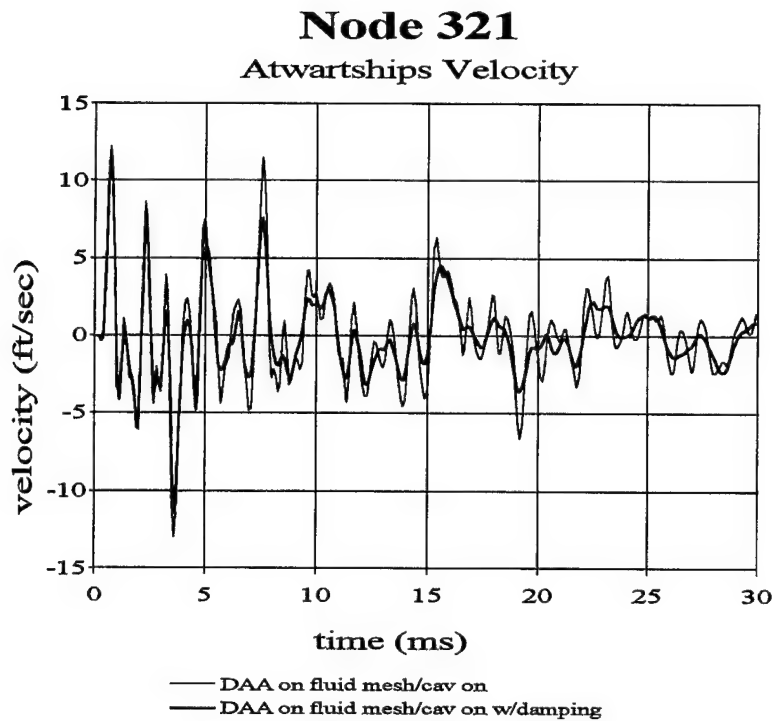


Figure 75. 3-D Model w/Charge Under Keel Damped Response Comparison

V. CONCLUSIONS AND RECOMMENDATIONS

This thesis investigated the effect of cavitation on ship-like box structure subjected to an underwater explosion. In the course of the investigation, both two and three-dimensional models were run through underwater shock simulations. The nodal velocity response results obtained clearly demonstrated that cavitation plays a role in the overall velocity response of the model. Rayleigh damping was added to the three-dimensional model and it was also found to play a vital role in the velocity response.

Shock simulation runs with the DAA boundary on the wetted surface provide a basic prediction of the model response, but inclusion of the fluid mesh in the finite element model is essential to get accurate results. Models with the DAA on the exterior of the fluid mesh and cavitation flag off also provide a basic prediction of model behavior, but the cavitation flag must be turned on to get the best prediction of the structural behavior due to the underwater explosion event.

The modeling and simulation process used in this investigation seems to be valid in that the velocity responses obtained from the finite element models agree with expected behavior based on the physics of the situation. It was also observed that three-dimensional models with the fluid mesh included as computationally expensive to run through underwater shock simulations.

It is recommended that additional studies be conducted to more fully examine fluid mesh modeling in underwater shock simulation, as well as the fluid-structure interaction. Specifically, the following areas need to be studied:

1. The effect of varying the number of rows of critical size fluid elements next to the structure to find the optimum number of rows.
2. The effect of fluid element size adjacent to and away from the critical element rows.
3. Vary the overall size of the fluid mesh in the longitudinal direction (x and y direction) from the structure to find the optimum dimensions.

APPENDIX A. BULK CAVITATION PROGRAM

The following program code calculates the bulk cavitation zone by solving Equations (2.20) and (2.21). The code is written for MATLAB version 5 [Ref. 11].

```
%Bulk Cavitation Program Using HBX-1 as charge type
%Written by: Steven L. Wood
%Last Modified: 10 Jul 98
%MATLAB Version 5
%
%Program to compute both the upper and lower cavitation boundaries
%for a given user input of charge weight of HBX1 and charge depth.
%Program can easily be modified to handle other explosive types:
%-shock wave parameters (K1,K2,A1,A2) must be updated.
%"Standard" atm pressure and seawater specific weight are used by
%default,
% these can be changed to achieve desired accuracy for a particular
%problem.
%Speed of sound can also be modified to suit different conditions.
%Program cavitation boundaries can be modified as required by changing
%x and y limits in the loop indices (both in upper boundary loop, only
%y in lower boundary loop.
%Axis limits on the plot can also be modified as required.
%
%Begin Program
clear all;

%Define constants
%C = acoustic velocity, ft/s
%Pa = atmospheric pressure, psi
%K1,K2,A1,K2 = shock wave parameters, explosive type specific
%gamma = specific weight of seawater, lbf/in^3 @ 60F and 1 atm
Pa = 14.7;
C = 4929.6;
K1 = 22347.6;
K2 = 0.056;
A1 = 1.144;
A2 = -0.247;
gamma = 0.037037;

%User is prompted to enter charge weight and depth
W = input('Enter the charge weight of HBX-1 in lb: ');
D = input('Enter the charge depth in feet: ');
%Begin calculation of cavitation boundaries, upper and lower

%theta = decay constant
%x = horizontal distance
%y = vertical distance
%r1,R = standoff distance from charge to point
%r2 = standoff distance from image charge to point
%Pi = incident shock wave pressure at tc
```



```

data_u = []; %Create matrix to store upper boundary data
data_l = []; %Create matrix to store lower boundary data

%Calculate Upper Boundary
for x = 0:1500
    for y = 0:0.1:60
        r1 = sqrt((D-y)^2+x^2);
        r2 = sqrt((D+y)^2+x^2);
        theta = K2*W^(1/3)*(W^(1/3)/r1)^A2/1000;
        F = (K1*(W^(1/3)/r1)^A1*exp(-(r2-
r1)/(C*theta)))+Pa+(gamma*y^12)-(K1*(W^(1/3)/r2)^A1);

        if F <= 0 %Test for cavitation
            data_u = [data_u; F x -(y)];
            break,end
    end
end

%Calculate lower boundary
for x = 0:(length(data_u)-1)
    for y = 0:0.1:60
        r1 = sqrt((D-y)^2+x^2);
        r2 = sqrt((D+y)^2+x^2);
        theta = K2*W^(1/3)*(W^(1/3)/r1)^A2/1000;
        Pi = K1*(W^(1/3)/r1)^A1*exp(-(r2-r1)/(C*theta));
        G = -(Pi/(C*theta))*(1+((r2-
(2*D*(D+y)/r2))/r1)*((A2*r2)/r1-A2-1))-((A1*Pi)/r1^2)*(r2-
2*D*((D+y)/r2)))+(gamma^12)*((D+y)/r2)+(A1/r2)*(Pi+Pa+(gamma*y^12));

        if G >= 0 %Test for cavitation
            data_l = [data_l; G x -(y)];
            break,end
    end
end

%Truncate cavitation boundaries at intersection
index_u = find(data_u(:,3)<data_l(:,3));
index_l = find(data_l(:,3)>data_u(:,3));
data_u(index_u,:)=[];
data_l(index_l,:)=[];

%Plot cavitation boundary
orient tall;
figure(1)
plot(data_u(:,2),data_u(:,3),data_l(:,2),data_l(:,3)); grid;
W_text = num2str(W);
D_text = num2str(D);
title(['Cavitation Zone for a ',W_text,' lb HBX-1 Charge']);
%title(['Cavitation Zone for a ',W_text,' lb HBX-1 Charge at a Depth of
',D_text,' feet']);
xlabel('Feet'); ylabel('Feet');

```

APPENDIX B. HELPFUL FEATURES IN MSC/PATRAN

MSC/PATRAN [Ref. 14] is a powerful finite element modeling and visualization tool. The program has many useful features to aid in visualizing and manipulating a finite element model. Different input and output formats are also supported, such as LS-DYNA keyword format. Basic familiarity with MSC/PATRAN is assumed. Important menu selections are featured in bold.

1. Creating **GROUPS** is useful for visualization of a complex mesh. The model can in effect be "sliced" into different sections for example and each put in a different group. The **CREATE** option is used to form a group. A group name must be entered. Elements to add to a group can then be selected with the mouse from the viewport. When selecting elements to add to a group, visible elements only can be selected by toggling the visible only button on the top left of the selection tool bar. This is only effective when using the hide view of the mesh (vice wireframe). The visible elements only selection feature is most useful when defining the wetted surface of a model. The **MODIFY** option provides for additions or removals from the target group. The target group can be changed with the **CHANGE TARGET** button. The **POST** option allows individual groups to be displayed in the current viewport. More than one group can be selected for display. The **shift** key must be held down to make multiple selections. This feature works also when selecting individual elements from the viewport. An individual element is selected, then, if additional elements are desired to be selected, they can be added to the list by holding down the shift key while highlighting them with the mouse.
2. A model can be moved in set increments using the **TRANSFORMATIONS** options found under the **VIEWING** menu. This option provides for rotation of the model about one of the three axes in a set fashion. The model can also be moved in set increments in any of the six main directions (x,y, and z). This provides for precise control over the model's positioning and aspect.

3. Multiple viewports can be created and posted using the **VIEWPORT** menu. The **CREATE** option allows the user to create and name a new viewport. Each created viewport can be posted/unposted using the **POST** menu. The **MODIFY** menu provides for the current and default viewports to be changed. The current viewport is the "active" viewing window and it is where all actions performed will take effect. Groups can also be posted/unposted from this menu option. This effects the current viewport. The **TILE** option automatically places two displayed viewports side by side.
4. The **LIST** creation option under the **TOOLS** menu provides the means to find objects (elements, nodes, etc.) with a common **ATTRIBUTE** or **ASSOCIATION** with other objects (such as groups or certain elements). FEM or geometry can be chosen. Nodes or different element types can be specified for association or attribute selection. For example, an empty group can be created (the group name is entered in the group create dialog box and apply is depressed; no elements are selected from the viewport) and then a list can be created of all the elements with a common attribute, such as a particular material property or property set. The list of elements can then be added to the newly created group and subsequently displayed. The list can also be added to any existing groups. The list can be output to one of two sub-windows, **A** or **B**. The destination window is selected via the radial buttons at the bottom of the create list window. The list tool can be a very powerful asset.
5. The **DISPLAY** menu option provides a number of menu selections. The **PLOT/ERASE** option provides the means to "unclutter" the display viewport. Specific element types can be selected and then erased from the display. The erased elements are not deleted from the model; they are only removed from view. They can then be re-posted to the viewport by selecting the **PLOT ALL POSTED FEM OPTION**. All the objects in the viewport can also have their labeling toggled on and off via the appropriate menu selection. The object color can also be changed from the set default color. This is accomplished by

simply clicking the small color patch next to the object name in the appropriate label selection menu. A small window of color choices will pop-up and a new color can be selected and applied the object.

6. The **FINITE ELEMENT** radial button has a number of useful mesh creation and diagnostic tools, one of which is the **VERIFY** option. By selecting **ELEMENTS** and **NORMALS**, element normal vectors can be displayed and even reversed if required. For the reverse option, a reference element must be designated. The **ELEMENTS/DUPLICATES** option allows any duplicate elements to be highlighted and deleted if the user desires. Either the higher or lower ID number element can be selected for deletion. **EQUIVALENCE** allows a tolerance to be set and any nodes falling within the tolerance will be merged and the database numbering reset. Nodes can be designated for exclusion from the equivalencing. The **RENUMBER** option allows nodes and/or elements to be renumber starting with a user specified number. The **SHOW** option displays the selected node's coordinates and ID number, and for elements the ID number, type, and property set is displayed. The selected nodes and elements are highlighted in the viewport if the ID number is input by hand rather than selected with the mouse.
7. Selecting the **LOADS/BCS** radial button allows creation of pressure load to define the wetted surface. When inputting the pressure set data, one has choices of top or bottom of the element (for two-dimensional elements). The correct choice is top, since this is the side with the normal vector pointing outward. For three-dimensional elements, such a fluid elements, the pressure load can be applied to free faces only (a button on the selection tool bar). This is useful for defining the outside surface of the fluid mesh for the DAA boundary. The visible only button should also be depressed when defining a wetted surface.
8. Results from a NASTRAN analysis can be input into PATRAN by selecting the **ANALYSIS** radial button, followed by choosing **READ OUTPUT2**

under the action menu. The desired results file name can then be selected and read in by clicking the apply button.

9. The imported results can then be viewed using the **RESULTS** button. If the results are in a form that can be plotted in an xy-plot, then the results type should be changed from **BASIC** to **ADVANCED**. Under **RESULT CASE OPTIONS**, the desired results should be selected (highlighted), then the **GET RESULTS** bar depressed. Under the **PLOT TYPE** menu, **XY-PLOT** can be selected. **PLOT TYPE OPTIONS** is used next to assign the global variable (usually time) and then the desired y-variable (such as displacement, velocity, and acceleration, depending on the results read in) can be selected to be plotted. The nodes whose response is desired can be input. Once the results curves are plotted, they can be further manipulated using the **XY data radial** button.
10. The **XY data** button has the normal menu selections, such as **CREATE**, **DELETE**, **MODIFY**, **POST**. These choices have options for both xy-windows and curves. Using create, new xy-windows can be generated and displayed with the post option. Curves cannot be generated here, they must be generated as in step 9 above. Curves can be deleted here and posted/unposted to/from different xy-windows.
11. ASCII files can be created from the generated curve data. Under the **xy** menu, **MODIFY/CURVE** should be selected. The desired curve is then selected (highlighted) from the middle window (which displays all of the curves currently created in the database file). The **DATA FROM KEYBOARD** option should be chosen and the **WRITE XY DATA TO FILE** button should be clicked on. Once apply is clicked, a filename can be input for the ASCII file and the destination directory selected. PATRAN does put a small text header in the file above the first xy-data pair. This header must be deleted prior to importing the file into UERD Tool.
12. The **PRINT** option can be found under the **FILE** menu. The user must be careful when printing to select what is to be printed. The top bar of the print

menu can be toggled between either **CURRENT VIEWPORT** printing or **CURRENT XY-WINDOW** printing. **ALL VIEWPORTS** or **ALL XY-WINDOWS** can also be chosen. Color or black&white can be toggled under the print **OPTIONS** menu. Under options is where the print to file option is chosen and a filename is input. PATRAN can output postscript or encapsulated postscript files. The **PAGE SETUP** menu provides for selection of page orientation and size, as well as turning borders on and off. The output is not created until the apply button is clicked. It should also be noted that the output file name need not be changed for subsequent print views. PATRAN automatically appends a sequentially numbered suffix to the postscript filename with each print output.

13. **NEUTRAL** files can be generated by selecting the **EXPORT** option under the **FILE** menu. Neutral files can be imported into PATRAN using the **IMPORT** option. PATRAN by default looks for a .out extension on neutral files.

APPENDIX C. FLUID MODELING USING TRUEGRID

This appendix covers the procedure for creating a fluid finite element mesh using TrueGrid's extrusion feature: the **BLUDE** command. The basics of using TrueGrid will not be covered here and some familiarity with the code is assumed. Additional information can be found in the TrueGrid user manual [Ref. 12].

Essentially the **BLUDE** feature pulls or "extrudes" the structural mesh through an "guide" mesh mated to the structural wetted surface in the form of a block part. The block part is actually attached to a surface definition created from a faceset of the wetted elements of the structural mesh. The resulting extruded mesh matches exactly to the structural mesh, a prerequisite for successful fluid modeling.

The extrusion procedure is as follows, with important commands and menu selections denoted in bold and all capital letters for emphasis:

1. A structural model must be created. TrueGrid can be used or the **READMESH** command can be used to input a mesh from another code format, such as LS-DYNA or NASTRAN. It is very important to remember though, that when TrueGrid reads in a finite element mesh from an outside code format, it renumbers every element and grid point. Therefore, once the mesh is through being manipulated in TrueGrid, and it is written an output file, the grid point and element ID numbers will not match between the original and newly output model from TrueGrid (even if the original model was not modified in TrueGrid).
2. The elements of the structural model that will be in contact with the fluid, i.e. the wetted surface, must be grouped into **FACESETS**. This option can be accessed from the environment window under the **PICK** option by choosing the **SETS** button. The **FACES** button should be selected. Each "face" of the structural model should be put in a separate faceset, meaning each side, bottom, bow, and stern should be grouped individually. The reason for this will be clear once the procedure is understood and used. The **HIDE** drawing mode vice **WIREFRAME** should be used for the mesh to ensure that only the

visible elements are picked. This will make faceset selection must easier, since it must be done by hand using the lasso tool guided by the mouse. The four-node selection option is the best to use when choosing the faceset. This means that four nodes of an element must be within the selection lasso for the element to be added to the faceset. The selected elements will be highlight in white. If some elements are selected that are not desired in the particular set, they can be easily selected and removed; using the one node selection option is best for this operation. The **REMOVE** button should be pushed also. The set must be named and saved once selected.

3. The **SURFACE** menu **SD** (surface definition) option should be chosen next. A surface number must be input. The faceset option should be selected from the end of the surface options list and the name of the desired faceset should then be input. This step converts the named faceset into a surface definition. The new surface will be displayed in red in the physical window.
4. Next, the **PARTS** menu should be selected and the **BLUDE** option chosen. Using this option, the user creates a block part that will be attached to the above created surface. This block will serve as the "guide" for the extrusion of the structural mesh; therefore, the block's mesh must match the structural mesh or be of finer quality in order to get a quality extrusion; an exact match is not required however. This block part is created in the same way as a block using the **BLOCK** command. The blude command requires two additional inputs, however. First, the face of the block where the extrusion begins must be input. This is simply the face closest to the structure. Next, the name of the faceset to be extruded must input.
5. The block part created must now be attached to the surface created in step 3. It can be attached using any of TrueGrid's available options. The easiest being selection of the face to be attached and then selecting the surface and clicking the **PROJECT** button in the environment window. This will work for simple cases, but a complex surface may require use of other TrueGrid methods.

6. The interface of the extrusion mesh and the structural mesh should be carefully examined. Orthogonality of the fluid and structural mesh is a must (next to the wetted surface) and should be verified; TrueGrid's **DIAGNOSTICS** menu provides the necessary tools. The block mesh can be modified as needed using various TrueGrid tools to ensure a quality mesh is constructed for the extrusion; two examples of useful tools are the mesh relaxation algorithms and use of a cubic spline to added curvature to the block mesh edges. Material properties can be assigned to the mesh also, just as with any other part in TrueGrid. In short, the extrusion mesh should be treated as any other part one would create in TrueGrid; all of the same options are available.
7. Once the user is satisfied with the extrusion mesh, the **MERGE** command should be used to end the **PARTS** phase and actually perform the extrusion. The result will be a fluid mesh, which matches exactly to the structural mesh. The mesh will consist of 8-noded solid elements. The **STP** option can be used also if required to ensure that the fluid mesh is merged with the structural mesh and there are no duplicate nodes. Additionally, prior to merging, the extrusion mesh can be replicated using the **LCT** and **LREP** commands. This will only be effective if the model is symmetric. Using these part replication features, the user only has to build one-half of the extrusion mesh.
8. Additional extrusions can be performed, including on any newly extruded mesh surfaces. This must usually be done to fully form a fluid mesh around the structural model.
9. Postscript images of the model and the mesh can be made using the **POSTSCRIPT** command. The command postscript is given at the command prompt with a the desired output filename. The **DRAW** button in the environment window should then be clicked to redraw the image. This creates the postscript file. Additional files will be generated as long as the command is active and the model is manipulated in any way so that it must be regenerated in the display window. The postscript command can be turned off

by typing **POSTSCRIPT OFF**. One additional command that is quite useful in generating quality image files is the **RESO** command. The **reso** command is entered prior to the **postscript** command. The syntax is the command followed by a number that is the desired resolution. This is system limited. A resolution of 2300 has been used with success. The **postscript** files generated are black and white only, but they consist of vector data. This means the images generated are crisp and very accurate.

APPENDIX D. USA/LS-DYNA INPUT DECKS

This section of this appendix provides example USA input decks for each of the three USA modules: FLUMAS, AUGMAT, and TIMINT. The decks are from the ship-like box model (both two and three-dimensional models) and are given for each of two cases: a DAA₂ on the wetted surface and a DAA₁ on the fluid mesh. Reference 18 provides information concerning the various input deck variables.

Example LS-DYNA KEYWORD input decks are included also from the three-dimensional models. Two cases are included: DAA on the wetted surface and DAA on the fluid mesh. In each case only the first line or two of each card is included. Reference 16 provides information as to the meaning of each field on the cards.

USA INPUT DECKS:

Two-dimensional model:

Input decks for DAA₂ on wetted surface:

```
FLUMAS DATA FOR BOX MODEL
flunam geonam strnam daanam
T T F T
T T F F
F F T F
F F F T
F T F T
F F F F
F F F F
F F
0 38 0 12
0 0 0
0.9389E-4 59155.2
10
12. 0. 0. 1.
14.7 386.088
0. 0. 0.
0. 90. 0.
0
3
0 1 3 1
1 4 9 1
0 10 12 1
```

```
AUGMAT DATA FOR BOX MODEL
strnam flunam geonam prenam
F F F F
F T F T
```

```
$ FLUNAM GEONAM GRDNAM DAANAM
$ PRTGMT PRTRN PRTAMF CALCAM
$ EIGMAF TWODIM HAFMOD QUAMOD
$ PCHCDS NASTAM STOMAS STOINV
$ FRWTFI FRWTGE FRWTGR FRESUR
$ RENUMB STOGMT ROTGEO ROTQUA
$ PRTCOE STRMAS SPHERE ROTSYM
$ OCTMOD CAVFLU FRWTFV INTCAV
$ BOTREF MASREF
$ NSTRC NSTRF NGEN NGENF
$ NBRA NCYL NCAV
$ RHO CEE
$ NVEC
$ DEPTH CXFS CYFS CZFS
$ PATM GRAVAC
$ QUATRN(1)QUATRN(2)QUATRN(3)
$ QUAANG(1)QUAANG(2)QUAANG(3)
$ NSRADI
$ NSORDR
$ NORD JBEG JEND JINC
$ NORD JBEG JEND JINC
$ NORD JBEG JEND JINC
```

```
$ STRNAM FLUNAM GEONAM PRENAM
$ FRWTGE FRWTST FRWTFI LUMPFM
$ FLUSKY DAAFRM SYMCON DOFTAB
```

```

F F F F
F F F F
4
0.5
38 114 3 3
1
0 1 12 1

```

TIMINT DATA FOR BOX MODEL

```

prenam posnam
resnam
F F
1
0.0 1.0E-6
T F F F
F T F F
F F
1
0.
55.45 0. -201.00
55.2 0. 0.
201
1. 0.
4.765E-6
1
20. 16.75 17.75
2000 2000
0 0 0 0
F F F
F

```

```

$ PRTGMT PRTRN PRTSTF PRTAUG
$ MODTRN STRLCL INTWAT CFADYN
$ NTYPDA
$ DAA2M
$ NSTR NSFR NFRE NFTR
$ NSETLC
$ NDICOS JSTART JSTOP JINC

```

```

$ PRENAM POSNAM
$ RESNAM WRTNAM
$ REFSEC FLUMEM
$ NTINT
$ STRTIM DELTIM
$ EXPWAV SPLINE VARLIN PACKET
$ HYPERB EXPLOS DOUBDC VELINP
$ BUBPUL SHKBUB
$ NCHARG
$ HYDPRE
$ XC YC ZC
$ SX SY SZ
$ JPHIST
$ PNORM DETIM
$ DTHIST
$ CHGTYP
$ WEIGHT SLANT CHGDEP
$ NSAVER NRESET
$ LOCBEG LOCRES LOCWRT NSTART
$ FORWRT STBDA2 ASCWRT
$ DISPLA

```

Input decks for DAA₁ on fluid mesh:

FLUMAS DATA FOR BOX MODEL

```

flunam geonam strnam daanam
T T F T
T T F F
F F T F
F F F T
F T F F
F F F F
F F F F
F F
0 2582 0 102
0 0 0
0.9389E-4 59155.2
10
12. 1. 0. 0.
14.7 386.088
0
3
0 1 6 1
1 7 12 1
0 13 102 1

```

```

$ FLUNAM GEONAM GRDNAM DAANAM
$ PRTGMT PRTRN PRTAMF CALCAM
$ EIGMAF TWODIM HAFMOD QUAMOD
$ PCHCDS NASTAM STOMAS STOINV
$ FRWTFI FRWTGE FRWTGR FRESUR
$ RENUMB STOGMT ROTGEO ROTQUA
$ PRTCOE STRMAS SPHERE ROTSYM
$ OCTMOD CAVFLU FRWTFV INTCAV
$ BOTREF MASREF
$ NSTRC NSTRF NGEN NGENF
$ NBRA NCYL NCAV
$ RHO CEE
$ NVEC
$ DEPTH CXFS CYFS CZFS
$ PATM GRAVAC
$ NSRADI
$ NSORDR
$ NORD JBEG JEND JINC
$ NORD JBEG JEND JINC
$ NORD JBEG JEND JINC

```

AUGMAT DATA FOR BOX MODEL
 strnam flunam geonam prenam
 F F F F
 F T F T
 F F F F
 F F F F
 11
 2582 7746 3 3
 1
 0 1 102 1

TIMINT DATA FOR BOX MODEL
 prenam posnam
 resnam
 F F
 1
 0.0 1.0E-6
 T F F F
 F T F F
 F F
 1
 0.
 -201.0 0. 4.8
 -80.0 0. 4.8
 201
 1. 0.
 4.766E-6
 1
 20. 16.75 17.75
 2000 2000
 0 0 0 0
 F F F
 -5. 0. 0.
 F

\$ STRNAM FLUNAM GEONAM PRENAM
 \$ FRWTGE FRWTST FRWTF L LUMPFM
 \$ FLUSKY DAAFRM SYMCON DOFTAB
 \$ PRTGMT PRTRN PRTSTF PRTAUG
 \$ MODTRN STRLCL INTWAT CFAPRE
 \$ NTYPDA
 \$ NSTR NSFR NFRE NFTR
 \$ NSETLC
 \$ NDICOS JSTART JSTOP JINC

\$ PRENAM POSNAM
 \$ RESNAM WRTNAM
 \$ REFSEC FLUMEM
 \$ NTINT
 \$ STRTIM DELTIM
 \$ EXPWAV SPLINE VARLIN PACKET
 \$ HYPERB EXPLOS DOUBDC VELINP
 \$ BUBPUL SHKBUB
 \$ NCHARG
 \$ HYDPRE
 \$ XC YC ZC
 \$ SX SY SZ
 \$ JPHIST
 \$ PNORM DETIM
 \$ DTHIST
 \$ CHGTYP
 \$ WEIGHT SLANT CHGDEP
 \$ NSAVR NRESET
 \$ LOCBEG LOCRES LOCWRT NSTART
 \$ FORWRT STBDA2 ASCWRT
 \$ XV YV ZV
 \$ DISPLA

Three-Dimensional model:

Input decks for DAA₂ on the wetted surface:

FLUMAS DATA
 flunam geonam strnam daanam
 F F F T
 T F F F
 F F T F
 F F F T
 F T F F
 F F F F
 F F F F
 F F
 0 1001 0 192
 0 0 0
 0.9389E-4 59155.2
 10

\$ FLUNAM GEONAM GRDNAM DAANAM
 \$ PRTGMT PRTRN PRTAMF CALCAM
 \$ EIGMAF TWODIM HAEMOD QUAMOD
 \$ PCHCDS NASTAM STOMAS STOINV
 \$ FRWTF L FRWTGE FRWTGR FRESUR
 \$ RENUMB STOGMT ROTGEO ROTQUA
 \$ PRTCOE STRMAS SPHERE ROTSYM
 \$ OCTMOD CAVFLU FRWTFV INTCAV
 \$ BOTREF MASREF
 \$ NSTRC NSTRE NGEN NGENF
 \$ NBRA NCYL NCAV
 \$ RHO CEE
 \$ NVEC

12. 0. 0. 1.
14.7 386.088
0
0

AUGMAT DATA

strnam flunam geonam prenam
F F F F
F T F T
F F F F
F F F F
4
0.5
1001 3003 3 3
1
0 1 192 1

TIMINT DATA

prenam posnam
resnam
F F
1
0.0 1.0E-5
T F F F
F T F F
F F
1
0.
60.0 -112.44 -174.00
55.2 -112.44 0.
201
1. 0.
4.765E-6
1
20. 16.7. 15.50
2000 2000
0 0 0 0
F F F
F

\$ DEPTH CXFS CYFS CZFS
\$ PATM GRAVAC
\$ NSRADI
\$ NSORDR

\$ STRNAM FLUNAM GEONAM PRENAM
\$ FRWTGE FRWTST FRWTF LUMPFM
\$ FLUSKY DAAFRM SYMCON DOFTAB
\$ PRTGMT PRTRN PRTSTF PRTAUG
\$ MODTRN STRLCL INTWAT CFADYN
\$ NTYPDA
\$ DAA2M
\$ NSTR NSFR NFRE NFTR
\$ NSETLC
\$ NDICOS JSTART JSTOP JINC

\$ PRENAM POSNAM
\$ RESNAM WRTNAM
\$ REFSEC FLUMEM
\$ NTINT
\$ STRTIM DELTIM
\$ EXPWAV SPLINE VARLIN PACKET
\$ HYPERB EXPLOS DOUBDC VELINP
\$ BUBPUL SHKBUB
\$ NCHARG
\$ HYDPRE
\$ XC YC ZC
\$ SX SY SZ
\$ JPHIST
\$ PNORM DETIM
\$ DTHIST
\$ CHGTYP
\$ WEIGHT SLANT CHGDEP
\$ NSAVR NRESET
\$ LOCBEG LOCRES LOCWRT NSTART
\$ FORWRT STBDA2 ASCWRT
\$ DISPLA

Input decks for DAA₁ on fluid mesh:

FLUMAS DATA

flunam geonam strnam daanam
F F F T
T F F F
F F T F
F F F T
F T F F
F F F F
F F F F
F F
0 63009 0 7226
0 0 0

\$ FLUNAM GEONAM GRDNAM DAANAM
\$ PRTGMT PRTRN PRTAMF CALCAM
\$ EIGMAF TWODIM HAFMOD QUAMOD
\$ PCHCDS NASTAM STOMAS STOINV
\$ FRWTF L FRWTGE FRWTGR FRESUR
\$ RENUMB STOGMT ROTGEO ROTQUA
\$ PRTCOE STRMAS SPHERE ROTSYM
\$ OCTMOD CAVFLU FRWTFV INTCAV
\$ BOTREF MASREF
\$ NSTRC NSTRF NGEN NGENF
\$ NBRA NCYL NCAV

0.9389E-4 59155.2
 10
 12. 0. 0. 1.
 14.7 386.088
 0
 0

AUGMAT DATA

strnam flunam geonam prenam
 F F F F
 F T F T
 F F F F
 F F F F
 11
 63009 189027 3 3
 1
 0 1 7226 1

TIMINT DATA

prenam posnam
 resnam
 F F
 1
 0.0 1.0E-5
 T F F F
 F T F F
 F F
 1
 0.
 60.0 -112.44 -174.00
 60.0 -58.17 -80.0
 201
 1. 0.
 4.765E-6
 1
 20. 16.75 15.50
 2000 2000
 0 0 0 0
 F F F
 55.2 -17.0 -5.0
 F

\$ RHO CEE
 \$ NVEC
 \$ DEPTH CXFS CYFS CZFS
 \$ PATM GRAVAC
 \$ NSRADI
 \$ NSORDR

\$ STRNAM FLUNAM GEONAM PRENAM
 \$ FRWTGE FRWTST FRWTFL LUMPFM
 \$ FLUSKY DAAFRM SYMCON DOFTAB
 \$ PRTGMT PRTRN PRTSTF PRTAUG
 \$ MODTRN STRLCL INTWAT CFADYN
 \$ NTYPDA
 \$ NSTR NSFR NFRE NFTR
 \$ NSETLC
 \$ NDICOS JSTART JSTOP JINC

\$ PRENAM POSNAM
 \$ RESNAM WRTNAM
 \$ REFSEC FLUMEM
 \$ NTINT
 \$ STRTIM DELTIM
 \$ EXPWAV SPLINE VARLIN PACKET
 \$ HYPERB EXPLOS DOUBDC VELINP
 \$ BUBPUL SHKBUB
 \$ NCHARG
 \$ HYDPRE
 \$ XC YC ZC
 \$ SX SY SZ
 \$ JPHIST
 \$ PNORM DETIM
 \$ DTHIST
 \$ CHGTYP
 \$ WEIGHT SLANT CHGDEP
 \$ NSAVR NRESET
 \$ LOCBEG LOCRES LOCWRT NSTART
 \$ FORWRT STBDA2 ASCWRT
 \$ XV YV ZV
 \$ DISPLA

LS-DYNA INPUT DECKS:

Input deck DAA₂ on the wetted surface:

*KEYWORD
 *TITLE
 ORIGINAL BOX MODEL
 *CONTROL TERMINATION
 0.03,0,0,0,0
 *CONTROL TIMESTEP
 0.00001,0.9,0,0.0,0.0,1,0
 *CONTROL OUTPUT
 1,0,1,0,0,1,1


```

*DEFINE_CURVE
1
0.,0.00001
0.03,0.00001
*DEFINE_CURVE
2
0.,0.
0.03,0.
*DATABASE_HISTORY_NODE
62,67,102,294,318,321,369
*DATABASE_NODOUT
0.00001
*DATABASE_BINARY_D3PLOT
0.0001
*DATABASE_BINARY_D3THDT
0.0001
*DATABASE_EXTENT_BINARY
0,0,3,1,1,1,1,1
0,0,0,0,0,0
*BOUNDARY_USA_SURFACE
2,1,0
*LOAD_SEGMENT_SET
2,2,1.0,0.0
*NODE
1,0.000,-12.000,0.000
*PART
1
1,1,1
*SECTION_BEAM
1,2
1.50,7.81E-3,19.15,14.68
*ELEMENT_BEAM
1,1,22,95,1001
*PART
2
2, 2,1
*SECTION_BEAM
2,2
0.25,3.26E-4,0.40,0.32
□
*ELEMENT_BEAM
14,2,29,96,1014
*PART
1
11,11, 1
*SECTION_SHELL
11 ,2, 0.83333
0.2500,0.2500,0.2500,0.2500
*ELEMENT_SHELL
616,11,1,2,9,8

*ELEMENT_MASS
1372 ,662 ,0.138

```

```

*MAT_ELASTIC
1,0.0007350,0.300E+08,0.300
*SET_SEGMENT
2
1,2,9,8
*END

```

Input deck for DAA₁ on the fluid mesh:

```

*KEYWORD
*TITLE
BOX MODEL WITH FLUID
*CONTROL_TERMINATION
0.030,0,0,0,0
*CONTROL_TIMESTEP
0.00001,0.9,0,0.0,0.0,1,0
*CONTROL_OUTPUT
1,0,1,0,0,1,1
*CONTROL_PARALLEL
2,2,1
*DEFINE_CURVE
1
0.,0.00001
0.030,0.00001
*DEFINE_CURVE
2
0.,0.
0.030,0.
*DATABASE_HISTORY_NODE
81059,34212,34533,81096,40778,81112,41161
*DATABASE_NODOUT
0.00001
*DATABASE_BINARY_D3PLOT
0.0001
*DATABASE_BINARY_D3THDT
0.001
*DATABASE_EXTENT_BINARY
0,0,3,1,1,1,1,1
0,0,0,0,0,0
*BOUNDARY_USA_SURFACE
2,1,0
*INITIAL_DETONATION
-1,60.,-112.44,-174.,0.0
18060.,0.0001592,60.,-92.18,-140.,39850
*NODE
1,-120.000,-132.000,-140.000
*PART
1
1,1,1
*SECTION_BEAM
1,2
1.50,7.81E-3,19.15,14.68
*ELEMENT_BEAM
1,1,24917,34359,100001

```

```

*PART
2
2,2,1
*SECTION_BEAM
2,2
0.25,3.26E-4,0.40,0.32
*ELEMENT_BEAM
14,2,24946,34388,100014

*PART
93
4001,4001,1
*SECTION_SHELL
4001,2,0.83333
0.2500,0.2500,0.2500,0.2500
*ELEMENT_SHELL
75960,4001,22964,23262,25167,24859
*PART
90
90,90,90
*SECTION_SOLID
90,8
*ELEMENT_SOLID
616,90,1,320,349,30,2,321,350,31
*ELEMENT_MASS
76338,34533,0.1380000
*MAT_ELASTIC
1,0.735E-03,0.300E+08,0.300000
*MAT_ACOUSTIC
90,0.9389E-4,59155.2,0.5,1.0
0.,0.,12.,0.,0.,1.
*SET_SEGMENT
2
1,320,321,2
*END

```

APPENDIX E. USEFUL FEATURES IN LS-TAURUS

TAURUS is an interactive post-processor and three-dimensional visualization tool for LS-DYNA [Ref. 16]. TAURUS has many useful features for viewing and manipulating model output responses obtained from LS-DYNA/USA simulations; a few of these features are detailed here. All TAURUS commands are fully documented in Appendix K of Reference 16. Basic familiarity with TAURUS is assumed.

1. A given state can be displayed in TAURUS by the following syntax: **s (state number) frin (fringe number)**. Note that the parentheses are not included (this syntax will be used to illustrate all commands); only the appropriate number is put in the command. In underwater shock simulations, pressure fringes are of concern; fringe 8 is pressure. The fringe numbers for other variables are listed in a set of tables in Reference 16.
2. Animation can be easily set-up with the command: **r (starting state number) (final state number) (step) frin (appropriate fringe code)**. The animation can be set-up to run between any desired starting and ending state. The **gif** command allows a gif image to output of the currently displayed state in the visualization window. TAURUS names the file by default, **pict#.gif** (where the # is a consecutive integer starting at one for each gif image created during the current TAURUS session). The command **noborder** removes the border and text information from the visualization window. **Logo** toggles the drawing of the TAURUS logo. The command **cb** can be used to change the background color from the default black. After entering the command, the user must input the amount of red, green, and blue to be mixed for the desired background color. As an example, 0,0,0 is black, and 1,1,1 is white. Other colors can be made by experimentation. The command **cline** is used to change the mesh line color on the screen. The default is white. As with **cb**, the amount of red, green, and blue must be input.
3. A video tape of the resulting animation can be made by selecting the **video out** application from the SGI desktop list of media tools. Note that this feature

must be installed and a VCR and TV must be hooked up to the SGI machine. The NPS SGI OCTANES have this option installed. The outline of a box will be visible on the screen. This is the capture window outline for what is sent to the VCR/TV. The size of this window can be changed between two sizes: full screen and a somewhat less than full screen size. The size is changed by clicking on the video out gray box that appears on the screen. The flicker filter can also be toggled on and off in the same way, and the function can be turned off here too. The full screen size does not give the best output; it is better to use the smaller size for better quality on the TV end. The VCR can then be used to record the images transmitted from the computer.

4. Phase II of TAURUS is used to plot time histories of desired variables for elements and nodes. The procedure for making the plot is as follows (example is for element time history): first the command **elem (number of elements) (element numbers)** is used to designate the desired elements; next **gather** is used to read the element data into memory; once the gathering is complete the desired time history can be plotted with **etime (fringe number) (number of elements to plot) (element numbers to be plotted)**. The commands **aset (min) (max)** and **oset (min) (max)** can be used to set the x and y axes appropriately for the desired range. The **keep** command can be used to generate an ascii file with the plotted data in it. This command must be issued prior to the **etime** command and once entered the user is prompted to enter a filename for the output file. The ascii file generated is in two column (x-y) format and contains the entire range of data for the element fringe requested (even if the data is only partially displayed in the plot window by use of the axis setting commands). It should be noted that this ascii file does contain some text header information above the data columns and the string "endplot" is placed at the end of the data.

LIST OF REFERENCES

1. NAVSEA 0908-LP-000-3010A, *Shock Design Criteria for Surface Ships*, October 1994.
2. Military Specification, MIL-S-901D, Shock Tests, High Impact Shipboard Machinery, Equipment, and Systems, Requirements for, March 1989.
3. OPNAV Instruction 9072.2, "Shock Hardening of Surface Ships", 12 January 1987.
4. USS John Paul Jones (DDG-53) Shock Trial Final Report, AEGIS Program Manager (PMS-400), November 1994.
5. Cole, R.H., *Underwater Explosions*, pp. 3-13, Princeton University Press, 1948.
6. Shin, Y.S., "Naval Ship-Shock Design and Analysis", Course Notes for Underwater Shock Analysis, Naval Postgraduate School, Monterey, CA, 1996.
7. Santiago, L.D., "Fluid-Interaction and Cavitation Effects on a Surface Ship Model Due to an Underwater Explosion", Master's Thesis, Naval Postgraduate School, Monterey, CA, September 1996.
8. Geers, T.L., "Residual Potential and Approximate Methods for Three-Dimensional Fluid-Structure Interaction Problems", The Journal of the Acoustical Society of America, Vol. 49, pp. 1505-1510, 1971.
9. DeRuntz, J.A. Jr., "The Underwater Shock Analysis Code and Its Applications", 60th Shock and Vibration Symposium Proceedings, Vol. I, November 1989.
10. Costanzo, F.A. and Gordon, J.D., "An Analysis of Bulk Cavitation in Deep Water", DTNSRDC, UERD Report, May 1980.
11. Hanselman, D. and Littlefield, B., *The Student Edition of MATLAB, Version 5 User's Guide*, Prentice Hall, 1997.
12. XYZ Scientific Applications, Inc., *TrueGrid Manual*, Livermore, CA, 1997.
13. Beiter, K.A., "The Effect of Stiffener Smearing in a Ship-Like Box Structure Subjected to an Underwater Explosion", Master's Thesis, Naval Postgraduate School, Monterey, CA, June 1998.
14. Macneal-Schwendler Corporation, *MSC/NASTRAN Quick Reference Guide, Version 69*, Los Angeles, CA, 1996.

15. Macneal-Schwendler Corporation, *MSC/PATRAN Installation and Operations Guide*, Version 7.0, Publication No. 903002, Los Angeles, CA, 1997.
16. Livermore Software Technology Corporation, *LS-DYNA Keyword User's Manual*, Version 940, Livermore, CA, 1997.
17. DeRuntz, J.A. Jr. and Rankin, C.C., "Applications of the USA-STAGS-CFA Code to Nonlinear Fluid-Structure Interaction Problems in Underwater Shock of Submerged Structures", 60th Shock and Vibration Symposium Proceedings, Vol. I, November 1989.
18. Shin, Y.S. and DeRuntz, J.A. Jr., USA/LS-DYNA3D Software Training Course Notes, June 1996.
19. ViewTech ASA, *Ghview Users Guide*, UNIX, Version 4, Norway, 1997.

INITIAL DISTRIBUTION LIST

		<u>No. Copies</u>
1.	Defense Technical Information Center 8725 John J. Kingman Rd., STE 0944 Ft. Belvoir, VA 22060-6218	2
2.	Dudley Knox Library Naval Postgraduate School 411 Dyer Rd. Monterey, CA 93943-5101	2
3.	Professor Y.S. Shin, Code ME/Sg Department of Mechanical Engineering Naval Postgraduate School Monterey, CA 93943	2
4.	Professor Y.W. Kwon, Code ME/Kw Department of Mechanical Engineering Naval Postgraduate School Monterey, CA 93943	1
5.	Naval/Mechanical Engineering Curricular Office (Code 34) Department of Mechanical Engineering Naval Postgraduate School Monterey, CA 93943	1
6.	LT Steven L. Wood 5313 Westover Lane Virginia Beach, VA 23464	1
7.	LCDR James Syring AEGIS Program Manager PMS 400D5 Naval Sea Systems Command 2531 Jefferson Davis Highway Arlington, VA 22242-5165	1

- | | | |
|-----|--|---|
| 8. | Gust Constant
PMS400D5
Naval Sea Systems Command
2531 Jefferson Davis Highway
Arlington, VA 22242-5165 | 1 |
| 9. | Robert Bowser
NAVSEA 03P3, NC4-Rm. 374
Naval Sea Systems Command
2531 Jefferson Davis Highway
Arlington, VA 22242-5165 | 1 |
| 10. | Dana Johanson
NAVSEA 03P4, NC4-Rm. 438
Naval Sea Systems Command
2531 Jefferson Davis Highway
Arlington, VA 22242-5165 | 1 |
| 11. | Michael Riley
Naval Surface Warface Center, Carderock Division
Underwater Explosions Research Department
1445 Crossways Blvd.
Chesapeake, VA 23320 | 1 |
| 12. | Michael Winnete
Naval Surface Warface Center, Carderock Division
Underwater Explosions Research Department
1445 Crossways Blvd.
Chesapeake, VA 23320 | 1 |
| 13. | Fred Costanzo
Naval Surface Warface Center, Carderock Division
Underwater Explosions Research Department
1445 Crossways Blvd.
Chesapeake, VA 23320 | 1 |
| 14. | John DeRuntz, Jr.
4172 Hampshire Place
Colorado Springs, CO 80906 | 1 |

- | | | |
|-----|---|---|
| 15. | Thomas L. Geers
Dept. of Mechanical Engineering
University of Colorado
Boulder, CO 80309 | 1 |
| 16. | Gordeon Everstine
Naval Surface Warface Center, Caderock Division
Code 1844
Bethesda, MD 20084-5000 | 1 |
| 17. | Harry Gray
Naval Surface Warface Center, Caderock Division
Code 673
Bethesda, MD 20084-5000 | 1 |
| 18. | Austin Alvarez
Electric Boat
75 Eastern Point Road
Groton, CT 06340-4989 | 1 |
| 19. | Hans Mair
Institute for Defense Analyses
Operational Evaluation Division
1801 North Beauregard Division
Alexandria, VA 22311-1772 | 1 |
| 20. | Robert Smilowitz
Weidlinger Associates
375 Hudson St., FL 12
New York, NY 10014 | 1 |
| 21. | Michael Harrington
Gibbs & Cox
1235 Jefferson Davis Highway
Crystal Gateway 1, Suite 700
Arlington, VA 22242 | 1 |